

## Small molecule inhibitors of ferrochelatase are antiangiogenic agents

Kamakshi Sishtla,<sup>1</sup> Nathan Lambert-Cheatham,<sup>1</sup> Bit Lee,<sup>2</sup> Duk Hee Han,<sup>3</sup> Jaehui Park,<sup>3</sup> Sheik Pran Babu Sardar Pasha,<sup>1</sup> Sanha Lee,<sup>2</sup> Sangil Kwon,<sup>2</sup> Anbukkarasi Muniyandi,<sup>1</sup> Bomina Park,<sup>1,4</sup> Noa Odell,<sup>1,5</sup> Sydney Waller,<sup>1</sup> Il Yeong Park,<sup>3</sup> Soo Jae Lee<sup>3,\*</sup>, Seung-Yong Seo<sup>2,\*</sup>, Timothy W. Corson<sup>1,4,6,7,\*</sup>

<sup>1</sup>Eugene and Marilyn Glick Eye Institute, Department of Ophthalmology, Indiana University School of Medicine, Indianapolis, IN 46202, USA

<sup>2</sup>College of Pharmacy, Gachon University, Incheon 21936, South Korea

<sup>3</sup>College of Pharmacy, Chungbuk National University, Chungbuk 28160, South Korea

<sup>4</sup>Department of Pharmacology & Toxicology, Indiana University School of Medicine, Indianapolis, IN 46202, USA

<sup>5</sup>Spelman College, Atlanta, GA 30314, USA

<sup>6</sup>Department of Biochemistry and Molecular Biology, Indiana University School of Medicine, Indianapolis, IN 46202, USA

<sup>7</sup>Lead Contact

\*Correspondence:

Soo Jae Lee, Osongsaengmyung 1, 194-21, Heungduk-gu, Cheongju, Chungbuk, South Korea 28160; +82-43-261-2816; sjlee@chungbuk.ac.kr  
Seung-Yong Seo, 191 Hambakmoero, Yeonsu-gu, Incheon, South Korea 21936; +82-32-820-4949; syseo@gachon.ac.kr  
Timothy W. Corson, 1160 West Michigan Street, Indianapolis, IN, 46202; +1-317-274-3305; tcorson@iu.edu

This is the author's manuscript of the work published in final edited form as:

Sishtla, K., Lambert-Cheatham, N., Lee, B., Han, D. H., Park, J., Sardar Pasha, S. P. B., Lee, S., Kwon, S., Muniyandi, A., Park, B., Odell, N., Waller, S., Park, I. Y., Lee, S. J., Seo, S.-Y., & Corson, T. W. (2022). Small-molecule inhibitors of ferrochelatase are antiangiogenic agents. *Cell Chemical Biology*. <https://doi.org/10.1016/j.chembiol.2022.01.001>

## **SUMMARY**

Activity of the heme synthesis enzyme ferrochelatase (FECH) is implicated in multiple diseases. In particular, it is a mediator of neovascularization in the eye and thus an appealing therapeutic target for preventing blindness. However, no drug-like direct FECH inhibitors are known. Here, we set out to identify small molecule inhibitors of FECH as potential therapeutic leads using a high throughput screening approach to identify potent inhibitors of FECH activity. A structure-activity relationship study of a class of triazolopyrimidinone hits yielded drug-like FECH inhibitors. These compounds inhibit FECH in cells, bind the active site in cocrystal structures, and are anti-angiogenic in multiple in vitro assays. One of these promising compounds was anti-angiogenic in vivo in a mouse model of choroidal neovascularization. This foundational work may be the basis for new therapeutic agents to combat not only ocular neovascularization, but also other diseases characterized by FECH activity.

## INTRODUCTION

The heme synthesis enzyme ferrochelatase (FECH; EC 4.99.1.1) has garnered considerable interest since it was first purified in 1981 (Taketani and Tokunaga, 1981). Found in the mitochondrion, the eukaryotic enzyme is responsible for the final step of heme biosynthesis, insertion of a ferrous ion into the center of the porphyrin ring of protoporphyrin IX (PPIX) (Hamza and Dailey, 2012). Partial loss-of-function mutations in the *FECH* gene cause erythropoietic protoporphyria, a blood disorder characterized by phototoxic buildup of PPIX (Lecha et al., 2009). Thus, there have been efforts to find small molecule activators of this enzyme to potentially treat conditions of reduced FECH activity (Hazama et al., 2008).

However, in recent years, *inhibition* of FECH has also emerged as a potential therapeutic avenue for multiple diseases. Two FECH inhibitors are widely used in preclinical studies. *N*-methylprotoporphyrin (NMPP) is a transition-state analog and fairly potent FECH inhibitor tool compound (Dailey and Fleming, 1983). Unfortunately, it is bulky, poorly soluble, and not amenable to medicinal chemistry optimization, rendering it a poor clinical candidate. The long-approved antifungal drug griseofulvin, interestingly, forms NMPP *in vivo* by alkylating the heme group of cytochrome P450 (Liu et al., 2015). Thus griseofulvin can be used as a FECH inhibitor in cells and intact organisms. However, given this unusual mechanism, it is difficult to develop novel griseofulvin analogs as FECH inhibitors. FECH is also a common off-target of kinase inhibitor cancer drugs (Klaeger et al., 2016). Of course these agents have other major biological targets making them poor models for developing FECH inhibitors. To our knowledge, no screening efforts to find drug-like FECH inhibitors have been published before. The need for useful, specific FECH inhibitors has been highlighted by a growing body of work implicating this protein in disease.

We identified FECH as a mediator of ocular neovascularization (Basavarajappa et al., 2017). Neovascularization is a key pathological determinant of several major, blinding eye diseases such as neovascular age-related macular degeneration (AMD), proliferative diabetic retinopathy (PDR), and retinopathy of prematurity (ROP). Neovascularization at the back of the eye is divided into choroidal neovascularization (neovascular AMD) and retinal neovascularization (PDR and ROP). FECH is upregulated in both human and murine eyes undergoing choroidal neovascularization (Basavarajappa et al., 2017). Moreover, knockdown or mutation of FECH blocks angiogenesis *in vitro* and *in vivo* (Basavarajappa et al., 2017). *In vitro*, both NMPP and griseofulvin selectively block endothelial cell growth without causing cell death. *In vivo*, oral or intravitreal (into the eye) griseofulvin reduces choroidal neovascularization (Basavarajappa et al., 2017). FECH is also upregulated in mouse eyes undergoing oxygen-induced retinopathy, a model of retinal neovascularization. Both griseofulvin and NMPP, delivered intravitreally, are effective therapies in this model (Pran Babu et al., 2020). A partial loss-of-function *Fech* mutant mouse

(Tutois et al., 1991) also displayed reduced choroidal (Basavarajappa et al., 2017) and retinal neovascularization (Pran Babu et al., 2020).

Depletion of the heme cofactor needed for the function of proangiogenic signaling proteins like mitochondrial Complex IV and endothelial nitric oxide synthase appears to be a key mechanism for the antiangiogenic effects of FECH inhibition (Basavarajappa et al., 2017; Shetty et al., 2020), although this is still an active area of investigation. Development of FECH-targeting small molecules will be helpful in these ongoing studies. Moreover, FECH inhibitors could provide a new way to target neovascularization therapeutically. They could complement or replace the agents that inhibit vascular endothelial growth factor (VEGF) currently used for neovascular eye diseases. These anti-VEGF drugs are biologics not effective in all patients (Lux et al., 2007), and can be associated with side effects.

Given this appealing potential utility of FECH inhibitors, and the limitations of griseofulvin, NMPP, and indirect methods of FECH inhibition, we sought to identify FECH inhibitors. We undertook a high throughput screen for small molecule FECH inhibition and identified a series of triazolopyrimidinone hits. We then synthesized derivatives of these hit compounds. Some of these perform as well as NMPP in FECH inhibition assays *in vitro*; crystal structures show active site binding and enzyme kinetics analysis confirms competitive inhibition by our lead compound. This compound was an effective antiangiogenic agent *in vivo*. These drug-like FECH inhibitors have promise for further development as tool compounds and therapeutic leads.

## **RESULTS**

### **High-throughput screen identifies FECH inhibitors**

To find FECH inhibitors, a kinetic assay to monitor FECH enzymatic activity was adapted from a published protocol (Burden et al., 1999). Recombinant human FECH activity was established by monitoring the increase of Ni<sup>2+</sup> mesoporphyrin IX reaction product at 550 nm over time (Figure 1A; Figure S1). Optimization of the high-throughput screen gave a  $Z'$  > 0.5 across multiple replicate assays, where the positive control was FECH activity inhibited by NMPP and the negative control was FECH activity with DMSO vehicle alone. A high  $Z'$  indicates a high-quality assay with low likelihood of false positives and negatives in the screen.

We screened 20,231 compounds in the initial screen (Figure 1B,C). Because each plate had both negative (uninhibited FECH activity) and positive (NMPP) controls, and there was considerable variability between plates, we established a hit on a given plate as a reduction > 3 standard deviations from the average activity of the negative control (100% activity) for each plate. Using this metric, 662 (3.3%) of the compounds tested in the initial screen were designated hits (Figure 1B). We selected these compounds for secondary screening.

Secondary screening with these hits was run identically to the initial screen. However, hits were defined in the secondary screen by their percent inhibition of FECH activity (the average of the activity from two plates compared to activity with the DMSO negative control wells set as 100%) (Figure 1D). The 93 compounds (0.5%) that inhibited FECH activity by 50% or more in this secondary screen were subjected to further scrutiny. Two were removed after pan-assay interference compound assessment (Baell and Holloway, 2010). Intriguingly, the 91 remaining 'hit' compounds from the secondary screen (0.5% of the initial screen) included a remarkable 62 triazolopyrimidinones (Supplemental Dataset S1). Twenty-one drug-like compounds selected to represent the diversity of the hits, including 18 triazolopyrimidinones (Table S1; Figure 1F), were reordered for dose-response testing.

### **Dose response assays confirm triazolopyrimidinone activity against FECH and in cells**

Ten of the eighteen triazolopyrimidinones tested had an  $IC_{50}$  value in the low micromolar range with eight in the mid- to high nanomolar range (Table S1), indicating potent FECH inhibition, comparable to NMPP ( $IC_{50} = 450$  nM in our assay). Figure 1E shows the  $IC_{50}$  curves of two of these potent FECH inhibitors along with NMPP as a positive control.

To assess the potential disease-treatment relevance of these hits, we explored what effect these compounds would have on angiogenesis. Since we have established that FECH knockdown and inhibition with NMPP or griseofulvin reduces Human Retinal Endothelial Cell (HREC) proliferation (Basavarajappa et al., 2017), we used this proliferation assay as an initial assessment of the bioactivity of our screening hits. HREC proliferation was inhibited only in the micromolar range (Table S1; Figure 2A), suggesting that further structure-activity relationship (SAR) assessment was needed to find potentially cell-active FECH inhibitors. Additionally, these screening hits have liabilities. For instance, D351-0310, a potent FECH inhibitor, contains an aniline moiety which could cause toxicity by aniline metabolites. Thus, our goal of developing FECH inhibitors based on the triazolopyrimidinone backbone was a balance between potency and promising drug-like properties.

### **Synthetic compounds inhibit recombinant FECH**

To explore the SAR of triazolopyrimidinone inhibition of FECH, we synthesized two series of triazolopyrimidinones, **4** and **5** (Schemes 1 and 2; Tables S2 and S3), focusing on varying the substitution of C2 and C5 positions (Figure S2). First, synthesis of compound series **4** was carried out by the general methodology shown in Scheme 1. Initially, 3-(4-*t*-butylphenyl)-1*H*-1,2,4-triazol-5-amine (**1**) was obtained through condensation of benzoic acid and aminoguanidine bicarbonate, but the yield was poor. To improve the chemical yield, a 4-*t*-butylbenzohydrazide was reacted with *S*-methylisothiourea hemisulfate salt upon heating in water to give the aminoguanidine intermediate. The subsequent cyclization in 10% aqueous NaOH at 100 °C gave the aminotriazole (**1**) in 61% yield. Condensation of **1** with ethyl 3-oxobutanoate and

ethyl 4-chloro-3-oxobutanoate under acidic conditions gave the 5-methyl and 5-chloromethyl triazolopyrimidinones (**2** and **3**), respectively. The 5-chloromethyl triazolopyrimidinone **3** could be converted to the 5-alkylaminomethyl triazolopyrimidinone derivatives (**4a~4h**) by reaction with the requisite amines under basic conditions.

Second, compounds **5a~5x** were prepared in accordance with the procedures shown in Scheme 2. Alkylation of ethyl 2-bromoacetate with the requisite anilines in the presence of K<sub>2</sub>CO<sub>3</sub> led to the formation of **6a~6n**. A series of 6-substituted or 5,6-disubstituted 2,3-diaminopyrimidin-4-ones (**7a~7d**) were provided by condensation of ethyl 3-oxohexanoate or ethyl 2-cyclopentane-1-carboxylate or ethyl 4-methyl-3-oxopentanoate or ethyl 3-oxobutanoate with aminoguanidine bicarbonate (see STAR Methods), followed by the condensation of **7a~7d** with **6a~6n** to afford the 2-arylaminomethyl triazolopyrimidinone derivatives (**5a~5x**). Using the same assay methods as in the high throughput screen, we tested compounds **1**, **2**, **3**, **4a~4h**, and **5a~5x** for FECH inhibition (Tables S2 and S3). Among 5-alkylaminomethyl triazolopyrimidinone derivatives, quinolin-2-yl and 3-chlorophenyl derivatives (**4e** and **4h**) showed inhibitory activity against recombinant FECH. Among 2-arylaminomethyl triazolopyrimidinone derivatives, the tolylamino and chlorophenylamino derivatives (**5a~5f**) having an *n*-propyl group at the C5 position showed better inhibitory activity than other derivatives (**5o~5x**) having methyl, isopropyl, and cyclopentylene groups. As a substituent of the phenyl group at the C2 position, *p*-tolyl and *p*-chlorophenyl derivatives exhibited improved activity rather than *o*- and *m*-substituent ones. However, bulky groups such as *t*-butyl and *n*-pentyl groups hampered the inhibitory activity against FECH, when the additional *n*-propyl derivatives (**5g~5n**) were evaluated. Although 3,4-disubstituted derivatives (**5i** and **5k**) showed the strongest inhibitory activity against recombinant FECH, they did not affect HREC proliferation. A summary of these SAR findings is provided in Figure S2. Several compounds were potent FECH inhibitors *in vitro*, such as **5f**, with two previously undescribed compounds, **4e** (Figure S1) and **5c**, showing IC<sub>50</sub> values in the high nanomolar range. These compounds also had an antiproliferative effect on HRECs (Tables S2 and S3; Figure 2A). While they are not as potent on HRECs as the known FECH inhibitor, NMPP (GI<sub>50</sub> = 30 μM (Basavarajappa et al., 2017)), they do have more drug-like structures amenable to further SAR. The triazolopyrimidinone skeleton is a bioisostere of a purine and also is an N-heterocycle, like the majority of modern new drugs (Vieth et al., 2004), whereas the porphyrin skeleton is uncommon in marketed drugs, and violates Lipinski's Rule of Five (Walters, 2012).

### **FECH inhibitors are effective and antiangiogenic *in vitro***

We have shown that inhibition of FECH by the canonical chemical inhibitor, NMPP, also inhibits angiogenic properties of HRECs beyond proliferation in migration and tube formation assays at single-digit micromolar concentrations (Basavarajappa et al., 2017). We sought to test our small molecule FECH inhibitors to see if they also inhibit angiogenesis *in vitro*. In this initial functional testing, we included two potent triazolopyrimidinones identified as FECH

inhibitors in the initial compound screen to see how they compare to the newly synthesized compounds. In a Matrigel based tube formation assay, which tests the angiogenic properties of HRECs, both screening hits, D351-0310 and D433-1848, blocked the ability of HRECs to form tubes effectively (Figure 2B). Importantly, the two compounds with the best balance of FECH inhibitory activity and HREC antiproliferative activity, **4e** and **5c**, both also blocked tube formation of HRECs (Figure 2B). Compound **4e** demonstrated the most potent antiangiogenic effect of the compounds tested in this assay.

Having demonstrated FECH inhibition in enzymatic assays using recombinant enzyme, we wanted to confirm that our compounds of interest are inhibiting FECH in the disease relevant cell type used in angiogenesis assays. Since FECH inhibition leads to a buildup of its substrate PPIX, assessment of PPIX levels is a facile measure of FECH activity in cells. HRECs co-treated with 5-aminolevulinic acid (5-ALA; to increase heme pathway throughput) had statistically significant PPIX accumulation after treatment with the highest dose of **4e** when compared to the vehicle DMSO (Figure 2C), suggesting an inhibition of heme production. Based on this combination of antiangiogenic activity and PPIX accumulation, **4e** was chosen for further examination.

### **Compound 4e inhibits FECH in HRECs with specificity, without cytotoxic effects**

Compound **4e** blocked the migration ability, another key facet of angiogenesis, of HRECs in a dose dependent manner (Figure 3A). Because FECH inhibition is expected to cause a reduction in hemoproteins (Basavarajappa et al., 2017; Shetty et al., 2020), we probed for hemoprotein COXIV subunit I expression in HRECs treated with known FECH inhibitor NMPP or **4e**. This protein is known to be reduced by NMPP or FECH knockdown. Treatment with **4e** decreased COXIV levels in HRECs in a dose dependent manner (Figure 3B). Two consequences of FECH inhibition are heme depletion and PPIX substrate accumulation. Succinylacetone mediated inhibition of 5-aminolevulinic acid dehydratase (ALAD, an enzyme upstream of FECH in the heme biosynthesis pathway) would decrease available PPIX in the cells. However, succinylacetone in HRECs did not reverse **4e**'s effect on COXIV expression, indicating that this effect is not due to PPIX accumulation in HRECs. But hemin supplementation did ameliorate the effects of **4e** on COXIV expression, indicating that heme depletion is the consequence of FECH inhibition that is causing the observed decrease in COXIV expression. Furthermore, HRECs treated with **4e** with and without treatment with 5-ALA showed a buildup of FECH substrate PPIX as well as a decrease in heme (Figure 3C). This verifies that **4e**-mediated FECH inhibition is taking place in cells and leads to heme reduction. Before testing **4e** in vivo, we wanted to rule out non-specific cytotoxic effects by testing the compound for antiproliferative effects on another normal ocular cell type from the retina. We chose ARPE19, a cell line derived from human retinal pigmented epithelial cells, in which FECH knockdown, NMPP, or griseofulvin treatment did not block proliferation (Basavarajappa et al., 2017). **4e** did not have a substantial antiproliferative effect on ARPE19 cells (Figure 3D), increasing confidence that

this compound would not have any deleterious effects on normal ocular tissue. We further tested **4e** and NMPP on an induced pluripotent stem cell-derived choroidal endothelial cell line, iCEC2 (Voigt et al., 2019), particularly relevant to the choroidal neovascularization seen in neovascular AMD. Compound **4e** was more potent than NMPP in blocking the proliferation of these cells (Figure 3D). Additionally, to confirm that **4e** was antiproliferative and not cell lethal, we stained **4e** treated HRECs for cleaved caspase-3 and ran a terminal deoxynucleotidyl transferase dUTP nick end labeling (TUNEL) assay to test for apoptosis. Treatment with **4e** did not lead to apoptosis in HRECs by either method of detection (Figure 3E).

### Inhibitors bind to FECH in the active site

X-ray structures of FECH complexed with potent in vitro inhibitors **4e** and **5f** were solved at a resolution of 2.0 Å (Figure 4, Table S4). In the asymmetric unit, there are two FECH molecules which form a dimer.

Three sandwich-like hydrophobic interactions between **4e** and FECH stabilize the FECH–**4e** complex (Figure 4A). The quinoline ring of **4e** is located between H263 and T198 of FECH to make the H263/quinoline(**4e**)/T198 hydrophobic interaction. Similarly, the triazolopyrimidinone ring of **4e** makes another W310/triazolopyrimidinone(**4e**)/L98 interaction, and the third V305/phenyl(**4e**)/M99 interaction assists the stabilization of FECH–**4e** complex at the substrate entrance site of FECH.

Similar to the FECH–**4e** complex, there are two sandwich-like hydrophobic interactions between FECH and **5f** (Figure 4B). The phenyl ring of **5f** is located between H263 and T198 of FECH to make the H263/phenyl(**5f**)/T198 interaction, and the triazolopyrimidinone of **5f** makes the W310/triazolopyrimidinone(**5f**)/L98 interaction. The chlorine atom of the chlorophenyl in **5f** contributes to the stabilization of the complex via a bound water bridged hydrogen bond. The bound water O3 near the chlorine atom is connected to A336 and N193 of FECH by hydrogen bonds and is hydrogen-bonded again to the chlorine atom of **5f**. Although **4e** and **5f** share a common triazolopyrimidinone ring in the middle of the molecules, the binding direction of the molecules to FECH is opposite to each other. The binding pocket of **4e** and **5f** in FECH is a part of the PPIX binding site (Figure 4C).

In the X-ray cocrystal structure, the quinoline in position C5 of the triazolopyrimidinone in **4e** is placed inside the binding pocket of FECH, and the *p*-chloro-phenylaminomethyl in position C2 of **5f** is placed inside the binding pocket. Thus, in 4-series analogs, the binding force is interpreted to be affected by the *N*-substituent at position C5, and in contrast, the effect of the 4-(*tert*-butyl)-phenyl placed in the solvent part appears to be small. In 5-series analogs, the binding force is shown to vary greatly depending on the *o*-, *m*-, and *p*-substituents of the phenyl in position 2. Therefore, the 3D structure provides information consistent with the in vitro SAR for FECH inhibition (Figure S2).



Given this active site binding, to investigate the mode of inhibition, we studied the kinetics of FECH inhibition by our lead compound, **4e**. Concentrations of the FECH assay substrate (mesoporphyrin IX) and FECH inhibitor **4e** were varied. The  $V_{max}$  of the reaction stayed consistent for each concentration of **4e** tested as the  $K_M$  increased. This indicates competitive inhibition of **4e** for the substrate mesoporphyrin (Figure 4D). This mode of inhibition is consistent with the cocrystal structure that shows **4e** binding to the active site of the enzyme.

### **Intravitreal injections of FECH inhibitor 4e decreased neovascularization in vivo**

With a validated FECH inhibitor in hand, we sought to assess therapeutic efficacy. The murine laser-induced choroidal neovascularization (L-CNV) model is widely used for assessing the antiangiogenic potential of small molecules for ocular indications (Grossniklaus et al., 2010). We previously showed that FECH inhibition via mutation, knockdown, and treatment with chemical inhibitors were all associated with reduced neovascularization in this L-CNV model (Basavarajappa et al., 2017). Above, we established that **4e** was antiproliferative in a choroidal endothelial cell line (Figure 3D). We therefore assessed intravitreal injection of our small molecule inhibitor **4e** in the L-CNV model (Figure 5A). To assess lesion volume and leakage, optical coherence tomography (OCT) and fluorescein angiography (FA) were performed. On day 7, OCT images of each lesion were taken (Figure 5B). On day 14, OCT was repeated along with FA (Figure 5A,B). Qualitatively, leakage on FA was smaller in **4e** treated eyes. OCT lesion volume was significantly reduced relative to control by final intravitreal concentrations of 50  $\mu\text{M}$  **4e** as well as 100  $\mu\text{M}$  **4e** (Figure 5C). This volumetric reduction was confirmed by staining choroidal flat mounts for vasculature markers agglutinin and *Griffonia simplicifolia* isolectin B4 (GS-IB4) (Figure 5D). Lesions in vehicle-treated eyes showed a typical L-CNV morphology. However, stained neovascular areas were dramatically smaller, and often barely identifiable, in **4e** treated eyes at both doses. Quantification of lesions based on both agglutinin and GS-IB4 signal revealed a profound decrease in lesion volume of >50% at both tested **4e** doses (Figure 5E,F).

To monitor for potential toxicity during the in vivo experiment, fundus images were taken on day 0, day 7, and day 14 after laser induction in each experimental group. Lesions were visible at the locations of laser induction on days 7 and 14. However, no obvious signs of toxicity were observed in fundi treated with **4e** (Figure 5A), nor did the compound induce changes in OCT retinal images outside CNV lesion areas (Figure 5B). To further support this, a SafetyScan off-target analysis of 78 GPCRs, ion channels, kinases, transporters and other enzymes only showed effects <100  $\mu\text{M}$  against dopamine D2 receptor DRD2S (agonist,  $EC_{50}$  = 98  $\mu\text{M}$ ) and  $\delta$  opioid receptor OPRD1 (agonist,  $EC_{50}$  = 0.47  $\mu\text{M}$ ) (Table S5).

## DISCUSSION

The enzyme FECH has significant promise for therapeutic targeting in multiple diseases but lacks good direct inhibitors. We undertook a high-throughput screen to find FECH inhibitors. There was a striking over-representation of triazolopyrimidinones amongst our screening hits, suggesting that this scaffold might have potential as the basis of FECH inhibitors. We followed up with SAR studies to optimize inhibition and developed several triazolopyrimidinone compounds that were largely good inhibitors of FECH activity. FECH inhibition was confirmed with the accumulation of PPIX, the FECH substrate, and reduction of heme, the FECH product, in cells treated with small molecule inhibitors. A consequence of FECH inhibition is the depletion of heme containing proteins. We observed a reduction in one of these (COXIV subunit I) in treated retinal endothelial cells. When the heme depletion in these cells was rescued by adding hemin to the culture media, the reduction in COXIV expression was ameliorated.

We tested these compounds' abilities to inhibit angiogenesis in three in vitro assays. The proliferation of human retinal or choroidal microvascular endothelial cells is a key step in ocular angiogenesis. Of the newly synthesized compounds we identified as FECH inhibitors, **4e** and **5c** were also anti-proliferative. Some compounds active against recombinant FECH did not have good antiproliferative activity, likely due to permeability issues; this warrants further optimization in future. However, compound **4e** also inhibited migration and tube formation in a dose dependent manner, without inducing apoptosis in HRECs or affecting the proliferation of the non-endothelial ocular cell line ARPE19. This efficacy translated to an in vivo model of choroidal neovascularization, with no obvious signs of toxicity in the fundus and OCT images. A more rigorous toxicity study of **4e** is warranted before developing this compound further.

FECH inhibitors based on a drug-like scaffold are appealing. Amongst our screening hits, the preponderance of triazolopyrimidinones is striking. The triazolopyrimidine scaffold such as [1,2,4]triazolo[1,5-a]pyrimidin-7(4*H*)-one is one of the most attractive [5,6]-bicyclic heterocycles. Several natural and synthetic triazolopyrimidine derivatives are known. For instance, the triazolopyrimidine natural product essramycin was isolated from *Streptomyces* species (El-Gendy et al., 2008). Essramycin and its analogs possess antibacterial activity as well as cytotoxicity (Wang et al., 2020). However, association with FECH has not been reported for this compound class previously.

Of compounds assessed for X-ray co-crystal structure determination, compounds **4e** and **5f** showed interpretable electron densities at the inhibitor binding site. Generally hydrogen bonding between a protein and inhibitor provides a directionality and specificity of interaction that is a fundamental aspect of molecular recognition (Hubbard and Kamran Haider, 2010). Though direct hydrogen bonds between FECH and the inhibitors were not found, three extensive hydrophobic interactions of **4e**, and one water bridged hydrogen bond

as well as two hydrophobic interactions of **5f** held the molecules and enabled us to get clear electron densities of the inhibitors. The interaction surfaces between FECH and **4e** and between FECH and **5f** were 415 Å and 325 Å, respectively, whereas that between FECH and its endogenous substrate PPIX was 517 Å. Therefore, the interaction sites of **4e** and **5f** with FECH are limited to just a partial area of the PPIX binding pocket of the enzyme. The complex structure of FECH–PPIX revealed that some hydrophobic residues at L92, L98, T198, V305, Y276, and W310 of FECH contact PPIX (Medlock et al., 2007). Our FECH-inhibitor structures also showed similar hydrophobic interactions between FECH and inhibitors: L92, L98, W310 in **5f** and L92, L98, V305, W310 in **4e**, respectively. In the FECH-PPIX complex structure, the conserved  $\pi$ -helix (residues 340-349) is unwound whereas the  $\pi$ -helix of FECH–inhibitor structures is in a well folded state which is quite similar to the wild type FECH structure without PPIX.

One potential liability of FECH inhibition as a therapeutic approach is the risk of protoporphyria. Erythropoietic protoporphyria (EPP) is caused by partial loss-of-function mutations in *FECH* (Lecha et al., 2009). This disease is characterized by cutaneous photosensitivity and in rare cases hepatotoxicity due to buildup of PPIX, which is a photosensitizer. In mice, complete loss of *Fech* is embryonic lethal, since some heme synthesis is presumedly essential for cellular function (Magness et al., 2002). But it appears that FECH activity is titratable: in our prior studies (Basavarajappa et al., 2017) with the *Fech*<sup>m1Pas</sup> partial loss-of-function mutant mouse (Tutois et al., 1991), heterozygotes had reduced L-CNV, but with ~50% FECH activity are otherwise phenotypically normal. The eyes of *Fech*<sup>m1Pas</sup> mice, even homozygotes, are normal in the absence of neovascular stimulus (Sardar Pasha et al., 2021). And griseofulvin, metabolized into the FECH inhibitor NMPP (Liu et al., 2015), is well-tolerated in most patients, even during high-dose, months-long therapy (Bennett et al., 2000). Careful dose-finding to avoid side effects with a potential FECH-targeting drug should therefore be possible. Direct delivery to the eye for neovascular eye diseases (as is done for the standard of care) further mitigates the risk of systemic side effects. Inhibition of glycine transporters GlyT1 and GlyT2 by available small molecules could also decrease PPIX accumulation after FECH inhibition (Halloy et al., 2021). Moreover, compound **4e** did not induce obvious cellular or ocular toxicity and did not have pronounced effects on off-target proteins. Agonism of the  $\delta$  opioid receptor (OPRD1) was the only sub-micromolar positive signal with **4e** in our SafetyScan analysis. One liability of  $\delta$  agonists (developed for pain and depression therapy) is risk of respiratory depression or seizures, but this does not appear to be a class effect (Peppin and Raffa, 2015). Again, local delivery of a compound like **4e** would largely mitigate any such risks. Indeed,  $\delta$  agonists are neuroprotective in the eye (Husain, 2018), although are not known to have antiangiogenic activity (Yamamizu et al., 2013). Moreover, OPRD1 expression is very low in the ocular vasculature (Voigt et al., 2020), suggesting that any effect of **4e** on the  $\delta$  receptor does not contribute to its antiangiogenic effect.

FECH inhibitors have potential therapeutic applications that reach beyond angiogenesis. These compounds could also be developed to treat malaria as

FECH plays an interesting role in the disease (Lelliott et al., 2015). Although the pathogenic *Plasmodium* species have their own *FECH* gene, it is dispensable (Nagaraj et al., 2013); the parasites are seemingly reliant on the host erythrocyte FECH. Thus, *Fech* mutant mice (characterized by reduced FECH activity) are resistant to plasmodium infection, and the erythrocytes of EPP patients, who are FECH deficient, poorly support *Plasmodium* growth (Smith et al., 2015). Moreover, NMPP blocks parasite growth in vitro (Smith et al., 2015), with griseofulvin having a similar effect (Smith et al., 2017). The blood of griseofulvin-treated patients also shows reduced *Plasmodium* growth (Smith et al., 2017). New treatments are sorely needed for this mosquito-borne parasitic disease, and host proteins are intriguing targets. Therefore, new ways of blocking FECH could have utility in treating malaria as well.

Finally, FECH inhibition may find utility in cancer treatment. One mode of photodynamic therapy (PDT) and photodynamic diagnosis (PDD) can benefit from FECH inhibition. Dosing patients with the first compound in the heme biosynthesis pathway, 5-ALA, leads to buildup of the phototoxic PPIX, especially in certain cancer types with already-low FECH activity, such as glioblastoma (Yang et al., 2015b). Given that FECH converts PPIX into heme, blockade of FECH can potentiate this process, enhancing PDT/PDD effect. This has been shown in multiple systems. Glioma (Teng et al., 2011), breast carcinoma (Yang et al., 2015a), and urothelial carcinoma (Miyake et al., 2009) cells with *FECH* knockdown showed enhanced 5-ALA-mediated PDT, and colon cancer cells showed increased PPIX (Kemmner et al., 2008). Griseofulvin enhanced ALA-PDT in osteosarcoma and an oral squamous cell carcinoma cell line (Nomura et al., 2006). In urothelial carcinoma cells and an animal model, using the iron chelator deferoxamine to indirectly block FECH function (by removing one of its substrates) led to enhanced PDT (Inoue et al., 2013). Similar effects were seen in prostate cancer models (Fukuhara et al., 2013), histiocytic lymphoma (Amo et al., 2009), and gastric cancer (Tan et al., 1997). And in mouse cutaneous tumors, blockade of FECH with  $Pb^{2+}$  (which interferes with normal,  $Fe^{2+}$  metalation of PPIX) enhanced PPIX buildup and phototoxicity (Bhasin et al., 2002). Most recently, work was published suggesting that a combination of MEK inhibition and FECH inhibition could significantly enhance the efficacy of PDT/PDD in a number of human cancers (Chelakkot et al., 2020).

In summary, we have identified and developed a class of more drug-like, non-porphyrin, small molecule FECH competitive inhibitors. These compounds have good in vitro and in vivo efficacy and bind directly to the enzyme. Our early SAR studies of triazolopyrimidinones for FECH inhibitory activity and X-ray co-crystallography with FECH will allow future structural optimization for the development of a promising lead compound for neovascular eye disease therapy. For instance, the introduction of various further *N*-aryl substituents at the C2 or C5 position is appealing. Because FECH activity has relevance to multiple disease states, the scope for therapeutic use of FECH inhibitors is expansive. These compounds provide a starting point for exploring this understudied area.

## **SIGNIFICANCE**

Ferrochelatase (FECH) is the final enzyme in heme biosynthesis. FECH is a key mediator of various disease processes, including ocular neovascular diseases, host response to malaria, and efficacy of photodynamic therapy. However, no drug-like direct FECH inhibitors are available for research and potential therapeutic development. Here we outline the hunt for and synthesis of small molecule inhibitors of FECH activity. Hit compounds bind to the active site of the enzyme, reduce heme-containing protein expression, and inhibit FECH activity in cells. Moreover, they show anti-angiogenic effects on endothelial cells in vitro and they inhibit ocular neovascularization in vivo. These inhibitors are valuable tools and emblematic of the therapeutic potential of small molecule FECH inhibitors for multiple diseases.

## **ACKNOWLEDGMENTS**

This work was supported by NIH/NEI R01EY025641 (T.W.C.), BrightFocus Foundation Macular Degeneration Research grant M2019069 (T.W.C.), National Research Foundation (S. Korea) grants 2017M3A9C8027781 and 2020R1A6A1A03043708 (S.-Y.S.) and 2011-0017405 (S.J.L.), a Challenge Grant from Research to Prevent Blindness, and the Indiana Clinical and Translational Sciences Institute funded, in part by NIH/NCATS UL1TR002529 (T.W.C.). N.O. was supported by NIH RISE Grant 5R25GM060566. This work was supported by the Chemical Genomics Core Facility (CGCF) at Indiana University School of Medicine and the Iron and Heme Core facility at the University of Utah, supported in part by NIH/NIDDK U54DK110858. The content is solely the responsibility of the authors and does not necessarily represent the official views of the National Institutes of Health.

## **AUTHOR CONTRIBUTIONS**

Conceptualization, S.J.L., S.-Y.S. and T.W.C.; Investigation, K.S., N.L.-C., B.L., D.H.H., J.P., S.P.B.S.P., S.L., S.K., A.M., B.P., N.O. and S.W.; Formal Analysis and Visualization, K.S., N.L.-C., B.L., S.P.B.S.P., S.L., S.K., N.O., and S.W.; Writing – Original Draft, K.S.; Writing – Review & Editing, K.S., N.L.-C., B.L., D.H.H., J.P., S.P.B.S.P., S.L., S.K., A.M., B.P., N.O., S.W., I.Y.P., S.J.L., S.-Y.S. and T.W.C.; Funding Acquisition, S.J.L., S.-Y.S. and T.W.C.

## **DECLARATION OF INTERESTS**

K.S., B.L., S.P.B., S.-Y.S., and T.W.C. are named inventors on patent applications related to this work. The other authors declare no competing interests.

## **INCLUSION AND DIVERSITY STATEMENT**

One or more of the authors of this paper self-identifies as an underrepresented ethnic minority in science. One or more of the authors of this

paper received support from a program designed to increase minority representation in science.

## FIGURE & SCHEME LEGENDS

### Figure 1. High-throughput screen identifies FECH inhibitors.

(A)  $Z'$  determination using 10  $\mu$ M NMPP (blue squares) or DMSO vehicle (red circles) indicates the signal-noise ratio for the FECH activity assay; 3 SD (dotted lines) around the mean (solid lines) for each treatment shown.  $Z'$  in this experiment was 0.73 ( $n = 192$  wells/treatment) with  $t=20$  min.

(B) Workflow for the high-throughput FECH screen. Number of compounds (% of the starting number) passing each stage is indicated.

(C) Compounds (20,231) from two small molecule libraries tested at 10  $\mu$ M. Only compounds that reduced FECH activity by 3 SD below FECH activity with DMSO alone (plate by plate) were tested further.

(D) Secondary screen results. Of 662 compounds tested at 10  $\mu$ M, hits were selected as those inhibiting activity by >50% (red zone) compared to DMSO control (mean $\pm$ SD, green zone). 93 compounds were selected as hits from this screen.

(E)  $IC_{50}$  curves with known FECH inhibitor NMPP (red), two triazolopyrimidinone hit compounds D433-1848 (orange) and D381-0310 (purple) and newly synthesized FECH inhibitor **4e** (blue). Mean $\pm$ SEM,  $n=3$  technical replicates. Representative data from 3 biological replicates.

(F) Selected hit compounds validated in  $IC_{50}$  assays.

See also Figure S1, Table S1, and Supplemental Dataset S1.

### Figure 2. FECH inhibitors are effective and antiangiogenic in vitro.

(A) FECH inhibitors show antiproliferative effects on human retinal endothelial cells (HRECs). 48 hour treatment. Mean $\pm$ SEM,  $n=3$  technical replicates. Representative data from 3 biological replicates.

(B) Triazolopyrimidinones dose-dependently block tube formation by HRECs. Images of HREC tube formation with DMSO control or highest tested concentration of compound. 8 hour treatment. Mean $\pm$ SEM,  $n=6$  technical replicates. Scale bar: 750  $\mu$ m. \*,  $p<0.05$ ; \*\*,  $p<0.01$ ; \*\*\*,  $p<0.001$  vs. DMSO control, ANOVA with Dunnett's post hoc tests. Representative data from 3 biological replicates.

(C) PPIX accumulation in HRECs after treatment with a known FECH inhibitor (10  $\mu$ M NMPP), or with screening hits and synthetic compounds. 3 hour treatment. Mean $\pm$ SEM,  $n=3$  technical replicates. \*,  $p<0.05$ ; \*\*,  $p<0.01$ ; \*\*\*,  $p<0.001$  vs. DMSO control, ANOVA with Dunnett's post hoc tests. Representative data from at least 2 biological replicates.

See also Tables S1–S3.

**Figure 3. Compound 4e inhibits FECH in HRECs with specificity, without cytotoxic effects.**

(A) Compound **4e** inhibited HREC migration in a dose dependent manner. 8 hour treatment. Mean±SEM, n=4 technical replicates. Scale bar: 250 μm. \*\*\*, p<0.001 vs. DMSO control, ANOVA with Dunnett's post hoc tests. Representative data from 3 biological replicates.

(B) Hemoprotein COX IV subunit I expression in HRECs treated with **4e** decreased in a dose dependent manner when exposed to FECH inhibitors for 16 hours. Hemin treatment (10 μM for 6 hours) rescued expression while succinylacetone (SA) treatment (100 μM for 6 hours) did not restore COXIV expression to more normal levels. Mean±SEM, n=3 biological replicates.

(C) PPIX and heme buildup in HRECs treated with 30 μM **4e** ± 1 mM 5-ALA. Mean±SEM, n=3 replicates. \*\*\*, p<0.001 vs. DMSO control, unpaired t-test.

(D) FECH inhibitors **4e** and NMPP are antiproliferative on iCEC2 choroidal endothelial cells, but neither canonical FECH inhibitor NMPP nor **4e** shows an antiproliferative effect on ARPE19 human retinal epithelial cell line. 48 hour treatment. Mean±SEM, n=3 technical replicates. Representative data from 3 biological replicates. NMPP ARPE19 data are reproduced from Basavarajappa et al., 2017.

(E) **4e** does not cause apoptosis in HRECs as shown by cleaved caspase-3 staining and a TUNEL assay (red); nuclei are stained with Hoechst 33342 (blue). 16 hour treatment. Mean±SEM, n=3 technical replicates. Scale bar: 100 μm. SP, staurosporine positive control. Representative data from 3 biological replicates.

**Figure 4. Inhibitors bind to FECH and 4e is a competitive inhibitor of FECH.**

Details of the interaction site in FECH-inhibitor complex structures. The 2Fo-Fc maps of **4e** and **5f** are shown at the 1.0 σ level. Enzyme kinetic studies with **4e** indicate that the small molecule is a competitive inhibitor.

(A) Amino acid residues involved in three hydrophobic interactions in FECH-**4e** (pink) complex structure are represented in the ball-and-stick model. [2Fe-2S] cluster depicted as spheres.

(B) A water (red sphere) bridged hydrogen bond between FECH and **5f** (red) are represented as black lines and amino acids involved in two hydrophobic interactions are shown as ball-and-stick models.

(C) Comparison of binding patterns of three chemicals, PPIX (green), **4e** (pink), and **5f** (red) at their binding pocket in FECH drawn transparently as a surface model.

(D) Michaelis-Menten kinetic analysis of **4e** inhibition of recombinant FECH. Mean±SEM, n=6 technical replicates. Representative data from 2 biological replicates.

See also Table S4.

**Figure 5. Intravitreal injections of FECH inhibitor 4e decreased neovascularization in vivo.**

(A) Fundus and fluorescein angiography (FA) images of mice with L-CNV treated

as indicated, imaged on day 7 and day 14 after laser. Red lines indicate cross sections for optical coherence tomography (OCT) images that were taken concurrently.

(B) OCT images of mice with L-CNV treated as indicated, imaged on day 7 and day 14 after laser. Scale bars: 100  $\mu\text{m}$ .

(C) Quantification of lesion volume on day 14 using OCT images. Individual lesions plotted, Mean $\pm$ SEM, n=10-16 eyes/treatment. \*, p<0.05; \*\*, p<0.01 vs. DMSO control, ANOVA with Dunnett's post-hoc tests.

(D) Ex vivo analysis of neovascular lesions stained with both agglutinin (red) and *Griffonia simplicifolia* isolectin B4 (GS-IB4) (green). Scale bars: 100  $\mu\text{m}$ .

(E & F) Quantification of (E) agglutinin-stained and (F) GS-IB4-stained lesion volume. Individual lesions plotted, Mean $\pm$ SEM, n=12-15 eyes/treatment. \*\*\*\*, p<0.0001 vs. DMSO control, ANOVA with Dunnett's post hoc tests.

See also Table S5.

### **Scheme 1. Synthesis of 2-(4-*tert*-butylphenyl)-5-(dialkylaminomethyl)-[1,2,4]triazolo[1,5-a]pyrimidin-7(4*H*)-one derivatives.**

**Reagents and conditions:** a) SOCl<sub>2</sub>, CH<sub>2</sub>Cl<sub>2</sub>, then aminoguanidine bicarbonate, reflux, 12%; b) S-methylisothiurea hemisulfate, NaOH, H<sub>2</sub>O, reflux, 61%; c) ethyl 3-oxobutanoate, *p*-TsOH, 48%; d) ethyl 4-chloro-3-oxobutanoate, AcOH, 80 °C, 74%; e) R<sub>1</sub>R<sub>2</sub>NH, NaH, DMA or DMF, 10%~40%; f) R<sub>1</sub>R<sub>2</sub>NH, NaOtBu, NaI, DMF, 40% for **4e**.

See also STAR Methods and Figure S2.

### **Scheme 2. Synthesis of 2-(arylaminomethyl)-[1,2,4]triazolo[1,5-a]pyrimidin-7(4*H*)-one derivatives.**

**Reagents and conditions:** a) ethyl 2-bromoacetate, K<sub>2</sub>CO<sub>3</sub>, acetone, 19%~99%; b) NaOEt, EtOH, reflux, ethyl 3-oxohexanoate (for **7a**) or ethyl 2-cyclopentane-1-carboxylate (for **7b**) or ethyl 4-methyl-3-oxopentanoate (for **7c**) or ethyl 3-oxobutanoate (for **7d**), 10%~21%; c) **6a**~**6n**, NaOEt, EtOH, 90 °C, 7%~69%.

See also STAR Methods and Figure S2.



## STAR Methods

### RESOURCE AVAILABILITY

#### *Lead Contact*

Further information and requests for resources and reagents should be directed to and will be fulfilled by the Lead Contact, Timothy W. Corson (tcorson@iu.edu).

#### *Materials Availability*

There are restrictions to the availability of synthetic compounds due to the lack of an external centralized repository for their distribution and our need to maintain the stock. We are glad to share compounds with reasonable compensation by requestor for its processing and shipping and completion of a Materials Transfer Agreement.

#### *Data and Code Availability*

The high-throughput screening data generated during this study is available at PubChem (BioAssay ID 1671448). The atomic coordinates for the R115L FECH-**4e** and FECH-**5f** complex structures are available in the Protein Data Bank (PDB ID 7CTC, 7CT7). This paper does not report original code. Any additional information required to reanalyze the data reported in this paper is available from the lead contact upon request.

### EXPERIMENTAL MODEL AND SUBJECT DETAILS

#### *Microbial strain*

For high-throughput screening, the human *FECH* expression plasmid pHisTF20E was obtained in JM109 *Escherichia coli* cells from the Dailey Lab (University of Georgia) (Burden et al., 1999). The cells were grown in Circlegrow® medium (MP Biomedicals, Irvine, CA, USA, Cat. No. #3000-122) with 100 µg/mL ampicillin for 20 hours at 30°C without induction. For protein crystallography, the R115L mutant of human FECH (residues 61-423) was cloned into the *Bam* HI and *Xho* I sites of pET-28a by Bionics (Seoul, South Korea) and was introduced into *E. coli* strain BL21(DE3) (Invitrogen, Seoul, South Korea). The R115L mutant was used because it has superior stability but with wild-type kinetics (Najahi-Missaoui and Dailey, 2005). The transformants containing the target plasmid were grown in Circlegrow® medium with 50 mg/mL kanamycin at 37°C.

#### *Cell culture*

Human primary retinal microvascular endothelial cells (HRECs) and Attachment Factor were purchased from Cell Systems (Kirkland, WA, USA). Female HRECs were grown in endothelial growth medium (EGM-2) and used between passages 4 and 8. EGM-2 was prepared by combining components of an EGM-2 “bullet kit” (Cat No. CC-4176) and endothelial basal medium (EBM, Lonza, Walkersville, MD, USA; Cat No. CC-3156). As primary cells, these were not subject to authentication. ARPE-19 male human retinal pigment epithelial

cells were obtained from ATCC (Manassas, VA, USA) and grown in a 50:50 mix of DMEM and Ham's-F12 growth medium (Thermo Scientific, Waltham, MA, USA) supplemented with 10% fetal bovine serum (FBS, Gibco Labs, Gaithersburg, MD, USA; Cat. No.10437-028). These cells were not authenticated after receipt from the supplier but were replenished annually. iCEC2 cells were a kind gift from Dr. Mullins at the University of Iowa (Voigt et al., 2019) and cultured in Endothelial Cell Growth Medium (R&D Systems, Minneapolis, MN; Cat. No. CCM027). All cells were grown at 37°C (30°C for iCEC2 maintenance stocks), 5% CO<sub>2</sub>, 100% humidity and tested for mycoplasma contamination regularly.

### *Animals*

All mouse experiments were approved by the Institutional Animal Care and Use Committee, Indiana University School of Medicine and followed the guidelines of the Association for Research in Vision and Ophthalmology (ARVO) Statement for the Use of Animals in Ophthalmic and Visual Research. Wild-type, treatment naïve, female C57BL/6J mice, 7–8 weeks of age were purchased from Jackson Laboratory (Bar Harbor, ME) and the mice were housed under standard conditions (Wenzel et al., 2015) in the Indiana University Laboratory Animal Resource Center (LARC). Mice were randomly assigned to treatment, and masked investigators analyzed all quantitative data.

## **METHOD DETAILS**

### *Compound synthesis*

**General methods and materials.** All starting materials and reagents were obtained from commercial suppliers and were used without further purification. Air and moisture sensitive reactions were performed under an argon atmosphere. Flash column chromatography was performed using silica gel 60 (230-400 mesh, Merck, Darmstadt, Germany) with the indicated solvents. Thin-layer chromatography was performed using 0.25 mm silica gel plates (Merck). <sup>1</sup>H and <sup>13</sup>C NMR spectra were recorded on a Bruker 600 MHz spectrometer as solutions in chloroform-d or dimethylsulfoxide-d<sub>6</sub> or methanol-d<sub>4</sub>. <sup>1</sup>H NMR data were reported in the order of chemical shift, multiplicity (s, singlet; d, doublet; t, triplet; m, multiplet and/or multiple resonances), number of protons, and coupling constant (*J*) in hertz (Hz). High-resolution mass spectra (HRMS) were recorded on a JEOL JMS-700 (FAB and EI) and an Agilent 6530 Q-TOF LC/MS/MS system (ESI).

**3-(4-(*tert*-Butyl)phenyl)-1H-1,2,4-triazol-5-amine (1).** Method A: To a solution of 4-*tert*-butylbenzoic acid (600 mg, 3.36 mmol) in CH<sub>2</sub>Cl<sub>2</sub> (5 mL) was added SOCl<sub>2</sub> (2 mL) with stirring and placed in an ice bath. After stirring for 2 h at 60 °C, the mixture was cooled to RT. The solvent was removed under reduced pressure. To the mixture was added toluene (2 mL) and aminoguanidine bicarbonate (460 mg, 3.38 mmol). After refluxing for 24 h, the mixture was cooled to RT. The reaction mixture was filtered and then the precipitates were purified by flash column chromatography on silica gel (MeOH / CH<sub>2</sub>Cl<sub>2</sub> = 1 : 10 ) to afford compound (**1**) (90 mg, 12%). Method B: A solution of *S*-methylisothiourea hemisulfate (5.56 g,

20 mmol), 4-(*tert*-butyl)benzohydrazide (3.84 g, 20 mmol), and water (15 mL) was refluxed for 15 h. The solvent was concentrated under reduced pressure and the residue was washed with ethanol (3 x 10 mL). The resulting solid was poured into 50 mL of 10% NaOH and heated to reflux for additional 6 h. The reaction was cooled to room temperature and adjusted to pH 5 using 1N HCl. The precipitate was filtered, washed with cold water and dried to afford 3-(4-(*tert*-butyl)phenyl)-1*H*-1,2,4-triazol-5-amine (**1**) (2.62 g, 61%). <sup>1</sup>H NMR (600 MHz, CDCl<sub>3</sub>) δ 7.70 (d, 2H, *J* = 9 Hz), 7.24 (d, 2H, *J* = 8.4 Hz), 1.17 (s, 9H); <sup>13</sup>C{<sup>1</sup>H} NMR (150 MHz, CDCl<sub>3</sub>) δ 159.6, 157.4, 153.0, 126.2, 126.0, 125.7, 34.7, 31.2; HRMS (ESI) *m/z*: [M+H]<sup>+</sup> Calcd for C<sub>12</sub>H<sub>16</sub>N<sub>4</sub>, 217.1448; found, 217.1447.

**2-(4-(*tert*-Butyl)phenyl)-5-methyl-[1,2,4]triazolo[1,5-*a*]pyrimidin-7(4*H*)-one (2).** A mixture of 3-(4-(*tert*-butyl)phenyl)-1*H*-1,2,4-triazol-5-amine (**1**) (1.45 g, 6.73 mmol) and ethyl 3-oxobutanoate (5.1 mL, 40.4 mmol) was stirred at RT for 30 min. To the mixture was added toluene (13 mL) and *p*-toluenesulfonic acid (134 mg, 036 mmol). After refluxing for 24 h, the mixture was cooled to RT. The reaction mixture was filtered and then the precipitates were washed with toluene and dried to afford compound (**2**) (916 mg, 48%). <sup>1</sup>H NMR (600 MHz, DMSO-*d*<sub>6</sub>) δ 13.25 (bs, 1H), 8.07 (d, 2H, *J* = 8.4 Hz), 7.55 (d, 2H, *J* = 8.4 Hz), 5.85 (s, 1H), 2.34 (s, 3H), 1.32 (s, 9H); <sup>13</sup>C{<sup>1</sup>H} NMR (150 MHz, DMSO- *d*<sub>6</sub>) δ 161.2, 156.2, 153.4, 151.7, 151.5, 127.9, 126.9, 126.1, 98.9, 35.0, 31.4, 19.0; HRMS (ESI) *m/z*: [M+H]<sup>+</sup> Calcd for C<sub>16</sub>H<sub>18</sub>N<sub>4</sub>O, 283.1559; found, 283.1554.

**2-(4-(*tert*-Butyl)phenyl)-5-(chloromethyl)-[1,2,4]triazolo[1,5-*a*]pyrimidin-7(4*H*)-one (3).** To a solution of 3-(4-(*tert*-butyl)phenyl)-1*H*-1,2,4-triazol-5-amine (**1**) (1.17 g, 5.14 mmol) in acetic acid (6 mL) was added ethyl 4-chloro-3-oxobutanoate (2.21 mL, 15.4 mmol). After stirring for 24 h at 80 °C, the mixture was cooled to RT. The reaction mixture was filtered and then the precipitates were washed with acetonitrile and dried to afford the product (**3**) (690 mg, 43%). <sup>1</sup>H NMR (600 MHz, DMSO-*d*<sub>6</sub>) δ 13.79 (bs, 1H), 8.06 (d, 2H, *J* = 8.4 Hz), 7.58 (d, 2H, *J* = 8.4 Hz), 6.2 (s, 1H), 4.69 (s, 2H), 1.32 (s, 9H); <sup>13</sup>C{<sup>1</sup>H} NMR (150 MHz, DMSO-*d*<sub>6</sub>) δ 158.5, 156.2, 153.8, 151.9, 149.4, 127.2, 126.9, 126.2, 100.4, 41.8, 35.1, 31.4; HRMS (ESI) *m/z*: [M+H]<sup>+</sup> Calcd for C<sub>16</sub>H<sub>17</sub>ClN<sub>4</sub>O, 317.1169; found, 317.1168.

**5-((Benzyl(methyl)amino)methyl)-2-(4-(*tert*-butyl)phenyl)-[1,2,4]triazolo[1,5-*a*]pyrimidin-7(4*H*)-one (4a).** A reaction mixture of chloromethyl compound (**3**) (55 mg, 0.17 mmol), *N*-benzylmethylamine (27 μL, 0.17 mmol) and sodium hydride (60% in oil, 20 mg, 0.51 mmol) in DMA (1 mL) was stirred in a microwave at 250 °C for 60 min. The solvent was removed under reduced pressure and purified by flash column chromatography on silica gel (MeOH / CH<sub>2</sub>Cl<sub>2</sub> / NH<sub>4</sub>OH = 1 : 20 : 0.1) to afford product (**4a**) (27.9 mg, 40%). <sup>1</sup>H NMR (600 MHz, DMSO-*d*<sub>6</sub>) δ 8.09 (d, 2H, *J* = 8.4 Hz), 7.45 (d, 2H, *J* = 7.8 Hz), 7.39 (t, 2H, *J* = 7.8 Hz), 7.31 (t, 1H, *J* = 7.2 Hz), 6.0 (s, 1H), 3.74 (s, 2H), 3.64 (s, 2H), 2.28 (s, 3H), 1.33 (s, 9H); <sup>13</sup>C{<sup>1</sup>H} NMR (150 MHz, DMSO-*d*<sub>6</sub>) δ 160.8, 156.5, 153.5, 153.3, 152.6, 137.0, 129.2, 128.3, 128.0, 127.5, 126.4, 125.6, 97.3, 60.6, 58.0, 41.4, 34.5, 31.0; HRMS (ESI) *m/z*: [M+H]<sup>+</sup> Calcd for C<sub>24</sub>H<sub>27</sub>N<sub>5</sub>O, 402.2294; found, 402.2290.

**2-(4-(tert-Butyl)phenyl)-5-(((1-phenyl-1H-pyrazol-5-yl)amino)methyl)-[1,2,4]triazolo[1,5-a]pyrimidin-7(4H)-one (4b).** A reaction mixture of chloromethyl compound (**3**) (50 mg, 0.158 mmol), 5-amino-1-phenylpyrazole (30 mg, 0.19 mmol) and sodium hydride (60% in oil, 19 mg, 0.47 mmol) in DMA (1 mL) was stirred in a microwave at 250 °C for 60 min. The solvent was removed under reduced pressure and purified by flash column chromatography on silica gel (MeOH / CH<sub>2</sub>Cl<sub>2</sub> / NH<sub>4</sub>OH = 1 : 20 : 0.1) to afford product (**4b**) (7.6 mg, 11%). <sup>1</sup>H NMR (600 MHz, DMSO-*d*<sub>6</sub>) δ 8.05 (d, 2H, *J* = 9 Hz), 7.68 (d, 2H, *J* = 7.2 Hz), 7.57-7.53 (m, 4H), 7.40 (t, 1H, *J* = 7.2 Hz), 7.36 (d, 1H, *J* = 1.8 Hz), 6.26 (t, 1H, *J* = 6 Hz), 6.06 (s, 1H), 5.58 (d, 1H, *J* = 1.8 Hz), 4.26 (d, 2H, *J* = 6 Hz), 1.33 (s, 9H); <sup>13</sup>C{<sup>1</sup>H} NMR (150 MHz, DMSO-*d*<sub>6</sub>) δ 162.2, 156.3, 153.6, 151.8, 147.7, 140.5, 139.8, 139.4, 129.8, 127.8, 127.2, 126.9, 126.2, 124.0, 97.6, 88.7, 46.3, 35.1, 31.4; HRMS (ESI) *m/z*: [M+H]<sup>+</sup> Calcd for C<sub>25</sub>H<sub>25</sub>N<sub>7</sub>O, 440.2199; found, 440.2198.

**2-(4-(tert-Butyl)phenyl)-5-((phenethylamino)methyl)-[1,2,4]triazolo[1,5-a]pyrimidin-7(4H)-one (4c).** A reaction mixture of chloromethyl compound (**3**) (50 mg, 0.158 mmol), phenethylamine (23 μL, 0.19 mmol) and sodium hydride (60% in oil, 19 mg, 0.47 mmol) in DMA (1 mL) was stirred in a microwave at 250 °C for 100 min. The solvent was removed under reduced pressure and purified by flash column chromatography on silica gel (MeOH / CH<sub>2</sub>Cl<sub>2</sub> / NH<sub>4</sub>OH = 1 : 20 : 0.1) to afford product (**4c**) (8.1 mg, 13%). <sup>1</sup>H NMR (600 MHz, DMSO-*d*<sub>6</sub>) δ 8.05 (d, 2H, *J* = 8.4 Hz), 7.57 (d, 2H, *J* = 8.4 Hz), 7.32-7.19 (m, 5H), 5.79 (d, 1H, *J* = 40.8 Hz), 4.50 (d, 2H, *J* = 5.4 Hz), 3.62 (t, 1H, *J* = 7.2 Hz), 3.52 (t, 1H, *J* = 7.2 Hz), 2.90 (t, 1H, *J* = 7.2 Hz), 2.80 (t, 1H, *J* = 7.2 Hz), 1.33 (d, 9H, *J* = 1.2 Hz); <sup>13</sup>C{<sup>1</sup>H} NMR (150 MHz, DMSO-*d*<sub>6</sub>) δ 171.2, 156.3, 153.6, 151.9, 139.0, 129.4, 129.1, 128.9, 128.8, 126.9, 126.6, 126.2, 96.7, 60.2, 50.8, 35.1, 34.5, 31.4; HRMS (ESI) *m/z*: [M+H]<sup>+</sup> Calcd for C<sub>24</sub>H<sub>27</sub>N<sub>5</sub>O, 402.02294; found, 402.2294.

**2-(4-(tert-Butyl)phenyl)-5-((pyrazin-2-ylamino)methyl)-[1,2,4]triazolo[1,5-a]pyrimidin-7(4H)-one (4d).** A reaction mixture of chloromethyl compound (**3**) (50 mg, 0.158 mmol), 2-aminopyrazine (22.5 mg, 0.237 mmol) and sodium hydride (60% in oil, 19 mg, 0.47 mmol) in DMA (1 mL) was stirred in a microwave at 250 °C for 50 min. The solvent was removed under reduced pressure and purified by flash column chromatography on silica gel (MeOH / CH<sub>2</sub>Cl<sub>2</sub> / NH<sub>4</sub>OH = 1 : 20 : 0.1) to afford the product (**4d**) (6.4 mg, 11%). <sup>1</sup>H NMR (600 MHz, CD<sub>3</sub>OD) δ 8.15 (d, 2H, *J* = 9 Hz), 8.09 (d, 1H, *J* = 1.8 Hz), 8.03 (q, 1H, *J* = 1.8 Hz), 7.79 (d, 1H, *J* = 3 Hz), 7.57 (d, 2H, *J* = 8.4 Hz), 6.03 (s, 1H), 4.62 (s, 2H), 1.39 (s, 9H); <sup>13</sup>C{<sup>1</sup>H} NMR (DMSO-*d*<sub>6</sub>, 150 MHz) δ 160.8, 156.0, 154.2, 153.1, 151.8, 141.4, 133.8, 132.3, 129.2, 127.4, 126.5, 125.7, 95.8, 41.2, 34.7, 31.0; HRMS (ESI) *m/z*: [M+H]<sup>+</sup> Calcd for C<sub>20</sub>H<sub>21</sub>N<sub>7</sub>O, 376.1886; found, 376.1882.

**2-(4-(tert-Butyl)phenyl)-5-((quinolin-2-ylamino)methyl)-[1,2,4]triazolo[1,5-a]pyrimidin-7(4H)-one (4e).** Method A: A reaction mixture of 2-aminoquinoline (34 mg, 0.237 mmol) and sodium hydride (60% in oil, 19 mg, 0.47 mmol) in DMF (1 mL) was stirred at 0°C for 30 minutes. To the resultant clear solution was added chloromethyl compound (**3**) (50 mg, 0.158 mmol). The reaction mixture

was stirred in a microwave oven at 150 °C for 30 minutes. The solvent was removed under reduced pressure and purified by flash column chromatography on silica gel (MeOH / CH<sub>2</sub>Cl<sub>2</sub> / NH<sub>4</sub>OH = 1 : 20 : 0.1) to afford the product (**4e**) (6.1 mg, 10 %). Method B: A reaction mixture of 2-aminoquinoline (47 mg, 0.33 mmol), sodium *tert*-butoxide (95 mg, 0.99 mmol) and sodium iodide (49 mg, 0.33 mmol) in DMF (3.0 mL) was stirred at 0 °C. To the resultant clear solution was added chloromethyl compound (**3**) (103 mg, 0.33 mmol). The reaction mixture was stirred at room temperature. After 12 h, the reaction mixture was filtered over a pad of Celite and washed. The solvent was removed under reduced pressure and the residue directly purified by flash column chromatography on silica gel (MeOH / CH<sub>2</sub>Cl<sub>2</sub> / AcOH = 1 : 60 : 0.1) to afford the product (**4e**) (45 mg, 40%). <sup>1</sup>H NMR (600 MHz, CD<sub>3</sub>OD) δ 8.02 (d, 2H, *J* = 8.4 Hz), 7.94 (d, 1H, *J* = 9 Hz), 7.62 (d, 1H, *J* = 8.4 Hz), 7.60 (d, 1H, *J* = 7.8 Hz), 7.49 (t, 1H, *J* = 7.2 Hz), 7.42 (d, 2H, *J* = 9 Hz), 7.21 (t, 1H, *J* = 7.2 Hz), 6.88 (d, 1H, *J* = 9 Hz), 5.93 (s, 1H), 4.60 (s, 2H), 1.26 (s, 9H); <sup>13</sup>C{<sup>1</sup>H} NMR (150 MHz, DMSO-*d*<sub>6</sub>) δ 170.0, 156.6, 156.5, 153.5, 152.1, 147.5, 137.4, 129.8, 128.1, 127.9, 126.9, 126.1, 126.1, 123.7, 122.4, 113.5, 96.5, 41.9, 35.1, 31.4; HRMS (ESI) *m/z*: [M+H]<sup>+</sup> Calcd for C<sub>25</sub>H<sub>24</sub>N<sub>6</sub>O, 425.2090; found, 425.2087.

**2-(4-(*tert*-Butyl)phenyl)-5-((cyclopentylamino)methyl)-[1,2,4]triazolo[1,5-*a*]pyrimidin-7(4H)-one (4f)**. A reaction mixture of cyclopentylamine (24 μL, 0.237 mmol) and sodium hydride (60% in oil, 19 mg, 0.47 mmol) in DMF (1 mL) was stirred at 0 °C for 10 minutes. To the resultant was added chloromethyl compound (**3**) (50 mg, 0.158 mmol). The reaction mixture was stirred in a microwave at 150 °C for 10 min. The solvent was removed under reduced pressure and purified by flash column chromatography on silica gel (MeOH / CH<sub>2</sub>Cl<sub>2</sub> / NH<sub>4</sub>OH = 1 : 20 : 0.1) to afford the product (**4f**) (32.6 mg, 10%). <sup>1</sup>H NMR (600 MHz, DMSO-*d*<sub>6</sub>) δ 8.06 (d, 2H, *J* = 9 Hz), 7.50 (d, 2H, *J* = 8.4 Hz), 5.66 (s, 1H), 4.02 (s, 2H), 3.53 (m, 1H), 2.00 (m, 2H), 1.72 (m, 4H), 1.55 (m, 2H), 1.32 (s, 9H); <sup>13</sup>C{<sup>1</sup>H} NMR (150 MHz, DMSO-*d*<sub>6</sub>) δ 160.5, 159.0, 157.8, 155.0, 151.7, 129.7, 126.2, 125.2, 94.4, 58.2, 49.2, 34.5, 31.1, 29.1, 23; HRMS (ESI) *m/z*: [M+H]<sup>+</sup> Calcd for C<sub>21</sub>H<sub>27</sub>N<sub>5</sub>O, 366.2289; found, 366.2288.

**2-(4-(*tert*-Butyl)phenyl)-5-((diethylamino)methyl)-[1,2,4]triazolo[1,5-*a*]pyrimidin-7(4H)-one (4g)**. A reaction mixture of diethylamine (13 μL, 0.12 mmol) and sodium hydride (60% in oil, 10 mg, 0.237 mmol) in DMF (1 mL) was stirred at 0 °C for 10 minutes. To the resultant clear solution was added chloromethyl compound (**3**) (25 mg, 0.079 mmol). The reaction mixture was stirred in a microwave at 150 °C for 10 min. The solvent was removed under reduced pressure and purified by flash column chromatography on silica gel (MeOH / CH<sub>2</sub>Cl<sub>2</sub> / NH<sub>4</sub>OH = 1 : 20 : 0.1) to afford product (**4g**) (6.4 mg, 23%). <sup>1</sup>H NMR (600 MHz, CD<sub>3</sub>OD) δ 8.03 (d, 2H, *J* = 8.4 Hz), 7.44 (d, 2H, *J* = 9 Hz), 5.86 (s, 1H), 4.15 (s, 2H), 3.19 (m, 4H), 1.28 (m, 15H); <sup>13</sup>C{<sup>1</sup>H} NMR (150 MHz, CD<sub>3</sub>OD) δ 161.8, 159.6, 158.3, 157.6, 153.1, 128.1, 126.5, 125.2, 95.6, 55.6, 48.2, 34.3, 30.3, 8.0; HRMS (ESI) *m/z*: [M+H]<sup>+</sup> Calcd for C<sub>20</sub>H<sub>27</sub>N<sub>5</sub>O, 354.2289; found, 354.2286.

**2-(4-(tert-Butyl)phenyl)-5-(((3-chlorophenyl)amino)methyl)-[1,2,4]triazolo[1,5-a]pyrimidin-7(4H)-one (4h).** A reaction mixture of 3-chloroaniline (13  $\mu$ L, 0.12 mmol) and sodium hydride (60% in oil, 20 mg, 0.47 mmol) in DMF (1 mL) was stirred at 0 °C for 10 minutes. To the resultant clear solution was added chloromethyl compound (**3**) (25 mg, 0.079 mmol). The reaction mixture was stirred in a microwave at 150 °C for 2 min. The solvent was removed under reduced pressure and purified by flash column chromatography on silica gel (MeOH / CH<sub>2</sub>Cl<sub>2</sub> / NH<sub>4</sub>OH = 1 : 30 : 0.1) to afford the product (**4h**) (8.4 mg, 26%). <sup>1</sup>H NMR (600 MHz, CD<sub>3</sub>OD)  $\delta$  8.15 (d, 2H, *J* = 9 Hz), 7.54 (d, 2H, *J* = 9 Hz), 7.08 (t, 1H, *J* = 8.4 Hz), 6.66 (t, 1H, *J* = 2.4 Hz), 6.61 (m, 1H), 6.57 (m, 1H), 6.06 (s, 1H), 4.32 (s, 2H), 1.38 (s, 9H); <sup>13</sup>C{<sup>1</sup>H} NMR (150 MHz, CD<sub>3</sub>OD)  $\delta$  162.0, 161.3, 159.3, 156.2, 153.1, 149.5, 134.5, 129.9, 127.9, 126.7, 125.1, 116.4, 112.0, 110.7, 94.4, 46.7, 34.3, 30.3; HRMS (ESI) *m/z*: [M+H]<sup>+</sup> Calcd for C<sub>21</sub>H<sub>21</sub>ClN<sub>5</sub>O, 408.1591; found, 408.1588.

**5-Propyl-2-((o-tolylamino)methyl)-[1,2,4]triazolo[1,5-a]pyrimidin-7(4H)-one (5a)** To a solution of NaOEt prepared from sodium (6 mg) and ethanol (1 mL), 2,3-diamino-6-propyl-pyrimidin-4-one (**7a**) (20 mg, 0.119 mmol) was added. After the reaction mixture was heated at 80 °C for 30 min, ethyl 2-(2-methylanilino)acetate (**6a**) (23 mg, 0.119 mmol) was added to the reaction mixture and heated at reflux for 15 h, and then stirred at RT overnight. The precipitate was filtered and dried under vacuum, then purified by flash column chromatography on silica gel (MeOH / CH<sub>2</sub>Cl<sub>2</sub> = 1 : 30) to afford 5-propyl-2-((o-tolylamino)methyl)-[1,2,4]triazolo[1,5-a]pyrimidin-7(4H)-one (**5a**) (8.7 mg, 25%). <sup>1</sup>H NMR (600 MHz, DMSO-*d*<sub>6</sub>)  $\delta$  13.09 (bs, 1H), 6.97 (m, 2H), 6.61 (d, 1H, *J* = 7.8 Hz), 6.52 (t, 1H, *J* = 7.2 Hz), 5.81 (s, 1H), 4.42 (s, 2H), 2.55 (t, 2H, *J* = 7.2 Hz), 2.13 (s, 3H), 1.68 (m, 2H), 0.92 (t, 3H, *J* = 7.2 Hz); <sup>13</sup>C{<sup>1</sup>H} NMR (150 MHz, DMSO-*d*<sub>6</sub>)  $\delta$  163.6, 156.3, 155.1, 151.4, 146.4, 130.2, 127.1, 122.2, 116.6, 110.0, 98.2, 41.6, 40.5, 21.6, 18.1, 13.7; HRMS (ESI) *m/z*: [M+H]<sup>+</sup> Calcd for C<sub>16</sub>H<sub>19</sub>N<sub>5</sub>O, 298.1668; found, 298.1665.

**5-Propyl-2-((m-tolylamino)methyl)-[1,2,4]triazolo[1,5-a]pyrimidin-7(4H)-one (5b)** To a solution of NaOEt prepared from sodium (6 mg) and ethanol (1 mL), 2,3-diamino-6-propyl-pyrimidin-4-one (**7a**) (20 mg, 0.119 mol) was added. After the reaction mixture was heated at 80 °C for 30 min, ethyl 2-(3-methylanilino)acetate (**6b**) (23 mg, 0.119 mmol) was added to the reaction mixture and heated at reflux for 15 h, and then stirred at RT overnight. The precipitate obtained was filtered and dried under vacuum, then purified by flash column chromatography on silica gel (MeOH / CH<sub>2</sub>Cl<sub>2</sub> = 1 : 30) to afford 5-propyl-2-((m-tolylamino)methyl)-[1,2,4]triazolo[1,5-a]pyrimidin-7(4H)-one (**5b**) (5.7 mg, 16%). <sup>1</sup>H NMR (600 MHz, DMSO-*d*<sub>6</sub>)  $\delta$  13.06 (bs, 1H), 6.94 (t, 1H, *J* = 7.8 Hz), 6.48 (s, 1H), 6.46 (d, 2H, *J* = 7.8 Hz), 6.36 (d, 1H, *J* = 7.2 Hz), 6.08 (t, 1H, *J* = 6.6 Hz), 5.79 (s, 1H), 4.32 (d, 2H, *J* = 60 Hz), 2.54 (t, 2H, *J* = 7.8 Hz), 2.16 (s, 3H), 1.68 (m, 2H), 0.91 (t, 3H, *J* = 7.2 Hz); <sup>13</sup>C{<sup>1</sup>H} NMR (150 MHz, DMSO-*d*<sub>6</sub>)  $\delta$  173.3, 156.4, 148.8, 138.2, 130.2, 129.1, 122.1, 117.5, 113.5, 110.0, 98.0, 41.4, 40.5, 21.8, 21.7, 13.7; HRMS (ESI) *m/z*: [M+H]<sup>+</sup> Calcd for C<sub>16</sub>H<sub>19</sub>N<sub>5</sub>O, 298.1668; found, 298.1665.

**5-Propyl-2-((*p*-tolylamino)methyl)-[1,2,4]triazolo[1,5-*a*]pyrimidin-7(4*H*)-one (5c)** To a solution of NaOEt prepared from sodium (6 mg) and ethanol (1 mL), 2,3-diamino-6-propyl-pyrimidin-4-one (**7a**) (20 mg, 0.119 mol) was added. After the reaction mixture was heated at 80 °C for 30 min, ethyl 2-(4-methylanilino)acetate (**6c**) (23 mg, 0.119 mmol) was added to the reaction mixture and heated at reflux for 15 h, and then stirred at RT overnight. The precipitate obtained was filtered and dried under vacuum, then purified by flash column chromatography on silica gel (MeOH / CH<sub>2</sub>Cl<sub>2</sub> = 1 : 30) to afford 5-propyl-2-((*p*-tolylamino)methyl)-[1,2,4]triazolo[1,5-*a*]pyrimidin-7(4*H*)-one (**5c**) (9.7 mg, 28%). <sup>1</sup>H NMR (600 MHz, DMSO-*d*<sub>6</sub>) δ 13.05 (bs, 1H), 6.87 (d, 2H, *J* = 8.4 Hz), 6.57 (d, 2H, *J* = 8.4 Hz), 5.97 (t, 1H, *J* = 6 Hz), 5.79 (s, 1H), 4.30 (d, 2H, *J* = 6 Hz), 2.54 (t, 2H, *J* = 7.2 Hz), 2.12 (s, 3H), 1.67 (m, 2H), 0.91 (t, 3H, *J* = 7.2 Hz); <sup>13</sup>C{<sup>1</sup>H} NMR (150 MHz, DMSO-*d*<sub>6</sub>) δ 168.9, 156.3, 151.4, 149.5, 146.5, 129.7, 124.9, 112.9, 98.1, 41.6, 40.5, 21.6, 20.5, 13.7; HRMS (ESI) *m/z*: [M+H]<sup>+</sup> Calcd for C<sub>16</sub>H<sub>19</sub>N<sub>5</sub>O, 298.1668; found, 298.1666.

**2-(((2-Chlorophenyl)amino)methyl)-5-propyl-[1,2,4]triazolo[1,5-*a*]pyrimidin-7(4*H*)-one (5d)** To a solution of NaOEt prepared from sodium (6 mg) and ethanol (1 mL), 2,3-diamino-6-propyl-pyrimidin-4-one (**7a**) (20 mg, 0.119 mmol) was added. After the reaction mixture was heated at 80 °C for 30 min, ethyl (2-chlorophenyl)glycinate (**6d**) (25 mg, 0.119 mmol) was added to the reaction mixture and heated at reflux for 15 h, and then stirred at RT overnight. The precipitate obtained was filtered and dried under vacuum, then purified by flash column chromatography on silica gel (MeOH / CH<sub>2</sub>Cl<sub>2</sub> = 1 : 30) to afford 2-(((2-chlorophenyl)amino)methyl)-5-propyl-[1,2,4]triazolo[1,5-*a*]pyrimidin-7(4*H*)-one (**5d**) (14.7 mg, 39%). <sup>1</sup>H NMR (600 MHz, DMSO-*d*<sub>6</sub>) δ 13.11 (bs, 1H), 7.27 (dd, 1H, *J* = 7.8 and 1.2 Hz), 7.11 (t, 1H, *J* = 8.4 Hz), 6.79 (dd, 1H, *J* = 7.8 and 0.6 Hz), 6.61 (td, 1H, *J* = 7.8 and 1.2 Hz), 5.96 (t, 1H, *J* = 6 Hz), 5.81 (s, 1H), 4.50 (d, 2H, *J* = 6 Hz), 2.54 (t, 2H, *J* = 7.2 Hz), 1.67 (m, 2H), 0.92 (t, 3H, *J* = 7.2 Hz); <sup>13</sup>C{<sup>1</sup>H} NMR (150 MHz, DMSO-*d*<sub>6</sub>) δ 162.8, 156.3, 155.3, 151.6, 144.2, 129.4, 128.4, 118.3, 117.4, 112.1, 98.2, 41.2, 34.6, 21.6, 13.7; HRMS (ESI) *m/z*: [M+H]<sup>+</sup> Calcd for C<sub>15</sub>H<sub>16</sub>ClN<sub>5</sub>O, 318.1121; found, 318.1117.

**2-(((3-Chlorophenyl)amino)methyl)-5-propyl-[1,2,4]triazolo[1,5-*a*]pyrimidin-7(4*H*)-one (5e)** To a solution of NaOEt prepared from sodium (6 mg) and ethanol (1 mL), 2,3-diamino-6-propyl-pyrimidin-4-one (**7a**) (20 mg, 0.119 mmol) was added. After the reaction mixture was heated at 80 °C for 30 min, ethyl (3-chlorophenyl)glycinate (**6e**) (25 mg, 0.119 mmol) was added to the reaction mixture and heated at reflux for 15 h, and then stirred at RT overnight. The precipitate obtained was filtered and dried under vacuum, then purified by flash column chromatography on silica gel (MeOH / CH<sub>2</sub>Cl<sub>2</sub> = 1 : 30) to afford 2-(((3-chlorophenyl)amino)methyl)-5-propyl-[1,2,4]triazolo[1,5-*a*]pyrimidin-7(4*H*)-one (**5e**) (12.3 mg, 33%). <sup>1</sup>H NMR (600 MHz, DMSO-*d*<sub>6</sub>) δ 13.07 (bs, 1H), 7.07 (td, 1H, *J* = 7.8 and 1.8 Hz), 6.70 (s, 1H), 6.62 (m, 2H), 6.54 (d, 1H, *J* = 7.8 Hz), 5.81 (d, 1H, *J* = 1.8 Hz), 4.37 (d, 2H, *J* = 6.6 Hz), 2.55 (t, 2H, *J* = 7.8 Hz), 1.68 (m, 2H), 0.92 (td, 3H, *J* = 7.8 Hz); <sup>13</sup>C{<sup>1</sup>H} NMR (150 MHz, DMSO-*d*<sub>6</sub>) δ 172.8, 162.9, 156.3, 151.5, 150.4, 134.0, 130.7, 115.9, 111.9, 111.5, 98.2, 41.1, 34.6, 21.6,

13.7; HRMS (ESI) m/z: [M+H]<sup>+</sup> Calcd for C<sub>15</sub>H<sub>16</sub>ClN<sub>5</sub>O, 318.1121; found, 318.1116.

**2-(((4-Chlorophenyl)amino)methyl)-5-propyl-[1,2,4]triazolo[1,5-a]pyrimidin-7(4H)-one (5f)** To a solution of NaOEt prepared from sodium (6 mg) and ethanol (1 mL), 2,3-diamino-6-propyl-pyrimidin-4-one (**7a**) (20 mg, 0.119 mmol) was added. After the reaction mixture was heated at 80 °C for 30 min, ethyl (4-chlorophenyl)glycinate (**6f**) (25 mg, 0.119 mmol) was added to the reaction mixture and heated at reflux for 15 h, and then stirred at RT overnight. The precipitate obtained was filtered and dried under vacuum, then purified by flash column chromatography on silica gel (MeOH / CH<sub>2</sub>Cl<sub>2</sub> = 1 : 30) to afford 2-(((4-chlorophenyl)amino)methyl)-5-propyl-[1,2,4]triazolo[1,5-a]pyrimidin-7(4H)-one (**5f**) (18.5 mg, 49%). <sup>1</sup>H NMR (600 MHz, DMSO-*d*<sub>6</sub>) δ 13.05 (bs, 1H), 7.08 (d, 2H, *J* = 8.4 Hz), 6.68 (d, 2H, *J* = 9 Hz), 6.47 (t, 1H, *J* = 6 Hz), 5.80 (s, 1H), 4.35 (d, 2H, *J* = 6 Hz), 2.54 (t, 2H, *J* = 7.2 Hz), 1.67-1.63 (m, 2H), 0.91 (t, 3H, *J* = 7.2 Hz); <sup>13</sup>C{<sup>1</sup>H} NMR (150 MHz, DMSO-*d*<sub>6</sub>) δ 172.4, 162.6, 155.8, 151.1, 147.3, 128.5, 119.3, 113.7, 97.7, 40.8, 34.1, 21.2, 13.2; HRMS (ESI) m/z: [M+H]<sup>+</sup> Calcd for C<sub>15</sub>H<sub>16</sub>ClN<sub>5</sub>O, 318.1121; found, 318.1117.

**2-(((1,1'-Biphenyl)-2-ylamino)methyl)-5-propyl-[1,2,4]triazolo[1,5-a]pyrimidin-7(4H)-one (5g)** To a solution of NaOEt prepared from sodium (13 mg) and ethanol (1 mL), 2,3-diamino-6-propyl-pyrimidin-4-one (**7a**) (30 mg, 0.178 mmol) was added. After the reaction mixture was heated at 80 °C for 30 min, ethyl [1,1'-biphenyl]-2-ylglycinate (**6g**) (45 mg, 0.178 mmol) was added to the reaction mixture and heated at reflux for 15 h, and then stirred at RT overnight. The precipitate obtained was filtered and dried under vacuum, then purified by flash column chromatography on silica gel (MeOH / CH<sub>2</sub>Cl<sub>2</sub> = 1 : 30) to afford 2-(((1,1'-biphenyl)-2-ylamino)methyl)-5-propyl-[1,2,4]triazolo[1,5-a]pyrimidin-7(4H)-one (**5g**) (18.9 mg, 30%). <sup>1</sup>H NMR (600 MHz, CDCl<sub>3</sub>) δ 12.41 (bs, 1H), 7.09 (d, 5H, *J* = 4.2 Hz), 7.05-7.03 (m, 1H), 6.95 (dd, 1H, *J* = 7.2 and 1.2 Hz), 6.71 (td, 1H, *J* = 7.8 and 1.2 Hz), 6.66 (d, 1H, *J* = 7.8 Hz), 5.65 (s, 1H), 4.55 (bs, 1H), 4.31 (s, 2H), 2.32 (t, 2H, *J* = 7.8 Hz), 1.44 (m, 2H), 0.77 (t, 3H, *J* = 7.8 Hz); <sup>13</sup>C{<sup>1</sup>H} NMR (150 MHz, CDCl<sub>3</sub>) δ 162.6, 156.3, 155.0, 150.6, 143.8, 138.8, 130.4, 128.8, 128.8, 128.6, 127.8, 127.1, 118.2, 110.8, 98.7, 42.0, 34.8, 20.9, 13.5; HRMS (ESI) m/z: [M+H]<sup>+</sup> Calcd for C<sub>21</sub>H<sub>21</sub>N<sub>5</sub>O, 360.1824; found, 360.1820.

**2-(((4-(tert-Butyl)phenyl)amino)methyl)-5-propyl-[1,2,4]triazolo[1,5-a]pyrimidin-7(4H)-one (5h)** To a solution of NaOEt prepared from sodium (13 mg) and ethanol (1 mL), 2,3-diamino-6-propyl-pyrimidin-4-one (**7a**) (30 mg, 0.178 mmol) was added. After the reaction mixture was heated at 80 °C for 30 min, ethyl (4-(*tert*-butyl)phenyl)glycinate (**6h**) (42 mg, 0.178 mmol) was added to the reaction mixture and heated at reflux for 15 h, and then stirred at RT overnight. The precipitate obtained was filtered and dried under vacuum, then purified by flash column chromatography on silica gel (MeOH / CH<sub>2</sub>Cl<sub>2</sub> = 1 : 30) to afford 2-(((4-(*tert*-butyl)phenyl)amino)methyl)-5-propyl-[1,2,4]triazolo[1,5-a]pyrimidin-7(4H)-one (**5h**) (31.2 mg, 52%). <sup>1</sup>H NMR (600 MHz, CDCl<sub>3</sub>) δ 7.15 (d, 2H, *J* = 8.4 Hz), 6.52 (d, 2H, *J* = 8.4 Hz), 5.77 (s, 1H), 4.47 (s, 2H), 2.54 (t, 2H, *J* = 7.8 Hz),



1.63 (m, 2H), 1.24 (s, 9H), 0.92 (t, 3H,  $J = 7.2$  Hz);  $^{13}\text{C}\{^1\text{H}\}$  NMR (150 MHz,  $\text{CDCl}_3$ )  $\delta$  163.0, 156.5, 155.3, 150.8, 144.7, 141.1, 126.0, 112.6, 98.7, 42.3, 34.8, 33.9, 31.5, 21.1, 13.4; HRMS (ESI)  $m/z$ :  $[\text{M}+\text{H}]^+$  Calcd for  $\text{C}_{19}\text{H}_{25}\text{N}_5\text{O}$ , 340.2137; found, 340.2133.

**2-(((3-Chloro-4-fluorophenyl)amino)methyl)-5-propyl-[1,2,4]triazolo[1,5-a]pyrimidin-7(4H)-one (5i)** To a solution of NaOEt prepared from sodium (13 mg) and ethanol (1 mL), 2,3-diamino-6-propyl-pyrimidin-4-one (**7a**) (30 mg, 0.178 mmol) was added. After the reaction mixture was heated at 80 °C for 30 min, ethyl (3-chloro-4-fluorophenyl)glycinate (**6i**) (42 mg, 0.178 mmol) was added to the reaction mixture and heated at reflux for 15 h, and then stirred at RT overnight. The precipitate obtained was filtered and dried under vacuum, then purified by flash column chromatography on silica gel ( $\text{MeOH} / \text{CH}_2\text{Cl}_2 = 1 : 30$ ) to afford 2-(((3-chloro-4-fluorophenyl)amino)methyl)-5-propyl-[1,2,4]triazolo[1,5-a]pyrimidin-7(4H)-one (**5i**) (10.1 mg, 17%).  $^1\text{H}$  NMR (600 MHz,  $\text{DMSO}-d_6$ )  $\delta$  13.03 (bs, 1H), 7.04 (t, 1H,  $J = 9$  Hz), 6.73 (dd, 1H,  $J = 6.6$  and 3 Hz), 6.57 (m, 1H), 6.40 (t, 1H,  $J = 6$  Hz), 5.72 (s, 1H), 4.27 (d, 2H,  $J = 6$  Hz), 2.47 (t, 2H,  $J = 7.2$  Hz), 1.61 (m, 1H), 0.85 (t, 3H,  $J = 7.2$  Hz);  $^{13}\text{C}\{^1\text{H}\}$  NMR (150 MHz,  $\text{DMSO}-d_6$ )  $\delta$  162.8, 156.4, 155.7, 151.8, 150.4, 148.9, 146.5, 119.7, 117.2, 113.0, 112.5, 98.0, 41.5, 34.8, 21.7, 13.7; HRMS (ESI)  $m/z$ :  $[\text{M}+\text{H}]^+$  Calcd for  $\text{C}_{15}\text{H}_{15}\text{ClFN}_5\text{O}$ , 336.1027; found, 336.1024.

**2-(((4-Ethylphenyl)amino)methyl)-5-propyl-[1,2,4]triazolo[1,5-a]pyrimidin-7(4H)-one (5j)** To a solution of NaOEt prepared from sodium (13 mg) and ethanol (1 mL), 2,3-diamino-6-propyl-pyrimidin-4-one (**7a**) (30 mg, 0.178 mmol) was added. After the reaction mixture was heated at 80 °C for 30 min, ethyl (4-ethylphenyl)glycinate (**6j**) (37 mg, 0.178 mmol) was added to the reaction mixture and heated at reflux for 15 h, and then stirred at RT overnight. The precipitate obtained was filtered and dried under vacuum, then purified by flash column chromatography on silica gel ( $\text{MeOH} / \text{CH}_2\text{Cl}_2 = 1 : 30$ ) to afford 2-(((4-ethylphenyl)amino)methyl)-5-propyl-[1,2,4]triazolo[1,5-a]pyrimidin-7(4H)-one (**5j**) (26 mg, 47%).  $^1\text{H}$  NMR (600 MHz,  $\text{DMSO}-d_6$ )  $\delta$  13.06 (bs, 1H), 6.90 (d, 2H,  $J = 8.4$  Hz), 6.60 (d, 2H,  $J = 8.4$  Hz), 5.99 (s, 1H), 5.80 (s, 1H), 4.32 (d, 2H,  $J = 3.6$  Hz), 2.54 (t, 2H,  $J = 7.2$  Hz), 2.44 (q, 2H,  $J = 7.8$  Hz), 1.68 (m, 2H), 1.10 (t, 3H,  $J = 7.8$  Hz), 0.92 (t, 3H,  $J = 7.8$  Hz);  $^{13}\text{C}\{^1\text{H}\}$  NMR (150 MHz,  $\text{DMSO}-d_6$ )  $\delta$  163.5, 156.3, 155.3, 151.5, 146.7, 131.7, 128.5, 112.9, 98.1, 41.6, 34.6, 27.8, 21.6, 16.6, 13.7; HRMS (ESI)  $m/z$ :  $[\text{M}+\text{H}]^+$  Calcd for  $\text{C}_{17}\text{H}_{21}\text{N}_5\text{O}$ , 312.1824; found, 312.1819.

**2-(((3,4-Difluorophenyl)amino)methyl)-5-propyl-[1,2,4]triazolo[1,5-a]pyrimidin-7(4H)-one (5k)** To a solution of NaOEt prepared from sodium (13 mg) and ethanol (1 mL), 2,3-diamino-6-propyl-pyrimidin-4-one (**7a**) (30 mg, 0.178 mmol) was added. After the reaction mixture was heated at 80 °C for 30 min, ethyl (3,4-difluorophenyl)glycinate (**6k**) (38 mg, 0.178 mmol) was added to the reaction mixture and heated at reflux for 15 h, and then stirred at RT overnight. The precipitate obtained was filtered and dried under vacuum, then purified by flash column chromatography on silica gel ( $\text{MeOH} / \text{CH}_2\text{Cl}_2 = 1 : 30$ ) to afford 2-

(((3,4-difluorophenyl)amino)methyl)-5-propyl-[1,2,4]triazolo[1,5-*a*]pyrimidin-7(4*H*)-one (**5k**) (16.1 mg, 28%). <sup>1</sup>H NMR (600 MHz, DMSO-*d*<sub>6</sub>) δ 13.08 (bs, 1H), 7.12 (q, 1H, *J* = 3 Hz), 6.67 (m, 1H), 6.49 (t, 1H, *J* = 6.6 Hz), 6.45 (d, 1H, *J* = 9 Hz), 5.81 (s, 1H), 4.34 (d, 2H, *J* = 6 Hz), 2.55 (t, 2H, *J* = 7.2 Hz), 1.67 (m, 2H), 0.92 (t, 3H, *J* = 7.2 Hz); <sup>13</sup>C{<sup>1</sup>H} NMR (150 MHz, DMSO-*d*<sub>6</sub>) δ 162.4, 155.8, 154.8, 151.0, 150.7, 149.0, 146.1, 142.0, 140.5, 117.3, 107.9, 100.4, 97.7, 41.0, 34.1, 21.1, 13.2; HRMS (ESI) *m/z*: [M+H]<sup>+</sup> Calcd for C<sub>15</sub>H<sub>15</sub>F<sub>2</sub>N<sub>5</sub>O, 320.1323; found, 320.1325.

**2-(((4-(Pentyloxy)phenyl)amino)methyl)-5-propyl-[1,2,4]triazolo[1,5-*a*]pyrimidin-7(4*H*)-one (5l)** To a solution of NaOEt prepared from sodium (13 mg) and ethanol (1 mL), 2,3-diamino-6-propyl-pyrimidin-4-one (**7a**) (30 mg, 0.178 mmol) was added. After the reaction mixture was heated at 80 °C for 30 min, ethyl (4-(pentyloxy)phenyl)glycinate (**6l**) (47 mg, 0.178 mmol) was added to the reaction mixture and heated at reflux for 15 h, and then stirred at RT overnight. The precipitate obtained was filtered and dried under vacuum, then purified by flash column chromatography on silica gel (MeOH / CH<sub>2</sub>Cl<sub>2</sub> = 1 : 30) to afford 2-(((4-(pentyloxy)phenyl)amino)methyl)-5-propyl-[1,2,4]triazolo[1,5-*a*]pyrimidin-7(4*H*)-one (**5l**) (4.5 mg, 7%). <sup>1</sup>H NMR (600 MHz, DMSO-*d*<sub>6</sub>) δ 13.06 (bs, 1H), 6.69 (d, 2H, *J* = 9 Hz), 6.61 (d, 2H, *J* = 9 Hz), 5.79 (s, 1H), 5.75 (bs, 1H), 4.28 (d, 2H, *J* = 6 Hz), 3.81 (t, 2H, *J* = 6.6 Hz), 2.54 (t, 2H, *J* = 7.2 Hz), 1.67-1.61 (m, 2H), 1.37-1.30 (m, 4H), 0.92 (t, 3H, *J* = 7.8 Hz), 0.89 (t, 3H, *J* = 7.2 Hz); <sup>13</sup>C{<sup>1</sup>H} NMR (150 MHz, DMSO-*d*<sub>6</sub>) δ 163.5, 156.4, 150.7, 143.0, 115.8, 113.8, 98.0, 68.3, 42.1, 34.7, 29.1, 28.2, 22.4, 21.7, 14.4, 13.7; HRMS (ESI) *m/z*: [M+H]<sup>+</sup> Calcd for C<sub>20</sub>H<sub>27</sub>N<sub>5</sub>O<sub>2</sub>, 370.2243; found, 370.2242.

**2-(((4-Fluorophenyl)amino)methyl)-5-propyl-[1,2,4]triazolo[1,5-*a*]pyrimidin-7(4*H*)-one (5m)** To a solution of NaOEt prepared from sodium (13 mg) and ethanol (1 mL), 2,3-diamino-6-propyl-pyrimidin-4-one (**7a**) (30 mg, 0.178 mmol) was added. After the reaction mixture was heated at 80 °C for 30 min, ethyl (4-fluorophenyl)glycinate (**6m**) (35 mg, 0.178 mmol) was added to the reaction mixture and heated at reflux for 15 h, and then stirred at RT overnight. The precipitate obtained was filtered and dried under vacuum, then purified by flash column chromatography on silica gel (MeOH / CH<sub>2</sub>Cl<sub>2</sub> = 1 : 30) to afford 2-(((4-fluorophenyl)amino)methyl)-5-propyl-[1,2,4]triazolo[1,5-*a*]pyrimidin-7(4*H*)-one (**5m**) (16 mg, 30%). <sup>1</sup>H NMR (600 MHz, DMSO-*d*<sub>6</sub>) δ 13.08 (bs, 1H), 6.92 (t, 2H, *J* = 9 Hz), 6.67 (dd, 2H, *J* = 9 and 4.8 Hz), 6.17 (t, 1H, *J* = 6 Hz), 5.80 (s, 1H), 4.33 (d, 2H, *J* = 6 Hz), 2.54 (t, 2H, *J* = 7.2 Hz), 1.68-1.62 (m, 2H), 0.92 (t, 3H, *J* = 7.2 Hz); <sup>13</sup>C{<sup>1</sup>H} NMR (150 MHz, DMSO-*d*<sub>6</sub>) δ 163.2, 156.3, 155.7, 155.4, 154.1, 151.5, 145.5, 115.5, 113.5, 98.1, 41.8, 34.6, 21.6, 13.7; HRMS (ESI) *m/z*: [M+H]<sup>+</sup> Calcd for C<sub>15</sub>H<sub>16</sub>FN<sub>5</sub>O, 302.1417; found, 302.1417.

**5-Propyl-2-(((4-(trifluoromethoxy)phenyl)amino)methyl)-[1,2,4]triazolo[1,5-*a*]pyrimidin-7(4*H*)-one (5n)** To a solution of NaOEt prepared from sodium (13 mg) and ethanol (1 mL), 2,3-diamino-6-propyl-pyrimidin-4-one (**7a**) (30 mg, 0.178 mmol) was added. After the reaction mixture was heated at 80 °C for 30 min, ethyl (4-(trifluoromethoxy)phenyl)glycinate (**6n**) (47 mg, 0.178 mmol) was added

to the reaction mixture and heated at reflux for 15 h, and then stirred at RT overnight. The precipitate obtained was filtered and dried under vacuum, then purified by flash column chromatography on silica gel (MeOH / CH<sub>2</sub>Cl<sub>2</sub> = 1 : 30) to afford 5-propyl-2-(((4-(trifluoromethoxy)phenyl)amino)methyl)-[1,2,4]triazolo[1,5-*a*]pyrimidin-7(4*H*)-one (**5n**) (19 mg, 29%). <sup>1</sup>H NMR (600 MHz, DMSO-*d*<sub>6</sub>) δ 13.08 (bs, 1H), 7.06 (d, 2H, *J* = 8.4 Hz), 6.71 (d, 2H, *J* = 8.4 Hz), 6.56 (t, 1H, *J* = 6.6 Hz), 5.81 (s, 1H), 4.37 (d, 2H, *J* = 6.6 Hz), 2.55 (t, 2H, *J* = 7.2 Hz), 1.67 (m, 2H), 0.92 (t, 3H, *J* = 7.2 Hz); <sup>13</sup>C{<sup>1</sup>H} NMR (150 MHz, DMSO-*d*<sub>6</sub>) δ 163.1, 156.3, 155.2, 151.5, 148.1, 139.1, 122.4, 121.7, 120.0, 113.1, 98.2, 41.3, 34.5, 21.6, 13.7; HRMS (ESI) *m/z*: [M+H]<sup>+</sup> Calcd for C<sub>16</sub>H<sub>16</sub>F<sub>3</sub>N<sub>5</sub>O<sub>2</sub>, 368.1334; found, 368.1330.

**2-((*o*-Tolylamino)methyl)-4,5,6,7-tetrahydro-8H-cyclopenta[*d*][1,2,4]triazolo[1,5-*a*]pyrimidin-8-one (5o)** To a solution of NaOEt prepared from sodium (6 mg) and ethanol (1 mL), 2,3-diamino-3,5,6,7-tetrahydro-4*H*-cyclopenta[*d*]pyrimidin-4-one (**7b**) (20 mg, 0.12 mmol) was added. After the reaction mixture was heated at 80 °C for 30 min, ethyl 2-(2-methylanilino)acetate (**6a**) (28 mg, 0.144 mmol) was added to the reaction mixture and heated at reflux for 15 h, and then stirred at RT overnight. The precipitate obtained was filtered and dried under vacuum, then purified by flash column chromatography on silica gel (MeOH / CH<sub>2</sub>Cl<sub>2</sub> = 1 : 30) to afford 2-((*o*-tolylamino)methyl)-4,5,6,7-tetrahydro-8*H*-cyclopenta[*d*][1,2,4]triazolo[1,5-*a*]pyrimidin-8-one (**5o**) (6.7 mg, 19%). <sup>1</sup>H NMR (600 MHz, DMSO-*d*<sub>6</sub>) δ 13.31 (bs, 1H), 6.97 (m, 2H), 6.59 (d, 1H, *J* = 7.8 Hz), 6.52 (t, 1H, *J* = 7.2 Hz), 5.50 (t, 1H, *J* = 6 Hz), 4.41 (d, 2H, *J* = 6 Hz), 2.91 (t, 2H, *J* = 7.2 Hz), 2.69 (t, 2H, *J* = 7.2 Hz), 2.13 (s, 3H), 2.11-2.06 (m, 2H); <sup>13</sup>C{<sup>1</sup>H} NMR (150 MHz, DMSO-*d*<sub>6</sub>) δ 173.2, 154.9, 151.9, 146.5, 130.2, 127.1, 122.2, 116.5, 110.0, 109.6, 41.7, 40.5, 31.9, 27.3, 22.2, 18.1; HRMS (ESI) *m/z*: [M+H]<sup>+</sup> Calcd for C<sub>16</sub>H<sub>17</sub>N<sub>5</sub>O, 296.1511; found, 296.1505.

**2-((*m*-Tolylamino)methyl)-4,5,6,7-tetrahydro-8H-cyclopenta[*d*][1,2,4]triazolo[1,5-*a*]pyrimidin-8-one (5p)** To a solution of NaOEt prepared from sodium (6 mg) and ethanol (1 mL), 2,3-diamino-3,5,6,7-tetrahydro-4*H*-cyclopenta[*d*]pyrimidin-4-one (**7b**) (20 mg, 0.12 mmol) was added. After the reaction mixture was heated at 80 °C for 30 min, ethyl 2-(3-methylanilino)acetate (**6b**) (28 mg, 0.144 mmol) was added to the reaction mixture and heated at reflux for 15 h, and then stirred at RT overnight. The precipitate obtained was filtered and dried under vacuum, then purified by flash column chromatography on silica gel (MeOH / CH<sub>2</sub>Cl<sub>2</sub> = 1 : 30) to afford 2-((*m*-tolylamino)methyl)-4,5,6,7-tetrahydro-8*H*-cyclopenta[*d*][1,2,4]triazolo[1,5-*a*]pyrimidin-8-one (**5p**) (15.7 mg, 45%). <sup>1</sup>H NMR (600 MHz, DMSO-*d*<sub>6</sub>) δ 13.22, (bs, 1H), 6.87 (t, 1H, *J* = 7.8 Hz), 6.41 (s, 1H), 6.39 (d, 1H, *J* = 8.4 Hz), 6.29 (d, 1H, *J* = 7.2 Hz), 6.00 (bs, 1H), 4.24 (d, 2H, *J* = 4.2 Hz), 2.84 (t, H, *J* = 7.8 Hz), 2.61 (t, 2H, *J* = 7.2 Hz), 2.09 (s, 3H), 2.03-1.98 (m, 2H); <sup>13</sup>C{<sup>1</sup>H} NMR (150 MHz, DMSO-*d*<sub>6</sub>) δ 163.1, 155.4, 154.8, 151.7, 148.8, 138.2, 129.1, 117.5, 113.5, 110.4, 110.0, 41.5, 31.8, 27.2, 22.2, 21.8; HRMS (ESI) *m/z*: [M+H]<sup>+</sup> Calcd for C<sub>16</sub>H<sub>17</sub>N<sub>5</sub>O, 296.1511; found, 296.1505.

**2-((*p*-Tolylamino)methyl)-4,5,6,7-tetrahydro-8H-cyclopenta[*d*][1,2,4]triazolo[1,5-*a*]pyrimidin-8-one (5q)** To a solution of NaOEt prepared from sodium (6 mg) and ethanol (1 mL), 2,3-diamino-3,5,6,7-tetrahydro-4*H*-cyclopenta[*d*]pyrimidin-4-one (**7b**) (20 mg, 0.120 mmol) was added. After the reaction mixture was heated at 80 °C for 30 min, ethyl 2-(4-methylanilino)acetate (**6c**) (28 mg, 0.144 mmol) was added to the reaction mixture and heated at reflux for 15 h, and then stirred at RT overnight. The precipitate obtained was filtered and dried under vacuum, then purified by flash column chromatography on silica gel (MeOH / CH<sub>2</sub>Cl<sub>2</sub> = 1 : 30) to afford 2-[(4-methylanilino)methyl]-5-propyl-4*H*-[1,2,4]triazolo[1,5-*a*]pyrimidin-7-one (**5q**) (9 mg, 25%). <sup>1</sup>H NMR (600 MHz, DMSO-*d*<sub>6</sub>) δ 13.29 (bs, 1H), 6.87 (d, 2H, *J* = 8.4 Hz), 6.58 (d, 2H, *J* = 8.4 Hz), 5.95 (s, 1H), 4.30 (d, 2H, *J* = 5.4 Hz), 2.92 (t, 2H, *J* = 7.8 Hz), 2.69 (t, 2H, *J* = 7.2 Hz), 2.13 (s, 3H), 2.11-2.06 (m, 2H); <sup>13</sup>C{<sup>1</sup>H} NMR (150 MHz, DMSO-*d*<sub>6</sub>) δ 173.3, 163.1, 154.8, 151.8, 146.5, 129.7, 124.9, 112.9, 110.3, 41.7, 31.8, 27.2, 22.2, 20.5; HRMS (ESI) *m/z*: [M+H]<sup>+</sup> Calcd for C<sub>16</sub>H<sub>17</sub>N<sub>5</sub>O, 296.1511; found, 296.1505.

**5-Isopropyl-2-((*o*-tolylamino)methyl)-[1,2,4]triazolo[1,5-*a*]pyrimidin-7(4*H*)-one (5r)** To a solution of NaOEt prepared from sodium (6 mg) and ethanol (1 mL), 2,3-diamino-6-isopropylpyrimidin-4(3*H*)-one (**7c**) (20 mg, 0.119 mmol) was added. After the reaction mixture was heated at 80 °C for 30 min, ethyl 2-(2-methylanilino)acetate (**6a**) (28 mg, 0.143 mmol) was added to the reaction mixture and heated at reflux for 15 h, and then stirred at RT overnight. The precipitate obtained was filtered and dried under vacuum, then purified by flash column chromatography on silica gel (MeOH / CH<sub>2</sub>Cl<sub>2</sub> = 1 : 30) to afford 5-isopropyl-2-((*o*-tolylamino)methyl)-[1,2,4]triazolo[1,5-*a*]pyrimidin-7(4*H*)-one (**5r**) (24.3 mg, 69%). <sup>1</sup>H NMR (600 MHz, DMSO-*d*<sub>6</sub>) δ 13.06 (BS, 1H), 6.98 (m, 2H), 6.6 (d, 1H, *J* = 8.4 Hz), 6.52 (t, 1H, *J* = 7.8 Hz), 5.81 (s, 1H), 5.51 (t, 1H, *J* = 5.4 Hz), 4.43 (d, 2H, *J* = 5.4 Hz), 2.87-2.82 (m, 1H), 2.13 (s, 3H), 1.24 (s, 3H), 1.23 (s, 3H); <sup>13</sup>C{<sup>1</sup>H} NMR (150 MHz, DMSO-*d*<sub>6</sub>) δ 173.2, 163.4, 156.6, 151.5, 146.4, 130.2, 127.1, 122.2, 116.5, 110.0, 95.7, 41.5, 32.2, 21.3, 18.1; HRMS (ESI) *m/z*: [M+H]<sup>+</sup> Calcd for C<sub>16</sub>H<sub>19</sub>N<sub>5</sub>O, 298.1668; found, 298.1665.

**5-Isopropyl-2-((*m*-tolylamino)methyl)-[1,2,4]triazolo[1,5-*a*]pyrimidin-7(4*H*)-one (5s)** To a solution of NaOEt prepared from sodium (6 mg) and ethanol (1 mL), 2,3-diamino-6-isopropylpyrimidin-4(3*H*)-one (**7c**) (20 mg, 0.119 mmol) was added. After the reaction mixture was heated at 80 °C for 30 min, ethyl 2-(3-methylanilino)acetate (**6b**) (28 mg, 0.143 mmol) was added to the reaction mixture and heated at reflux for 15 h, and then stirred at RT overnight. The precipitate obtained was filtered and dried under vacuum, then purified by flash column chromatography on silica gel (MeOH / CH<sub>2</sub>Cl<sub>2</sub> = 1 : 30) to afford 5-isopropyl-2-((*m*-tolylamino)methyl)-[1,2,4]triazolo[1,5-*a*]pyrimidin-7(4*H*)-one (**5s**) (13.4 mg, 38%). <sup>1</sup>H NMR (600 MHz, DMSO-*d*<sub>6</sub>) δ 13.03 (bs, 1H), 6.95 (t, 1H, *J* = 7.8 Hz), 6.48 (s, 1H), 6.47 (d, 1H, *J* = 7.8 Hz), 6.37 (d, 1H, *J* = 7.2 Hz), 6.09 (bs, 1H), 5.80 (s, 1H), 4.34 (d, 2H, *J* = 3.6 Hz), 2.88 (m, 1H), 2.16 (s, 3H), 1.24 (s, 3H), 1.23 (s, 3H); <sup>13</sup>C{<sup>1</sup>H} NMR (150 MHz, DMSO-*d*<sub>6</sub>) δ 172.7, 156.1, 151.0, 148.3, 137.8, 137.7, 128.7, 117.0, 113.0, 109.5, 95.2, 40.8, 31.7, 21.3, 20.9; HRMS (ESI) *m/z*: [M+H]<sup>+</sup> Calcd for C<sub>16</sub>H<sub>19</sub>N<sub>5</sub>O, 298.1668; found, 298.1665.

**5-Isopropyl-2-((p-tolylamino)methyl)-[1,2,4]triazolo[1,5-a]pyrimidin-7(4H)-one (5t)** To a solution of NaOEt prepared from sodium (6 mg) and ethanol (1 mL), 2,3-diamino-6-isopropylpyrimidin-4(3H)-one (**7c**) (20 mg, 0.119 mmol) was added. After the reaction mixture was heated at 80 °C for 30 min, ethyl 2-(4-methylanilino)acetate (**6c**) (28 mg, 0.143 mmol) was added to the reaction mixture and heated at reflux for 15 h, and then stirred at RT overnight. The precipitate obtained was filtered and dried under vacuum, then purified by flash column chromatography on silica gel (MeOH / CH<sub>2</sub>Cl<sub>2</sub> = 1 : 30) to afford 5-isopropyl-2-((p-tolylamino)methyl)-[1,2,4]triazolo[1,5-a]pyrimidin-7(4H)-one (**5t**) (11 mg, 32%). <sup>1</sup>H NMR (600 MHz, DMSO-*d*<sub>6</sub>) δ; 12.96 (bs, 1H), 6.87 (d, 2H, *J* = 7.8 Hz), 6.58 (d, 2H, *J* = 8.4 Hz), 5.97 (bs, 1H), 5.80 (s, 1H), 4.32 (s, 2H), 2.87-2.83 (m, 1H), 2.13 (s, 3H), 1.24 (s, 3H), 1.23 (s, 3H); <sup>13</sup>C{<sup>1</sup>H} NMR (150 MHz, DMSO-*d*<sub>6</sub>) δ 173.3, 156.6, 151.5, 146.5, 146.4, 129.7, 129.2, 112.9, 95.7, 41.6, 32.2, 21.4, 20.5; HRMS (ESI) *m/z*: [M+H]<sup>+</sup> Calcd for C<sub>16</sub>H<sub>19</sub>N<sub>5</sub>O, 298.1668; found, 298.1666.

**5-Methyl-2-((o-tolylamino)methyl)-[1,2,4]triazolo[1,5-a]pyrimidin-7(4H)-one (5u)** To a solution of NaOEt prepared from sodium (6 mg) and ethanol (1 mL), 2,3-diamino-6-methylpyrimidin-4(3H)-one (**7d**) (20 mg, 0.140 mmol) was added. After the reaction mixture was heated at 80 °C for 30 min, ethyl 2-(2-methylanilino)acetate (**6a**) (33 mg, 0.168 mmol) was added to the reaction mixture and heated at reflux for 15 h, and then stirred at RT overnight. The precipitate obtained was filtered and dried under vacuum, then purified by flash column chromatography on silica gel (MeOH / CH<sub>2</sub>Cl<sub>2</sub> = 1 : 30) to afford 5-methyl-2-((o-tolylamino)methyl)-[1,2,4]triazolo[1,5-a]pyrimidin-7(4H)-one (**5u**) (11.1 mg, 30%). <sup>1</sup>H NMR (600 MHz, DMSO-*d*<sub>6</sub>) δ 13.12 (bs, 1H), 6.97 (m, 2H), 6.60 (d, 1H, *J* = 7.8 Hz), 6.52 (t, 1H, *J* = 7.8 Hz), 5.79 (s, 1H), 5.49 (t, 1H, *J* = 6 Hz), 4.41 (d, 2H, *J* = 6 Hz), 2.29 (s, 3H), 2.13 (s, 3H); <sup>13</sup>C{<sup>1</sup>H} NMR (150 MHz, DMSO-*d*<sub>6</sub>) δ 172.8, 162.9, 155.7, 150.9, 146.0, 129.7, 126.7, 121.8, 116.1, 109.6, 98.2, 41.1, 18.6, 17.6; HRMS (ESI) *m/z*: [M+H]<sup>+</sup> Calcd for C<sub>14</sub>H<sub>15</sub>N<sub>5</sub>O, 270.1355; found, 270.1350.

**5-Methyl-2-((m-tolylamino)methyl)-[1,2,4]triazolo[1,5-a]pyrimidin-7(4H)-one (5v)** To a solution of NaOEt prepared from sodium (6 mg) and ethanol (1 mL), 2,3-diamino-6-methylpyrimidin-4(3H)-one (**7d**) (20 mg, 0.14 mmol) was added. After the reaction mixture was heated at 80 °C for 30 min, ethyl 2-(3-methylanilino)acetate (**6b**) (33 mg, 0.168 mmol) was added to the reaction mixture and heated at reflux for 15 h, and then stirred at RT overnight. The precipitate obtained was filtered and dried under vacuum, then purified by flash column chromatography on silica gel (MeOH / CH<sub>2</sub>Cl<sub>2</sub> = 1 : 30) to afford 5-methyl-2-((m-tolylamino)methyl)-[1,2,4]triazolo[1,5-a]pyrimidin-7(4H)-one (**5v**) (4.8 mg, 13%). <sup>1</sup>H NMR (600 MHz, DMSO-*d*<sub>6</sub>) δ 13.10 (bs, 1H), 6.95 (t, 1H, *J* = 7.8 Hz), 6.48 (s, 1H), 6.47 (d, 1H, *J* = 7.8 Hz), 6.37 (d, 1H, *J* = 7.2 Hz), 6.09 (t, 1H, *J* = 6 Hz), 5.80 (s, 1H), 4.33 (d, 2H, *J* = 6 Hz), 2.30 (s, 3H), 2.16 (s, 3H); <sup>13</sup>C{<sup>1</sup>H} NMR (150 MHz, DMSO-*d*<sub>6</sub>) δ 163.3, 156.2, 151.7, 151.4, 148.8, 138.2, 129.1, 117.5, 113.5, 110.0, 98.7, 41.4, 21.8, 19.1; HRMS (ESI) *m/z*: [M+H]<sup>+</sup> Calcd for C<sub>14</sub>H<sub>15</sub>N<sub>5</sub>O, 270.1355; found, 270.1350.

**5-Methyl-2-((*p*-tolylamino)methyl)-[1,2,4]triazolo[1,5-*a*]pyrimidin-7(4*H*)-one (5x)** To a solution of NaOEt prepared from sodium (6 mg) and ethanol (1 mL), 2,3-diamino-6-methylpyrimidin-4(3*H*)-one (**7d**) (20 mg, 0.168 mmol) was added. After the reaction mixture was heated at 80 °C for 30 min, ethyl 2-(4-methylanilino)acetate (**6c**) (33 mg, 0.168 mmol) was added to the reaction mixture and heated at reflux for 15 h, and then stirred at RT overnight. The precipitate obtained was filtered and dried under vacuum, then purified by flash column chromatography on silica gel (MeOH / CH<sub>2</sub>Cl<sub>2</sub> = 1 : 30) to afford 5-methyl-2-((*p*-tolylamino)methyl)-[1,2,4]triazolo[1,5-*a*]pyrimidin-7(4*H*)-one (**5x**) (5.2 mg, 14%). <sup>1</sup>H NMR (600 MHz, DMSO-*d*<sub>6</sub>) δ 13.08 (bs, 1H), 6.87 (d, 2H, *J* = 7.8 Hz), 6.58 (d, 2H, *J* = 8.4 Hz), 5.98 (s, 1H), 5.79 (s, 1H), 4.31 (d, 2H), 2.29 (s, 3H), 2.13 (s, 3H); <sup>13</sup>C{<sup>1</sup>H} NMR (150 MHz, DMSO-*d*<sub>6</sub>) δ 163.4, 156.2, 151.7, 151.3, 146.5, 129.7, 124.9, 112.9, 98.7, 41.6, 20.5, 19.1; HRMS (ESI) *m/z*: [M+H]<sup>+</sup> Calcd for C<sub>14</sub>H<sub>15</sub>N<sub>5</sub>O, 270.1355; found, 270.1350.

**Ethyl *o*-tolylglycinate (6a)** To a THF (5 mL) solution of ethyl 2-bromoacetate (220 μL, 2 mmol), *o*-toluidine (214 μL, 2 mmol) and K<sub>2</sub>CO<sub>3</sub> (830 mg, 6 mmol) were added. After refluxing for 24 h, the reaction mixture was diluted with ethyl acetate and the organic phase was washed with water and brine, dried over MgSO<sub>4</sub>, and concentrated under reduced pressure. The residue was purified by flash column chromatography on silica gel (ethyl acetate / *n*-hexane = 1:5) to afford the ethyl *o*-tolylglycinate (**6a**) (386 mg, 99%). <sup>1</sup>H NMR (600 MHz, CDCl<sub>3</sub>) δ 7.14 (td, 1H, *J* = 7.8 and 1.2 Hz), 7.09 (d, 1H, *J* = 7.2 Hz), 6.73 (td, 1H, *J* = 7.8 and 0.6 Hz), 6.52 (d, 1H, *J* = 7.8 Hz), 4.28 (q, 2H, *J* = 7.2 Hz), 3.95 (s, 2H), 2.23 (s, 3H), 1.33 (t, 3H, *J* = 7.2 Hz); <sup>13</sup>C{<sup>1</sup>H} NMR (150 MHz, CDCl<sub>3</sub>) δ 171.2, 144.9, 130.3, 127.1, 122.7, 118.0, 110.1, 61.4, 46.0, 17.4, 14.2.

**Ethyl *m*-tolylglycinate (6b)** To a THF (5 mL) solution of ethyl 2-bromoacetate (220 μL, 2 mmol), *m*-toluidine (214 μL, 2 mmol) and K<sub>2</sub>CO<sub>3</sub> (830 mg, 6 mmol) were added. After refluxing for 24 h, the reaction mixture was diluted with ethyl acetate and the organic phase was washed with water and brine, dried over MgSO<sub>4</sub>, and concentrated under reduced pressure. The residue was purified by flash column chromatography on silica gel (ethyl acetate / *n*-hexane = 1 : 5) to afford the ethyl *m*-tolylglycinate (**6b**) (364 mg, 94%). <sup>1</sup>H NMR (600 MHz, CDCl<sub>3</sub>) δ 7.11 (td, 1H, *J* = 7.8 and 1.2 Hz), 6.26 (t, 1H, *J* = 7.8 Hz), 6.49 (s, 2H), 4.26 (q, 2H, *J* = 7.2 Hz), 3.91 (t, 2H, *J* = 1.8 Hz), 2.29 (s, 3H), 1.31 (t, 3H, *J* = 7.2 Hz); <sup>13</sup>C{<sup>1</sup>H} NMR (150 MHz, CDCl<sub>3</sub>) δ 171.1, 146.8, 139.2, 129.2, 119.5, 114.1, 110.4, 61.3, 46.1, 21.6, 14.2.

**Ethyl *p*-tolylglycinate (6c)** To a THF (5 mL) solution of ethyl 2-bromoacetate (220 μL, 2 mmol), *p*-toluidine (214 μL, 2 mmol) and K<sub>2</sub>CO<sub>3</sub> (830 mg, 6 mmol) were added. After refluxing for 24 h, the reaction mixture was diluted with ethyl acetate and the organic phase was washed with water and brine, dried over MgSO<sub>4</sub>, and concentrated under reduced pressure. The residue was purified by flash column chromatography on silica gel (ethyl acetate / *n*-hexane = 1 : 5) to afford the ethyl *p*-tolylglycinate (**6c**) (331 mg, 86%). <sup>1</sup>H NMR (600 MHz, CDCl<sub>3</sub>) δ 7.01 (d, 2H, *J* = 8.4 Hz), 6.57 (d, 2H, *J* = 8.4 Hz), 4.25 (q, 2H, *J* = 6.6 Hz), 3.88

(s, 2H), 2.24 (s, 3H), 1.30 (t, 3H,  $J = 7.2$  Hz);  $^{13}\text{C}\{^1\text{H}\}$  NMR (150 MHz,  $\text{CDCl}_3$ )  $\delta$  171.2, 144.6, 129.8, 127.7, 113.4, 61.3, 46.4, 20.4, 14.2.

**Ethyl (2-chlorophenyl)glycinate (6d)** To a THF (5 mL) solution of ethyl 2-bromoacetate (220  $\mu\text{L}$ , 2 mmol), 2-chloroaniline (328 mg, 2 mmol) and  $\text{K}_2\text{CO}_3$  (830 mg, 6 mmol) were added. After refluxing for 24 h, the reaction mixture was diluted with ethyl acetate and the organic phase was washed with water and brine, dried over  $\text{MgSO}_4$ , and concentrated under reduced pressure. The residue was purified by flash column chromatography on silica gel (ethyl acetate / *n*-hexane = 1 : 5) to afford the ethyl (2-chlorophenyl)glycinate (**6d**) (96 mg, 23%).  $^1\text{H}$  NMR (600 MHz,  $\text{CDCl}_3$ )  $\delta$  7.22 (dd, 1H,  $J = 8.4$  and 1.8 Hz), 7.09 (td, 1H,  $J = 7.8$  and 1.2 Hz), 6.64 (t, 1H,  $J = 8.4$  Hz), 6.50 (t, 1H,  $J = 7.2$  Hz), 4.21 (q, 2H,  $J = 7.2$  Hz), 3.89 (s, 3H), 1.25 (t, 3H,  $J = 7.2$  Hz);  $^{13}\text{C}\{^1\text{H}\}$  NMR (150 MHz,  $\text{CDCl}_3$ )  $\delta$  170.5, 142.8, 129.3, 127.8, 119.8, 118.3, 111.5, 61.5, 46.7, 14.2.

**Ethyl (3-chlorophenyl)glycinate (6e)** To a THF (5 mL) solution of ethyl 2-bromoacetate (220  $\mu\text{L}$ , 2 mmol), 3-chloroaniline (328 mg, 2 mmol) and  $\text{K}_2\text{CO}_3$  (830 mg, 6 mmol) were added. After refluxing for 24 h, the reaction mixture was diluted with ethyl acetate and the organic phase was washed with water and brine, dried over  $\text{MgSO}_4$ , and concentrated under reduced pressure. The residue was purified by flash column chromatography on silica gel (ethyl acetate / *n*-hexane = 1:10) to afford the ethyl (3-chlorophenyl)glycinate (**6e**) (274 mg, 64%).  $^1\text{H}$  NMR (600 MHz,  $\text{CDCl}_3$ )  $\delta$  7.04 (t, 1H,  $J = 8.4$  Hz), 6.67 (d, 1H,  $J = 7.8$  Hz), 6.54 (d, 1H,  $J = 1.8$  Hz), 6.46 (dd, 1H,  $J = 8.4$  and 2.4 Hz), 4.20 (q, 2H,  $J = 7.2$  Hz), 3.81 (s, 2H), 1.25 (t, 3H,  $J = 7.2$  Hz);  $^{13}\text{C}\{^1\text{H}\}$  NMR (150 MHz,  $\text{CDCl}_3$ )  $\delta$  170.5, 147.8, 135.1, 130.3, 118.4, 113.0, 111.7, 64.6, 45.7, 14.2.

**Ethyl (4-chlorophenyl)glycinate (6f)** To a THF (5 mL) solution of ethyl 2-bromoacetate (220  $\mu\text{L}$ , 2 mmol), 4-chloroaniline (255 mg, 2 mmol) and  $\text{K}_2\text{CO}_3$  (830 mg, 6 mmol) were added. After refluxing for 24 h, the reaction mixture was diluted with ethyl acetate and the organic phase was washed with water and brine, dried over  $\text{MgSO}_4$ , and concentrated under reduced pressure. The residue was purified by flash column chromatography on silica gel (ethyl acetate / *n*-hexane = 1 : 5) to afford the ethyl (4-chlorophenyl)glycinate (**6f**) (322 mg, 76%).  $^1\text{H}$  NMR (600 MHz,  $\text{CDCl}_3$ )  $\delta$  7.09 (d, 2H,  $J = 8.4$  Hz), 6.52 (m, 2H), 4.19 (q, 2H,  $J = 7.2$  Hz), 3.81 (s, 2H), 1.24 (t, 3H,  $J = 7.2$  Hz);  $^{13}\text{C}\{^1\text{H}\}$  NMR (150 MHz,  $\text{CDCl}_3$ )  $\delta$  170.6, 145.2, 129.9, 129.2, 114.6, 61.5, 46.2, 14.2.

**Ethyl [1,1'-biphenyl]-2-ylglycinate (6g)** To a THF (5 mL) solution of ethyl 2-bromoacetate (220  $\mu\text{L}$ , 2 mmol), 2-aminobiphenyl (340 mg, 2 mmol) and  $\text{K}_2\text{CO}_3$  (830 mg, 6 mmol) were added. After refluxing for 24 h, the reaction mixture was diluted with ethyl acetate and the organic phase was washed with water and brine, dried over  $\text{MgSO}_4$ , and concentrated under reduced pressure. The residue was purified by flash column chromatography on silica gel (ethyl acetate / *n*-hexane = 1 : 10) to afford ethyl [1,1'-biphenyl]-2-ylglycinate (**6g**) (100 mg, 19%).  $^1\text{H}$  NMR (600 MHz,  $\text{CDCl}_3$ )  $\delta$  7.50 (d, 4H,  $J = 4.2$  Hz), 7.41 (m, 1H), 7.29 (td, 1H,  $J = 7.8$  and 1.2 Hz), 7.18 (dd, 1H,  $J = 7.2$  and 1.2 Hz), 6.87 (td, 1H,  $J = 7.2$  and

0.6 Hz), 6.63 (d, 1H,  $J = 7.8$  Hz), 4.24 (q, 2H,  $J = 7.2$  Hz), 3.92 (s, 2H), 1.31 (t, 3H,  $J = 7.2$  Hz);  $^{13}\text{C}\{^1\text{H}\}$  NMR (150 MHz,  $\text{CDCl}_3$ )  $\delta$  171.0, 143.9, 139.1, 130.4, 129.3, 129.0, 128.7, 128.2, 127.4, 117.9, 110.5, 61.3, 45.9, 14.2.

**Ethyl (4-(tert-butyl)phenyl)glycinate (6h)** To a THF (5 mL) solution of ethyl 2-bromoacetate (322 mg, 2 mmol), 4-*tert*-butylaniline (315  $\mu\text{L}$ , 2 mmol) and  $\text{K}_2\text{CO}_3$  (830 mg, 6 mmol) were added. After refluxing for 24 h, the reaction mixture was diluted with ethyl acetate and the organic phase was washed with water and brine, dried over  $\text{MgSO}_4$ , and concentrated under reduced pressure. The residue was purified by flash column chromatography on silica gel (ethyl acetate / *n*-hexane = 1 : 10) to afford the ethyl (4-(*tert*-butyl)phenyl)glycinate (**6h**) (306 mg, 65%).  $^1\text{H}$  NMR (600 MHz,  $\text{CDCl}_3$ )  $\delta$  7.26 (d, 2H,  $J = 9$  Hz), 6.64 (m, 2H), 4.29 (q, 2H,  $J = 6.6$  Hz), 3.92 (s, 2H), 1.33 (t, 3H,  $J = 7.2$  Hz), 1.30 (s, 9H);  $^{13}\text{C}\{^1\text{H}\}$  NMR (150 MHz,  $\text{CDCl}_3$ )  $\delta$  171.2, 144.3, 141.4, 126.1, 113.1, 61.3, 46.3, 33.9, 31.5, 14.2.

**Ethyl (3-chloro-4-fluorophenyl)glycinate (6i)** To a THF (5 mL) solution of ethyl 2-bromoacetate (322 mg, 2 mmol), 3-chloro-4-fluoroaniline (291 mg, 2 mmol) and  $\text{K}_2\text{CO}_3$  (830 mg, 6 mmol) were added. After refluxing for 24 h, the reaction mixture was diluted with ethyl acetate and the organic phase was washed with water and brine, dried over  $\text{MgSO}_4$ , and concentrated under reduced pressure. The residue was purified by flash column chromatography on silica gel (ethyl acetate / *n*-hexane = 1 : 5) to afford the ethyl (3-chloro-4-fluorophenyl)glycinate (**6i**) (119 mg, 26%).  $^1\text{H}$  NMR (600 MHz,  $\text{CDCl}_3$ )  $\delta$  6.90 (t, 1H,  $J = 9$  Hz), 6.53 (dd, 1H,  $J = 6$  and 3 Hz), 6.38-6.35 (m, 1H), 4.19 (q, 2H,  $J = 7.2$  Hz), 3.77 (s, 2H), 1.24 (t, 3H,  $J = 7.2$  Hz);  $^{13}\text{C}\{^1\text{H}\}$  NMR (150 MHz,  $\text{CDCl}_3$ )  $\delta$  170.7, 152.2, 150.6, 144.0, 121.2, 116.9, 114.0, 112.3, 61.5, 46.1, 14.2.

**Ethyl (4-ethylphenyl)glycinate (6j)** To a THF (5 mL) solution of the ethyl 2-bromoacetate (322 mg, 2 mmol), 4-ethylaniline (249  $\mu\text{L}$ , 2 mmol) and  $\text{K}_2\text{CO}_3$  (830 mg, 6 mmol) were added. After refluxing for 24 h, the reaction mixture was diluted with ethyl acetate and the organic phase was washed with water and brine, dried over  $\text{MgSO}_4$ , and concentrated under reduced pressure. The residue was purified by flash column chromatography on silica gel (ethyl acetate / *n*-hexane = 1 : 10) to afford the ethyl (4-ethylphenyl)glycinate (**6j**) (245 mg, 59%).  $^1\text{H}$  NMR (600 MHz,  $\text{CDCl}_3$ )  $\delta$  7.07 (d, 2H,  $J = 8.4$  Hz), 6.62 (dd, 2H,  $J = 6.6$  and 2.4 Hz), 4.28 (q, 2H,  $J = 7.2$  Hz), 3.92 (s, 2H), 2.59 (q, 2H,  $J = 7.8$  Hz), 1.33 (t, 3H,  $J = 7.2$  Hz), 1.22 (t, 3H,  $J = 7.8$  Hz);  $^{13}\text{C}\{^1\text{H}\}$  NMR (150 MHz,  $\text{CDCl}_3$ )  $\delta$  171.2, 144.7, 134.4, 128.7, 113.4, 61.3, 46.4, 27.9, 15.9, 14.2.

**Ethyl (3,4-difluorophenyl)glycinate (6k)** To a THF (5 mL) solution of ethyl 2-bromoacetate (322 mg, 2 mmol), 3,4-difluoroaniline (258 mg, 2 mmol) and  $\text{K}_2\text{CO}_3$  (830 mg, 6 mmol) were added. After refluxing for 24 h, the reaction mixture was diluted with ethyl acetate and the organic phase was washed with water and brine, dried over  $\text{MgSO}_4$ , and concentrated under reduced pressure. The residue was purified by flash column chromatography on silica gel (ethyl acetate / *n*-hexane = 1 : 7) to afford the ethyl (3,4-difluorophenyl)glycinate (**6k**) (125 mg,



29%).  $^1\text{H}$  NMR (600 MHz,  $\text{CDCl}_3$ )  $\delta$  6.90 (q, 1H,  $J = 9$  Hz), 6.31 (dd, 1H,  $J = 6.6$  Hz), 6.19 (d, 1H,  $J = 9$  Hz), 4.24 (bs, 1H), 4.18 (q, 2H,  $J = 7.2$  Hz), 3.74 (s, 2H), 1.22 (td, 3H,  $J = 7.2$  and 1.2 Hz);  $^{13}\text{C}\{^1\text{H}\}$  NMR (150 MHz,  $\text{CDCl}_3$ )  $\delta$  170.7, 151.7, 150.0, 144.2, 144.1, 142.7, 117.5, 108.1, 101.7, 61.5, 46.0, 14.1.

**Ethyl (4-(pentyloxy)phenyl)glycinate (6l)** To a THF (5 mL) solution of ethyl 2-bromoacetate (322 mg, 2 mmol), 4-(pentyloxy)aniline (370  $\mu\text{L}$ , 2 mmol) and  $\text{K}_2\text{CO}_3$  (830 mg, 6 mmol) were added. After refluxing for 24 h, the reaction mixture was diluted with ethyl acetate and the organic phase was washed with water and brine, dried over  $\text{MgSO}_4$ , and concentrated under reduced pressure. The residue was purified by flash column chromatography on silica gel (ethyl acetate / *n*-hexane = 1 : 5) to afford the ethyl (4-(pentyloxy)phenyl)glycinate (**6l**) (171 mg, 32%).  $^1\text{H}$  NMR (600 MHz,  $\text{CDCl}_3$ )  $\delta$  6.71 (d, 2H,  $J = 8.9$  Hz), 6.51 (d, 2H,  $J = 8.9$  Hz), 4.16 (q, 2H,  $J = 7.1$  Hz), 3.96 (s, 1H), 3.81 (t, 2H,  $J = 6.6$  Hz), 3.78 (s, 2H), 1.71–1.64 (m, 2H), 1.39–1.27 (m, 3H), 1.21 (t, 4H,  $J = 7.1$  Hz), 0.86 (t, 3H,  $J = 7.2$  Hz).  $^{13}\text{C}\{^1\text{H}\}$  NMR (150 MHz,  $\text{CDCl}_3$ )  $\delta$  171.3, 152.1, 141.0, 115.6, 114.4, 68.6, 61.1, 46.8, 29.1, 28.2, 22.4, 14.1, 14.0.

**Ethyl (4-fluorophenyl)glycinate (6m)** To a THF (5 mL) solution of the ethyl 2-bromoacetate (322 mg, 2 mmol), 4-fluoroaniline (190  $\mu\text{L}$ , 2 mmol) and  $\text{K}_2\text{CO}_3$  (830 mg, 6 mmol) were added. After refluxing for 24 h, the reaction mixture was diluted with ethyl acetate and the organic phase was washed with water and brine, dried over  $\text{MgSO}_4$ , and concentrated under reduced pressure. The residue was purified by flash column chromatography on silica gel (ethyl acetate / *n*-hexane = 1 : 5) to afford the ethyl (4-fluorophenyl)glycinate (**6m**) (193 mg, 49%).  $^1\text{H}$  NMR (600 MHz,  $\text{CDCl}_3$ )  $\delta$  6.85 (d, 2H,  $J = 8.4$  Hz), 6.49 (dd, 2H,  $J = 9$  and 4.2 Hz), 4.19 (q, 2H,  $J = 7.2$  Hz), 3.79 (s, 2H), 1.24 (t, 3H,  $J = 7.2$  Hz);  $^{13}\text{C}\{^1\text{H}\}$  NMR (150 MHz,  $\text{CDCl}_3$ )  $\delta$  171.1, 157.0, 155.5, 143.4, 115.9, 113.9, 61.4, 46.5, 14.2.

**Ethyl (4-(trifluoromethoxy)phenyl)glycinate (6n)** To a THF (5 mL) solution of ethyl 2-bromoacetate (322 mg, 2 mmol), 4-(trifluoromethoxy)aniline (268  $\mu\text{L}$ , 2 mmol) and  $\text{K}_2\text{CO}_3$  (830 mg, 6 mmol) were added. After refluxing for 24 h, the reaction mixture was diluted with ethyl acetate and the organic phase was washed with water and brine, dried over  $\text{MgSO}_4$ , and concentrated under reduced pressure. The residue was purified by flash column chromatography on silica gel (ethyl acetate / *n*-hexane = 1:5) to afford the ethyl (4-(*tert*-butyl)phenyl)glycinate (**6n**) (134 mg, 25%).  $^1\text{H}$  NMR (600 MHz,  $\text{CDCl}_3$ )  $\delta$  7.08 (d, 2H,  $J = 8.4$  Hz), 6.58 (d, 2H,  $J = 9$  Hz), 4.44 (bs, 1H), 4.29 (q, 2H,  $J = 6.6$  Hz), 3.89 (s, 2H), 1.33 (t, 3H,  $J = 7.2$  Hz);  $^{13}\text{C}\{^1\text{H}\}$  NMR (150 MHz,  $\text{CDCl}_3$ )  $\delta$  170.9, 145.9, 141.0, 122.4, 121.5, 119.9, 113.2, 61.5, 45.8, 14.1.

**2,3-Diamino-6-propylpyrimidin-4(3H)-one (7a)** To a solution of NaOEt prepared from sodium (340 mg, 14.7 mmol) and ethanol (10 mL), aminoguanidine bicarbonate (2.0 g, 14.7 mmol) was added and the reaction was heated at 90 °C for 30 min. After NaCl filtering, ethyl 3-oxohexanoate (2.34 mL, 14.7 mmol) was added to the reaction mixture and heated at reflux for 15 h. The precipitate obtained was filtered and dried under vacuum to afford 2,3-diamino-6-

propylpyrimidin-4(3*H*)-one (**7a**) (515 mg, 21%). <sup>1</sup>H NMR (600 MHz, DMSO-*d*<sub>6</sub>) δ 7.07 (bs, 2H), 5.53 (s, 1H), 5.35 (m, 2H), 2.23 (t, 2H, *J* = 7.2 Hz), 1.57 (m, 2H), 0.88-0.85 (m, 3H); <sup>13</sup>C{<sup>1</sup>H} NMR (150 MHz, DMSO-*d*<sub>6</sub>) δ 166.8, 161.8, 156.0, 98.6, 39.3, 21.4, 14.0.

**2,3-Diamino-3,5,6,7-tetrahydro-4*H*-cyclopenta[*d*]pyrimidin-4-one (7b)** To a solution of NaOEt prepared from sodium (340 mg, 14.7 mmol) and ethanol (10 mL), aminoguanidine bicarbonate (2.0 g, 14.7 mmol) was added and the reaction was heated at 90 °C for 30 min. After NaCl filtering, ethyl 2-cyclopentane-1-carboxylate (2.12 mL, 14.7 mmol) was added to the reaction mixture and heated at reflux for 15 h. The precipitate obtained was filtered and dried under vacuum to afford 2,3-diamino-3,5,6,7-tetrahydro-4*H*-cyclopenta[*d*]pyrimidin-4-one (**7b**) (250 mg, 10%). <sup>1</sup>H NMR (600 MHz, DMSO-*d*<sub>6</sub>) δ 6.92 (bs, 2H), 5.30 (s, 2H), 2.56 (q, 4H, *J* = 9 Hz), 1.92 (m, 2H); <sup>13</sup>C{<sup>1</sup>H} NMR (150 MHz, DMSO-*d*<sub>6</sub>) δ 167.1, 158.6, 155.3, 108.3, 33.8, 26.6, 20.7.

**2,3-Diamino-6-isopropylpyrimidin-4(3*H*)-one (7c)** To a solution of NaOEt prepared from sodium (340 mg, 14.7 mmol) and ethanol (10 mL), aminoguanidine bicarbonate (2.0 g, 14.7 mmol) was added and the reaction was heated at 90 °C for 30 min. After NaCl filtering, ethyl 4-methyl-3-oxopentanoate (2.37 mL, 14.7 mmol) was added to the reaction mixture and heated at reflux for 15 h. The precipitate obtained was filtered and dried under vacuum to afford 2,3-diamino-6-isopropylpyrimidin-4(3*H*)-one (**7c**) (469 mg, 19%). <sup>1</sup>H NMR (600 MHz, DMSO-*d*<sub>6</sub>) δ 7.02 (bs, 2H), 5.53 (s, 1H), 5.32 (s, 2H), 2.50 (m, 1H), 1.10 (s, 3H), 1.09 (s, 3H); <sup>13</sup>C{<sup>1</sup>H} NMR (150 MHz, DMSO-*d*<sub>6</sub>) δ 170.8, 160.9, 155.0, 95.2, 34.4, 20.7.

**2,3-Diamino-6-methylpyrimidin-4(3*H*)-one (7d)** To a solution of NaOEt prepared from sodium (340 mg, 14.7 mmol) and ethanol (10 mL), aminoguanidine (2.0 g, 14.7 mmol) was added and the reaction was heated at 90 °C for 30 min. After NaCl filtering, ethyl 3-oxobutanoate (1.35 mL, 14.7 mmol) was added to the reaction mixture and heated at reflux for 15 h. The precipitate obtained was filtered and dried under vacuum to afford 2,3-diamino-6-methylpyrimidin-4(3*H*)-one (**7d**) (335 mg, 16%). <sup>1</sup>H NMR (600 MHz, DMSO-*d*<sub>6</sub>) δ 7.03 (bs, 2H), 5.52 (s, 1H), 5.30 (s, 2H), 1.99 (s, 3H); <sup>13</sup>C{<sup>1</sup>H} NMR (150 MHz, DMSO-*d*<sub>6</sub>) δ 162.4, 160.5, 154.8, 98.0, 22.9.

#### *FECH expression and assay*

*E. coli* cells expressing FECH were harvested after 20 hours' growth, lysed in a Tris-MOPS buffer and purified by immobilized metal affinity chromatography using HisPur Cobalt resin (Thermo Cat. No. 89965). Protein was dialyzed overnight in a Tris-MOPS buffer with 10% glycerol.

The activity assay buffer was 100 mM Tris-HCl pH 8.0 with 0.05% octyl glucoside detergent. Assay reagents included 100 μM NiCl (Sigma, St. Louis, MO, USA, Cat. No. 339350), 0.75 μM FECH enzyme and 100 μM mesoporphyrin IX (Sigma Cat. No. 258806) prepared in ammonium hydroxide (Santa Cruz,

Santa Cruz, CA, USA, Cat. No. sc-214535). FECH activity can be completely inhibited with 10  $\mu\text{M}$  NMPP (Santa Cruz Cat. No. sc-263846) and this was used as a positive control in the screen (Figure S1).

#### *Screening optimization*

A kinetic assay was optimized for a 384 well format. Each well contained a 50  $\mu\text{L}$  reaction with 40  $\mu\text{L}$  buffer, 5  $\mu\text{L}$  mesoporphyrin IX solution, 5  $\mu\text{L}$  NiCl and FECH solution. FECH activity was monitored by the formation of Ni<sup>2+</sup>-mesoporphyrin IX at 550 nm, and the slope was consistently linear over the first 20 minutes of the reaction (Figure S1). This time point was used for the chemical screen.

#### *Small molecule screen*

Initial screening took place at the Indiana University School of Medicine Chemical Genomics Core Facility (CGCF) using selected portions of the ChemDiv 10K library and the ChemBridge 50K library of chemical compounds assembled by the core facility. The compounds were diluted from parent plates with compounds in DMSO to our 384 well assay plate as 20  $\mu\text{L}$  of a 25  $\mu\text{M}$  solution in water for a final assay concentration of 10  $\mu\text{M}$  for each test compound. NMPP (2  $\mu\text{L}$ ) was added to two columns of wells on the assay plate left without compounds for a positive control. Two columns were also left without compounds to assay uninhibited FECH activity.

A mixture of assay buffer, NiCl and FECH enzyme (15  $\mu\text{L}$ ) was added to all wells on the assay plate using a MultiFlo dispenser. To start the reaction, 15  $\mu\text{L}$  of a 333  $\mu\text{M}$  mesoporphyrin solution in assay buffer was added to the plate, the plate spun down and the absorbance at OD = 550 nm immediately read on a SpectraMax 384 Plus (Molecular Devices, San Jose, CA, USA) (for the primary screen) or a Synergy H1 (BioTek, Winooski, VT, USA) (for follow-up screens) to establish a read at time 0. Plates were read for absorbance at OD = 550 nm again at  $t = 20$  minutes and the activity was expressed as the change in the absorbance over the 20-minute reaction.

#### *IC<sub>50</sub> determination*

Hit compounds, reordered from ChemDiv (San Diego, CA, USA), were made to 10 mM in DMSO and tested in the FECH enzymatic assay at final concentrations of 100 pM to 100  $\mu\text{M}$  (1% final DMSO concentration). IC<sub>50</sub> values for the compounds were determined using Prism software (GraphPad, San Diego, CA, USA).

#### *Cell-based GI<sub>50</sub> determination*

The cell proliferation assays were performed as previously described (Basavarajappa et al., 2017). Briefly, primary HRECs, induced pluripotent stem cell-derived choroidal endothelial cells (iCEC2), or ARPE19 RPE cells were plated at 2500 cells/well in 100  $\mu\text{L}$  medium in the center of a 96 well black with clear bottom tissue culture treated plate and allowed to attach overnight. The cells were dosed with compounds ranging from 100 pM to 100  $\mu\text{M}$  as 1  $\mu\text{L}$  of a

100x stock of compound per well in triplicate. Cells proliferated for 44 hours prior to addition of alamarBlue (BioRad, Hercules, CA, USA, Cat. No. BUF012B). Fluorescence readings of the wells were taken at excitation of 560 nm and emission of 590 nm. GI<sub>50</sub> values were determined using Prism software.

#### *Tube formation assay*

The Matrigel-based tube formation assay was performed as previously described (Basavarajappa et al., 2017). Briefly, 50  $\mu$ L Matrigel was allowed to solidify in a 96 well black, clear bottom plate at 37°C for 20 minutes. HRECs were added to the solid Matrigel at 15,000 cells/well in 100  $\mu$ L EGM-2 and dosed with appropriate concentrations of compound in DMSO, 1  $\mu$ L/well. Tube formation was observed every 2 hours by brightfield microscopy and images were taken after 8 hours of tube formation. Six images per treatment were analyzed using the AngiogenesisAnalyzer plugin for ImageJ (Carpentier et al., 2020) and HREC total tubule length for treated cells was normalized to DMSO controls.

#### *Protoporphyrin IX buildup assay*

Because FECH inserts Fe<sup>2+</sup> into its substrate PPIX during heme synthesis, a buildup of fluorescent PPIX in cells is an effective metric of FECH inhibition (Basavarajappa et al., 2017). To detect PPIX accumulation in HRECs, cells were dosed with heme precursor compound 5-ALA to increase the total flux through the heme biosynthetic pathway. HRECs were thus incubated with FECH inhibitors for 1 hour and 1 mM 5-ALA was added to the cells and incubated for another 2 hours. Cells were then lysed with RIPA buffer on ice and centrifuged at 12,000 g for 15 minutes to isolate cell lysates. 15  $\mu$ L of the lysate was added in triplicate to a black 384 well plate and PPIX was extracted with 15  $\mu$ L of 2M perchloric acid:methanol solution added to the wells and the plate shaken and read immediately at ex. 406 nm and em. 610 nm. PPIX in the lysates was quantified as pmol/mg protein by comparison to PPIX standards and cell lysate protein concentration (determined by Bradford assay).

#### *Scratch wound migration assay*

The scratch wound assay was also described previously (Basavarajappa et al., 2017). HRECs were allowed to grow to confluency in a 96 well plate at 37°C. A scratch was introduced down the center of the well with a 10  $\mu$ L micropipette tip. Cell migration across the gap was observed by brightfield microscopy (EVOS/fl, AMG, Mill Creek, WA, USA) and images were taken after 8 hours. Six images per treatment were analyzed by manually counting cells that migrated into the scratch with these tallies for treated cells normalized to DMSO controls. Replicate experiments were imaged using an IncuCyte Live imaging system (Essen Biosciences, Ann Arbor, MI, USA), with similar manual analysis.

#### *Immunoblot*

HRECs were plated and split into three groups. Group one was treated with 100  $\mu$ M succinylacetone (SA) (Sigma Cat. No. D1415) for 6 hours and subsequently treated with DMSO, 10  $\mu$ M NMPP, or 10, 30 or 100  $\mu$ M **4e** for 16

hours. Group two was treated with water (vehicle for SA) for 6 hours and then treated with the same compounds as group one for 16 hours. Group three was treated with compounds for 16 hours as with previous groups and then medium was aspirated and replaced with EBM-2 with 0.2% serum and 10  $\mu$ M hemin (Sigma Cat. No. H9039) prepared fresh in DMSO. Immunoblots were performed as described previously (Basavarajappa et al., 2017; Shetty et al., 2020). HRECs were lysed for 15 min on ice in RIPA buffer (Sigma Cat. No. R0278) with protease and phosphatase inhibitors added (Roche, Indianapolis, IN, USA, Cat. No. 4693132001, Cat. No. 4906845001) and then centrifuged at 12,000  $g$  for 15 min at 4°C. Supernatant was collected and protein concentration was determined using a Bradford assay. Protein samples (40  $\mu$ g) were resolved by 12% SDS-PAGE and transferred onto PVDF membranes. Proteins were immunoblotted with antibodies against cytochrome *c* oxidase COXIV subunit 1 (COX4I1; Thermo Fisher Cat. No. PA5-19471) (1:1000) and  $\beta$ -actin (Sigma Cat. No. A5316) (1:2000). All of the dilutions were made in Tris-buffered saline buffer containing 2.5% bovine serum albumin (BSA).

#### *Porphyrin analysis*

HRECs were grown to 80% confluency in 10 cm dishes, serum starved overnight, and treated with either DMSO or 30  $\mu$ M **4e** for 1 hour and then either 1 mM 5-ALA or vehicle (water) for an additional 2 hours. Cells were pelleted in cold PBS and pellets were frozen. Heme and porphyrin analysis was performed at the Iron and Heme Core facility at the University of Utah according to their posted core protocols (<http://cihd.cores.utah.edu/ironheme/#1467136333172-56f37fbb-2816>).

#### *In vitro apoptosis assays*

Treated HRECs were assayed for apoptosis by cleaved caspase-3 staining and by using a TUNEL assay to identify double stranded DNA breaks. For both assays, HRECs were seeded in 8 well Nunc™ Lab-Tek™ II Chamber Slides (Thermo Fisher) after the chamber growth surface was coated in Attachment Factor (Cell Systems Cat. No. 4Z0-210). HRECs were grown to 70% confluency and then treated with DMSO (vehicle), positive control (1  $\mu$ M staurosporine for cleaved caspase-3 staining or 10  $\mu$ M DNase I for TUNEL assay), 10  $\mu$ M, 30  $\mu$ M, and 100  $\mu$ M **4e** with one condition per chamber for 16 hours. Six slides in total were prepared in this manner using 3 different passages of HRECs. After overnight treatment, the cells were fixed in 4% paraformaldehyde. For cleaved caspase-3 staining, the fixed cells were then permeabilized using 0.5% Triton X-100 solution prepared in PBS. The cells were incubated with a 1:200 dilution of cleaved caspase-3 (5A1E) antibody (Cell Signaling, Danvers, MA, USA; Cat. No. 9664) in 1% BSA in PBS overnight at 4°C. Slides were washed and incubated for 1 hour in the dark with AlexaFluor 555-conjugated goat anti-rabbit secondary antibody (Invitrogen, Carlsbad, CA, USA, Cat. No. A21428) prepared at 1:400 in 1% BSA in PBS. The secondary antibody was aspirated and nuclei were stained with Hoechst 33342. Cells were washed thrice more. Coverslips were mounted using EverBrite mounting media (Biotium, Fremont, CA, USA, Cat. No. 23001). For the TUNEL assay, directions were followed for the Click-iT TUNEL Alexa

Fluor 594 Imaging Assay (Thermo Fisher Cat. No. C10246). Stained cells were imaged using an Axio Imager (Zeiss, Jena, Germany) and counted manually. Three 40x objective fields were recorded for each cell treatment per experiment and stained cells were expressed as a percentage of the total cells (stained nuclei) counted. The full experiment was done with three independent biological repetitions.

#### *Cocrystal structure determination*

The R115L mutant of human FECH (residues 61-423) cloned in pET-28a in *E. coli* was induced with 0.1 mM IPTG for 20 h at 303 K. The cells were harvested and resuspended in binding buffer (50 mM Tris-HCl pH 8.0, 0.1 M KCl, 1% Na cholate, 1 mM PMSF). The cells were sonicated for 3 min and the lysate was then collected by centrifugation at 18,000xg for 30 min at 277 K. The supernatant was loaded onto Ni-NTA beads for 1 h and eluted. After repeating the Ni-NTA bead purification, the protein purity was suitable for crystallization. Red crystals of FECH R115L mutant were obtained in hanging drops by mixing 22 mg/mL protein solution with an equal volume of reservoir solution (0.1 M PCB buffer pH 5.6, PEG 3350 15%). For soaking ligands and cryoprotection, crystals were moved into a reservoir solution containing 1 mM ligand and 25% glycerol for 1 day and flash-cooled in liquid nitrogen. Data sets were collected at 100 K using the Eiger 9M detector at PAL beamline, 5C, Pohang, Korea and Eiger 16M detector at SPring-8 beamline, BL44XU, Hyogo, Japan. All data sets were processed with XDS (Kabsch, 2010). The crystal structures of FECH:ligand complexes were solved by the molecular replacement method in Phenix software (Adams et al., 2010) with FECH-salicylic acid complex structure (PDB ID 3W1W) as a search model. Structure refinement was carried out using Phenix and Coot (Emsley et al., 2010). Data collection and refinement statistics are summarized in Table 4. The molecular representations in this paper were created by PyMOL (Schrodinger LLC, 2015).

#### *4e-FECH enzyme kinetic analysis*

FECH activity assay was run as described above with varying concentrations of mesoporphyrin substrate (0, 3, 10, 30, 100, 300, 100  $\mu$ M) and varying concentrations of **4e** (0, 0.03, 0.1, 0.3, 1, 3, 10  $\mu$ M) with 0.75  $\mu$ M FECH and 100  $\mu$ M NiCl. A Ni-mesoporphyrin IX (Frontier, Logan, UT, USA; Cat. No. M40146) solution was used to generate standards. The reaction was read for 45 minutes and Ni-mesoporphyrin IX product formed in 20 min (within the linear phase) was calculated based on Ni-mesoporphyrin IX standards. Product formed in  $\mu$ M/min was plotted against concentration of substrate for each concentration of **4e** tested. Michaelis-Menten analysis was conducted in Prism.

#### *Laser-induced choroidal neovascularization (L-CNV)*

L-CNV was performed as described previously (Basavarajappa et al., 2017; Sardar Pasha et al., 2018). Briefly, mice were anesthetized for all procedures by intraperitoneal (i.p.) injections of 80 mg/kg ketamine hydrochloride and 10 mg/kg xylazine mixture. Pupils were dilated with drops of 1% tropicamide and 2.5% phenylephrine. After 5 mins of dilation, 2.5% hydroxypropyl methylcellulose

ophthalmic solution (Gonak, Akorn, Lake Forest, IL, USA) was applied to the cornea. The fundus was viewed with an imaging camera and laser burns were introduced using a green argon laser (Micron IV, Phoenix Research Laboratories, Pleasanton, CA, USA). Orientation on the fundus was obtained by centering the optic nerve on the field of view and adjusting the focus until the strands of the nerve fiber layer or pigment of the retinal pigment epithelium were in focus in all quadrants. Each eye received up to 4 laser burns surrounding the optic nerve. Laser burns were focused at 1-2 optic disk diameters from the optic disk. Laser was set to 50  $\mu$ m diameter, wavelength 532 nm, laser duration 70 ms, and laser power of 240 mW.

#### *Compound preparation and intravitreal injections*

Triazolopyrimidinone **4e** was dissolved in DMSO to 100 mM and was then diluted into PBS solution up to 1 mM (final [DMSO] = 0.5%). For mice, injecting 0.5  $\mu$ L of a 0.5 or 1 mM aqueous solution of **4e**, we estimate a final intravitreal concentration of 50 or 100  $\mu$ M compound in adult mice (based on an average vitreous volume of approximately 5  $\mu$ L (Kaplan et al., 2010)).

Compound was delivered via an intravitreal injection immediately after laser induction while mice were still anesthetized. All instruments were sterilized before starting the procedures. Eyes were locally anesthetized with proparacaine eyedrops. A small incision was made at the nasal ora serrata (approximately 4 mm below the iris) to get access to the posterior chamber with the use of a 30-G insulin syringe needle. High precision sterile Hamilton syringes (0.5–5  $\mu$ L volume) with a sharp 33-G beveled tip were used for injections. 0.5  $\mu$ L of vehicle with or without **4e** was injected intravitreally at an angle of about 45-60° towards the plane of injection. The needle was kept in place for 1 min to prevent the reflux of solution when the needle was removed. Triple antibiotic ointment was used immediately after the injection to prevent infection.

#### *Fundus imaging, OCT imaging, and fluorescein angiography*

OCT and fundus imaging were performed on day 7 and day 14 after L-CNV on the Micron IV OCT2 system. OCT images were taken as a cube of multiple vertical and horizontal slices through each lesion. Fluorescein angiography (FA) was performed to determine the vascular leakage on day 14 after L-CNV. For this, 50  $\mu$ L of 12.5% fluorescein sodium (Fisher Scientific Acros, Fair Lawn, NJ, USA; Cat. No. 173241000) was injected i.p. and fundus images were taken using the Micron IV system with the GFP filter set.

Analysis of OCT images was done by modeling the lesions as ellipsoids. ImageJ was used to measure the maximum dimensions of the lesion in all three planes based on OCT images. Volumes were then calculated using the equation  $V = 4/3 \pi abc$  (Sulaiman et al., 2015).

#### *Choroidal flatmounts and staining*

Flatmounting and staining were performed according to a protocol described previously (Merrigan et al., 2020; Sardar Pasha et al., 2018) and summarized

here. After FA, 14 days after L-CNV induction, mice were euthanized by isoflurane overdose and eyes were harvested. The eyes were enucleated and fixed in 4% paraformaldehyde/PBS overnight. After dissection the posterior eye cups were prepared for choroidal flat mounts. The posterior eye cups were washed with PBS and permeabilized in blocking buffer containing 0.3% Triton X-100 and 5% bovine serum albumin (BSA) in PBS for 2 hours at 4°C. The eye cups were then double stained for vasculature with rhodamine-labeled *Ricinus communis* agglutinin I (Vector Laboratories, Burlingame, CA, USA) and Alexa Fluor 488-conjugated-Isolectin B4 from *Griffonia simplicifolia* (GS-IB4) (Molecular Probes/Thermo Fisher Scientific) at 1:250 dilution in buffer containing 0.3% Triton X-100, 0.5% BSA in PBS for 24-48 hours at 4°C. After antibody incubation, whole mounts were washed three times with PBS for 15 minutes. After washing, tissue was mounted in Fluoromount-G aqueous mounting medium (SouthernBiotech, Birmingham, AL, USA; Cat. No. 0100-01) to a Superfrost Plus Microscope Slide (Fisher Scientific) and cover-slipped.

#### *Confocal imaging and lesion quantification*

An LSM 700 (Zeiss) confocal microscope was used to image choroidal flat mounts stained with agglutinin (red channel) and GS-IB4 (green channel) with an objective power of 20x (Merrigan et al., 2020; Sardar Pasha et al., 2018). Three images through the largest, central section of the lesion were taken with a gap of 3 µm between images. ImageJ was used to calculate the area of staining in each image. The volume was calculated by averaging the stained area of each image and multiplying by the total depth of the images (6 µm). Lesions were only included for analysis if they met quality control standards (Poor et al., 2014), namely (1) circular or oval, not linear, lesions; and (2) not the only usable lesion in an eye. Additional exclusion criteria for lesions included bleeding, no FA leakage, retinal detachment, merged lesions, failure to form CNV lesion, lesions with volumes greater than twice the next largest lesion, and lesions with volumes smaller than half the next smallest lesion.

#### *Off-target analysis*

The SAFETYscan E/IC<sub>50</sub> ELECT assay of 78 targets was performed by Eurofins DiscoverX Corporation (San Diego, CA, USA).

## **QUANTIFICATION AND STATISTICAL ANALYSIS**

Data are presented as mean ± SEM; n is listed and defined in figure legends. One-way ANOVA was used with Dunnett's post-hoc test to compare three or more treatment groups, while Student's t-test was used to compare two treatment groups. Two-sided p-values < 0.05 were treated as significant. Sample sizes for animal experiments were based on power analyses. All statistical analyses and graphical analyses were performed using Prism 9 software (GraphPad).



## SUPPLEMENTAL INFORMATION

**Supplemental Information.** Contains Figures S1 and S2, Tables S1–S5, and chemical characterization data.

**Supplemental Dataset S1. Structures of confirmed hits,** Related to Figure 1

## REFERENCES

Adams, P.D., Afonine, P.V., Bunkoczi, G., Chen, V.B., Davis, I.W., Echols, N., Headd, J.J., Hung, L.W., Kapral, G.J., Grosse-Kunstleve, R.W., *et al.* (2010). PHENIX: a comprehensive Python-based system for macromolecular structure solution. *Acta Crystallogr D Biol Crystallogr* 66, 213-221.

Amo, T., Kawanishi, N., Uchida, M., Fujita, H., Oyanagi, E., Utsumi, T., Ogino, T., Inoue, K., Shuin, T., Utsumi, K., *et al.* (2009). Mechanism of cell death by 5-aminolevulinic acid-based photodynamic action and its enhancement by ferrochelatase inhibitors in human histiocytic lymphoma cell line U937. *Cell Biochem Funct* 27, 503-515.

Baell, J.B., and Holloway, G.A. (2010). New substructure filters for removal of pan assay interference compounds (PAINS) from screening libraries and for their exclusion in bioassays. *J Med Chem* 53, 2719-2740.

Basavarajappa, H.D., Sulaiman, R.S., Qi, X., Shetty, T., Sheik Pran Babu, S., Sishtla, K.L., Lee, B., Quigley, J., Alkhairy, S., Briggs, C.M., *et al.* (2017). Ferrochelatase is a therapeutic target for ocular neovascularization. *EMBO Mol Med* 9, 786-801.

Bennett, M.L., Fleischer, A.B., Loveless, J.W., and Feldman, S.R. (2000). Oral griseofulvin remains the treatment of choice for tinea capitis in children. *Pediatr Dermatol* 17, 304-309.

Bhasin, G., Kausar, H., and Athar, M. (2002). Protoporphyrin-IX accumulation and cutaneous tumor regression in mice using a ferrochelatase inhibitor. *Cancer Lett* 187, 9-16.

Burden, A.E., Wu, C., Dailey, T.A., Busch, J.L., Dhawan, I.K., Rose, J.P., Wang, B., and Dailey, H.A. (1999). Human ferrochelatase: crystallization, characterization of the [2Fe-2S] cluster and determination that the enzyme is a homodimer. *Biochim Biophys Acta* 1435, 191-197.

Carpentier, G., Berndt, S., Ferratge, S., Rasband, W., Cuendet, M., Uzan, G., and Albanese, P. (2020). Angiogenesis Analyzer for ImageJ - A comparative morphometric analysis of "Endothelial Tube Formation Assay" and "Fibrin Bead Assay". *Sci Rep* 10, 11568.

Chelakkot, V.S., Liu, K., Yoshioka, E., Saha, S., Xu, D., Licursi, M., Dorward, A., and Hirasawa, K. (2020). MEK reduces cancer-specific PpIX accumulation through the RSK-ABCB1 and HIF-1 $\alpha$ -FECH axes. *Sci Rep* 10, 22124.

Dailey, H.A., and Fleming, J.E. (1983). Bovine ferrochelatase. Kinetic analysis of inhibition by N-methylprotoporphyrin, manganese, and heme. *J Biol Chem* 258, 11453-11459.

El-Gendy, M.M., Shaaban, M., Shaaban, K.A., El-Bondkly, A.M., and Laatsch, H. (2008). Essramycin: a first triazolopyrimidine antibiotic isolated from nature. *J Antibiot (Tokyo)* 61, 149-157.

Emsley, P., Lohkamp, B., Scott, W.G., and Cowtan, K. (2010). Features and development of Coot. *Acta Crystallogr D Biol Crystallogr* 66, 486-501.

Fukuhara, H., Inoue, K., Kurabayashi, A., Furihata, M., Fujita, H., Utsumi, K., Sasaki, J., and Shuin, T. (2013). The inhibition of ferrochelatase enhances 5-aminolevulinic acid-based photodynamic action for prostate cancer. *Photodiagnosis Photodyn Ther* 10, 399-409.

Grossniklaus, H.E., Kang, S.J., and Berglin, L. (2010). Animal models of choroidal and retinal neovascularization. *Prog Retinal Eye Res* 29, 500-519.

Halloy, F., Iyer, P.S., Ghidini, A., Lysenko, V., Barman-Aksozen, J., Grubenmann, C.P., Jucker, J., Wildner-Verhey van Wijk, N., Ruepp, M.D., Minder, E.I., *et al.* (2021). Repurposing of glycine transport inhibitors for the treatment of erythropoietic protoporphyria. *Cell Chem Biol* 28, 1221-1234 e1226.

Hamza, I., and Dailey, H.A. (2012). One ring to rule them all: trafficking of heme and heme synthesis intermediates in the metazoans. *Biochim Biophys Acta* 1823, 1617-1632.

Hazama, M., Iwakami, N., and Yashiro, H. (2008). Screening Method. Patent Application, WO 2008/010511.

Hubbard, R.E., and Kamran Haider, M. (2010). Hydrogen bonds in proteins: role and strength. *eLS*,  
10.1002/9780470015902.a9780470003011.pub9780470015902.

Husain, S. (2018). Delta opioids: neuroprotective roles in preclinical studies. *J Ocul Pharmacol Ther* 34, 119-128.

Inoue, K., Fukuhara, H., Kurabayashi, A., Furihata, M., Tsuda, M., Nagakawa, K., Fujita, H., Utsumi, K., and Shuin, T. (2013). Photodynamic therapy involves an antiangiogenic mechanism and is enhanced by ferrochelatase inhibitor in urothelial carcinoma. *Cancer Sci* 104, 765-772.

Kabsch, W. (2010). Xds. *Acta Crystallogr D Biol Crystallogr* 66, 125-132.

Kaplan, H.J., Chiang, C.-W., Chen, J., and Song, S.-K. (2010). Vitreous volume of the mouse measured by quantitative high-resolution MRI. *Invest Ophthalmol Vis Sci* 43, E-abstract 4414.

Kemmner, W., Wan, K., Ruttinger, S., Ebert, B., Macdonald, R., Klamm, U., and Moesta, K.T. (2008). Silencing of human ferrochelatase causes abundant protoporphyrin-IX accumulation in colon cancer. *FASEB J* 22, 500-509.

Klaeger, S., Gohlke, B., Perrin, J., Gupta, V., Heinzlmeir, S., Helm, D., Qiao, H., Bergamini, G., Handa, H., Savitski, M.M., *et al.* (2016). Chemical proteomics reveals ferrochelatase as a common off-target of kinase inhibitors. *ACS Chem Biol* 11, 1245-1254.

Lecha, M., Puy, H., and Deybach, J.C. (2009). Erythropoietic protoporphyria. *Orphanet J Rare Dis* 4, 19.

Lelliott, P.M., McMorran, B.J., Foote, S.J., and Burgio, G. (2015). The influence of host genetics on erythrocytes and malaria infection: is there therapeutic potential? *Malar J* 14, 289.

Liu, K., Yan, J., Sachar, M., Zhang, X., Guan, M., Xie, W., and Ma, X. (2015). A metabolomic perspective of griseofulvin-induced liver injury in mice. *Biochem Pharmacol* 98, 493-501.

Lux, A., Llacer, H., Heussen, F.M., and Jousseaume, A.M. (2007). Non-responders to bevacizumab (Avastin) therapy of choroidal neovascular lesions. *Br J Ophthalmol* 91, 1318-1322.

Magness, S.T., Maeda, N., and Brenner, D.A. (2002). An exon 10 deletion in the mouse ferrochelatase gene has a dominant-negative effect and causes mild protoporphyria. *Blood* 100, 1470-1477.

Medlock, A.E., Dailey, T.A., Ross, T.A., Dailey, H.A., and Lanzilotta, W.N. (2007). A pi-helix switch selective for porphyrin deprotonation and product release in human ferrochelatase. *J Mol Biol* 373, 1006-1016.

Merrigan, S.L., Park, B., Ali, Z., Jensen, L.D., Corson, T.W., and Kennedy, B.N. (2020). Calcitriol and non-calcemic vitamin D analogue, 22-oxacalcitriol, attenuate developmental and pathological choroidal vasculature angiogenesis *ex vivo* and *in vivo*. *Oncotarget* 11, 493-509.

Miyake, M., Ishii, M., Kawashima, K., Kodama, T., Sugano, K., Fujimoto, K., and Hirao, Y. (2009). siRNA-mediated knockdown of the heme synthesis and degradation pathways: modulation of treatment effect of 5-aminolevulinic acid-based photodynamic therapy in urothelial cancer cell lines. *Photochem Photobiol* 85, 1020-1027.

- Nagaraj, V.A., Sundaram, B., Varadarajan, N.M., Subramani, P.A., Kalappa, D.M., Ghosh, S.K., and Padmanaban, G. (2013). Malaria parasite-synthesized heme is essential in the mosquito and liver stages and complements host heme in the blood stages of infection. *PLoS Pathog* 9, e1003522.
- Najahi-Missaoui, W., and Dailey, H.A. (2005). Production and characterization of erythropoietic protoporphyrin heterodimeric ferrochelatases. *Blood* 106, 1098-1104.
- Nomura, J., Yanase, S., Tokuda, T., Matsumura, Y., Sekida, M., and Tagawa, T. (2006). Griseofulvin enhances the effect of aminolevulinic acid-based photodynamic therapy in vitro. *Photomed Laser Surg* 24, 186-191.
- Peppin, J.F., and Raffa, R.B. (2015). Delta opioid agonists: a concise update on potential therapeutic applications. *J Clin Pharm Ther* 40, 155-166.
- Poor, S.H., Qiu, Y., Fassbender, E.S., Shen, S., Woolfenden, A., Delpero, A., Kim, Y., Buchanan, N., Gebuhr, T.C., Hanks, S.M., *et al.* (2014). Reliability of the mouse model of choroidal neovascularization induced by laser photocoagulation. *Invest Ophthalmol Vis Sci* 55, 6525-6534.
- Pran Babu, S.P.S., White, D., and Corson, T.W. (2020). Ferrochelatase regulates retinal neovascularization. *FASEB J* 34, 12419-12435.
- Sardar Pasha, S.P.B., Shetty, T., Lambert-Cheatham, N.A., Sishtla, K., Mathew, D., Muniyandi, A., Patwari, N., Bhatwadekar, A.D., and Corson, T.W. (2021). Retinal phenotyping of ferrochelatase mutant mice reveals protoporphyrin accumulation and reduced neovascular response. *Invest Ophthalmol Vis Sci* 62, 36.
- Sardar Pasha, S.P.B., Sishtla, K., Sulaiman, R.S., Park, B., Shetty, T., Shah, F., Fishel, M.L., Wikel, J.H., Kelley, M.R., and Corson, T.W. (2018). Ref-1/APE1 inhibition with novel small molecules blocks ocular neovascularization. *J Pharmacol Exp Ther* 367, 108-118.
- Schrodinger LLC (2015). The PyMOL Molecular Graphics System.
- Shetty, T., Sishtla, K., Park, B., Repass, M.J., and Corson, T.W. (2020). Heme synthesis inhibition blocks angiogenesis via mitochondrial dysfunction. *iScience* 23, 101391.
- Smith, C.M., Jerkovic, A., Puy, H., Winship, I., Deybach, J.C., Gouya, L., van Dooren, G., Goodman, C.D., Sturm, A., Manceau, H., *et al.* (2015). Red cells from ferrochelatase-deficient erythropoietic protoporphyria patients are resistant to growth of malarial parasites. *Blood* 125, 534-541.
- Smith, C.M., Jerkovic, A., Truong, T.T., Foote, S.J., McCarthy, J.S., and McMorran, B.J. (2017). Griseofulvin impairs intraerythrocytic growth of

Plasmodium falciparum through ferrochelatase inhibition but lacks activity in an experimental human infection study. *Sci Rep* 7, 41975.

Sulaiman, R.S., Quigley, J., Qi, X., O'Hare, M.N., Grant, M.B., Boulton, M.E., and Corson, T.W. (2015). A simple optical coherence tomography quantification method for choroidal neovascularization. *J Ocul Pharmacol Ther* 31, 447-454.

Taketani, S., and Tokunaga, R. (1981). Rat liver ferrochelatase. Purification, properties, and stimulation by fatty acids. *J Biol Chem* 256, 12748-12753.

Tan, W.C., Krasner, N., O'Toole, P., and Lombard, M. (1997). Enhancement of photodynamic therapy in gastric cancer cells by removal of iron. *Gut* 41, 14-18.

Teng, L., Nakada, M., Zhao, S.G., Endo, Y., Furuyama, N., Nambu, E., Pyko, I.V., Hayashi, Y., and Hamada, J.I. (2011). Silencing of ferrochelatase enhances 5-aminolevulinic acid-based fluorescence and photodynamic therapy efficacy. *Br J Cancer* 104, 798-807.

Tutois, S., Montagutelli, X., Da Silva, V., Jouault, H., Rouyer-Fessard, P., Leroy-Viard, K., Guenet, J.L., Nordmann, Y., Beuzard, Y., and Deybach, J.C. (1991). Erythropoietic protoporphyria in the house mouse. A recessive inherited ferrochelatase deficiency with anemia, photosensitivity, and liver disease. *J Clin Invest* 88, 1730-1736.

Vieth, M., Siegel, M.G., Higgs, R.E., Watson, I.A., Robertson, D.H., Savin, K.A., Durst, G.L., and Hipkind, P.A. (2004). Characteristic physical properties and structural fragments of marketed oral drugs. *J Med Chem* 47, 224-232.

Voigt, A.P., Mulfaul, K., Mullin, N.K., Flamme-Wiese, M.J., Giacalone, J.C., Stone, E.M., Tucker, B.A., Scheetz, T.E., and Mullins, R.F. (2019). Single-cell transcriptomics of the human retinal pigment epithelium and choroid in health and macular degeneration. *Proc Natl Acad Sci U S A* 116, 24100-24107.

Voigt, A.P., Whitmore, S.S., Lessing, N.D., DeLuca, A.P., Tucker, B.A., Stone, E.M., Mullins, R.F., and Scheetz, T.E. (2020). Spectacle: An interactive resource for ocular single-cell RNA sequencing data analysis. *Exp Eye Res* 200, 108204.

Walters, W.P. (2012). Going further than Lipinski's rule in drug design. *Expert Opin Drug Discov* 7, 99-107.

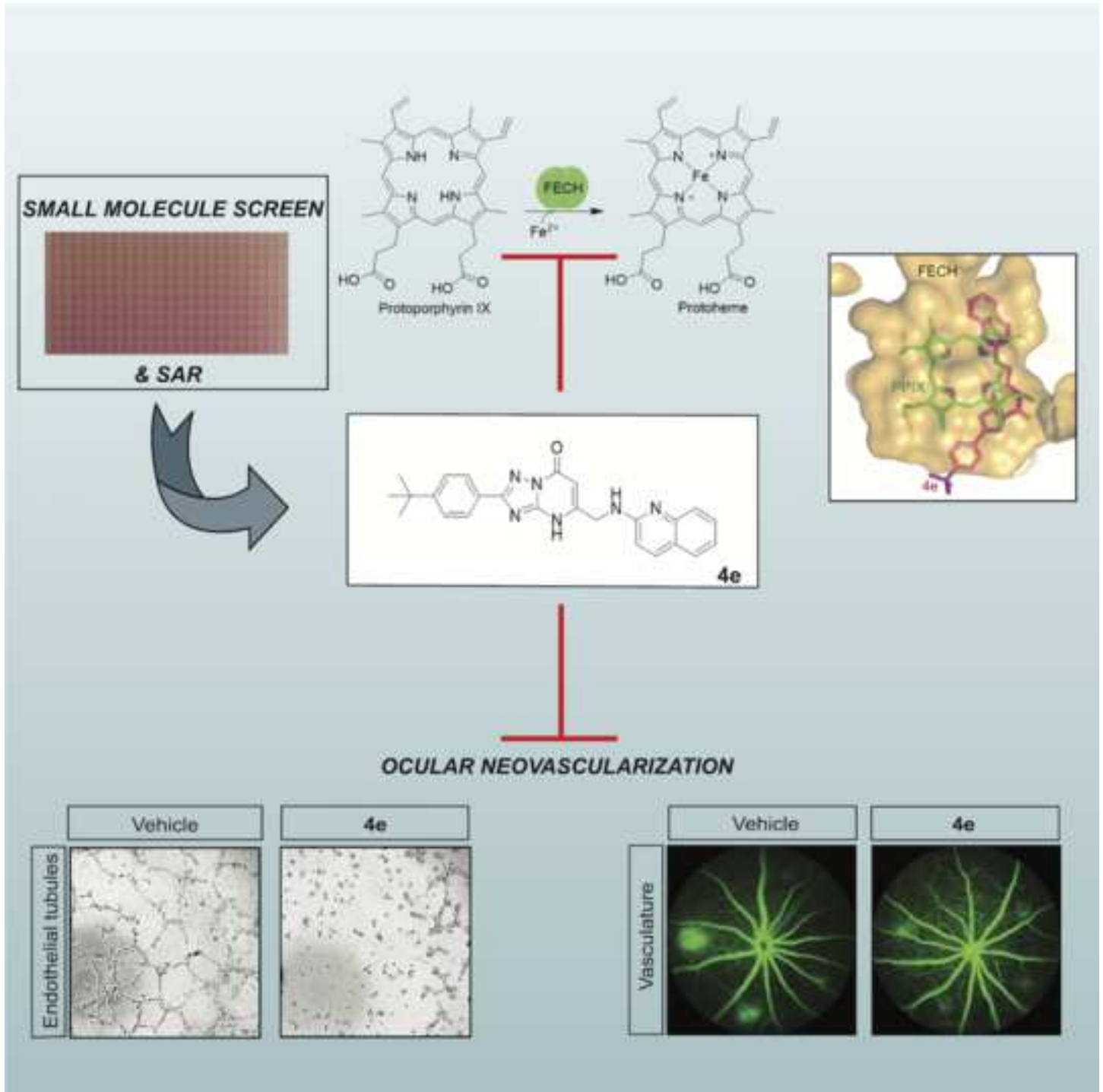
Wang, T., Yang, S., Li, H., Lu, A., Wang, Z., Yao, Y., and Wang, Q. (2020). Discovery, structural optimization, and mode of action of essramycin alkaloid and its derivatives as anti-tobacco mosaic virus and anti-phytopathogenic fungus agents. *J Agric Food Chem* 68, 471-484.

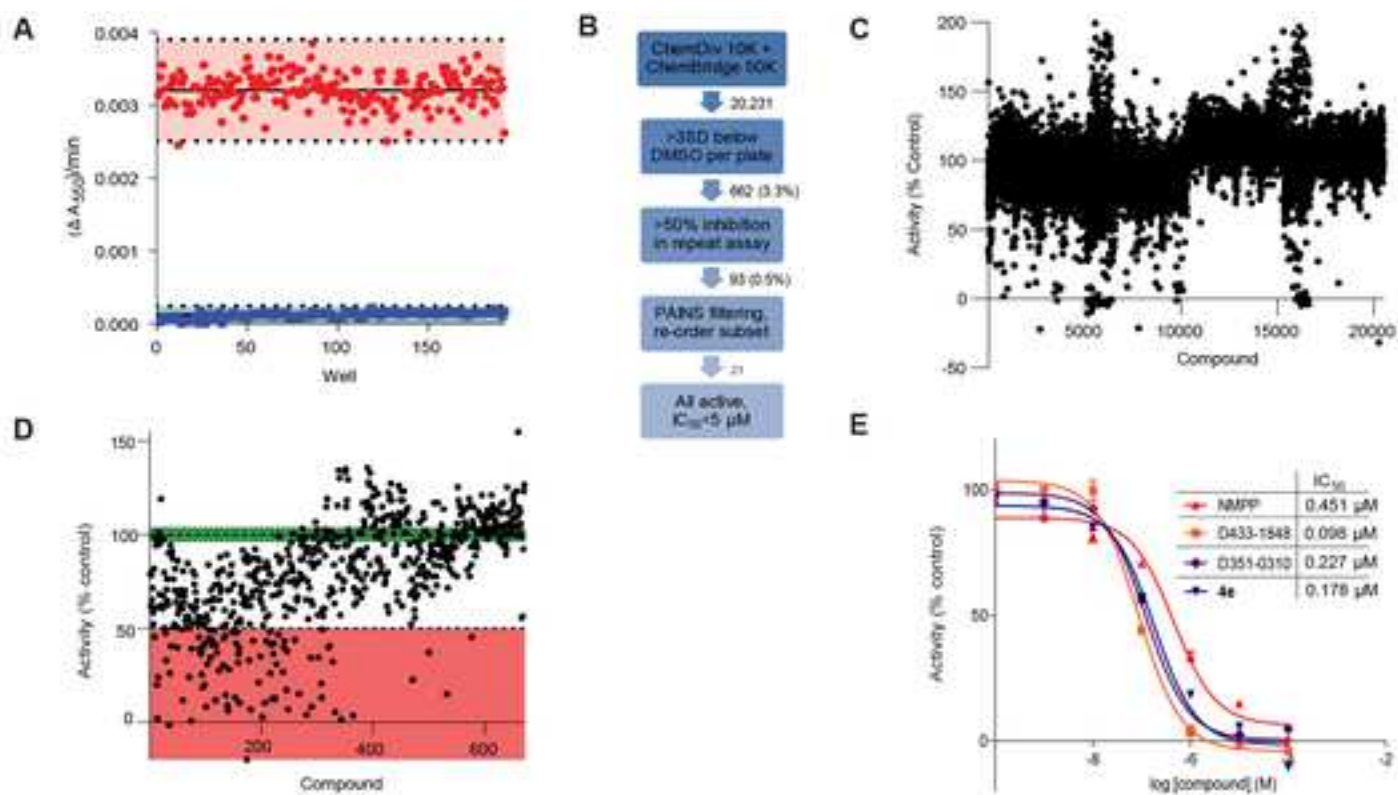
Wenzel, A.A., O'Hare, M.N., Shadmard, M., and Corson, T.W. (2015). Optical coherence tomography enables imaging of tumor initiation in the TAg-RB mouse model of retinoblastoma. *Mol Vis* 21, 515-522.

Yamamizu, K., Furuta, S., Hamada, Y., Yamashita, A., Kuzumaki, N., Narita, M., Doi, K., Katayama, S., Nagase, H., Yamashita, J.K., *et al.* (2013). Kappa opioids inhibit tumor angiogenesis by suppressing VEGF signaling. *Sci Rep* 3, 3213.

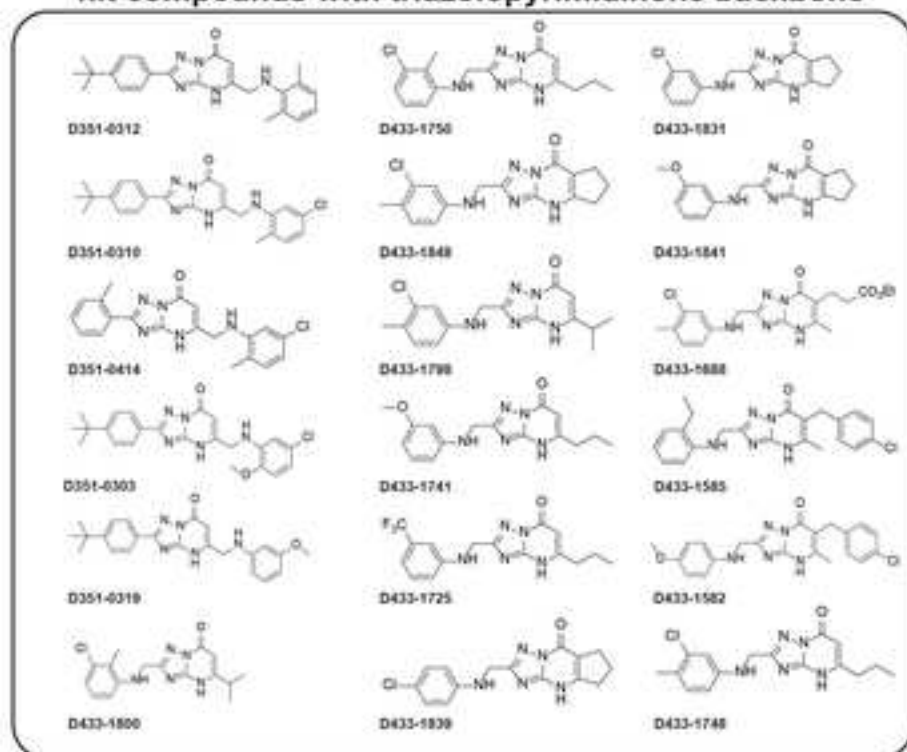
Yang, X., Li, W., Palasuberniam, P., Myers, K.A., Wang, C., and Chen, B. (2015a). Effects of silencing heme biosynthesis enzymes on 5-aminolevulinic acid-mediated protoporphyrin IX fluorescence and photodynamic therapy. *Photochem Photobiol* 91, 923-930.

Yang, X., Palasuberniam, P., Kraus, D., and Chen, B. (2015b). Aminolevulinic acid-based tumor detection and therapy: molecular mechanisms and strategies for enhancement. *Int J Mol Sci* 16, 25865-25880.

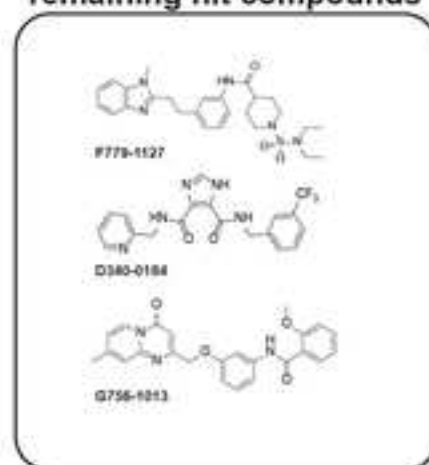




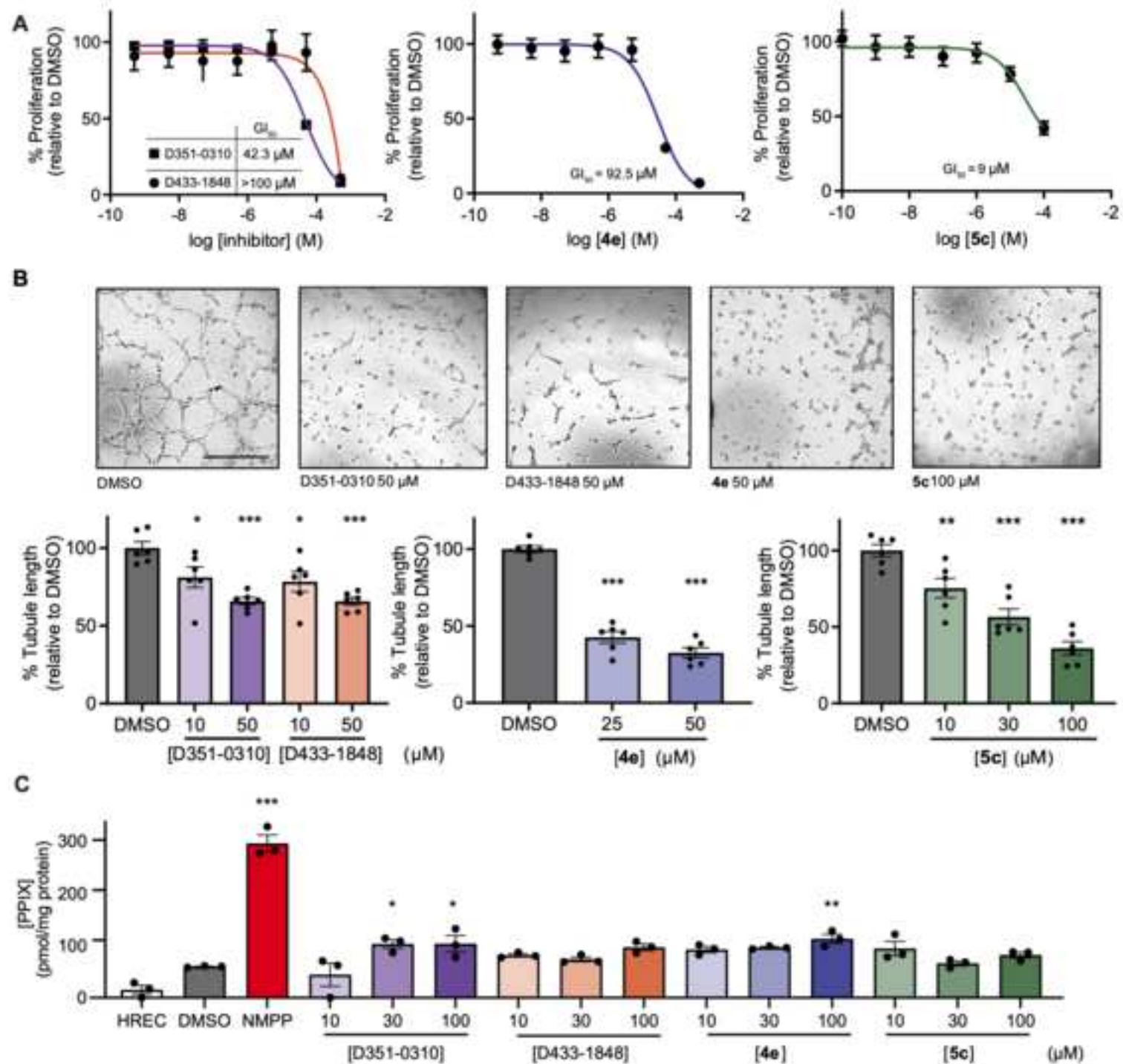
**F** hit compounds with triazolopyrimidinone backbone

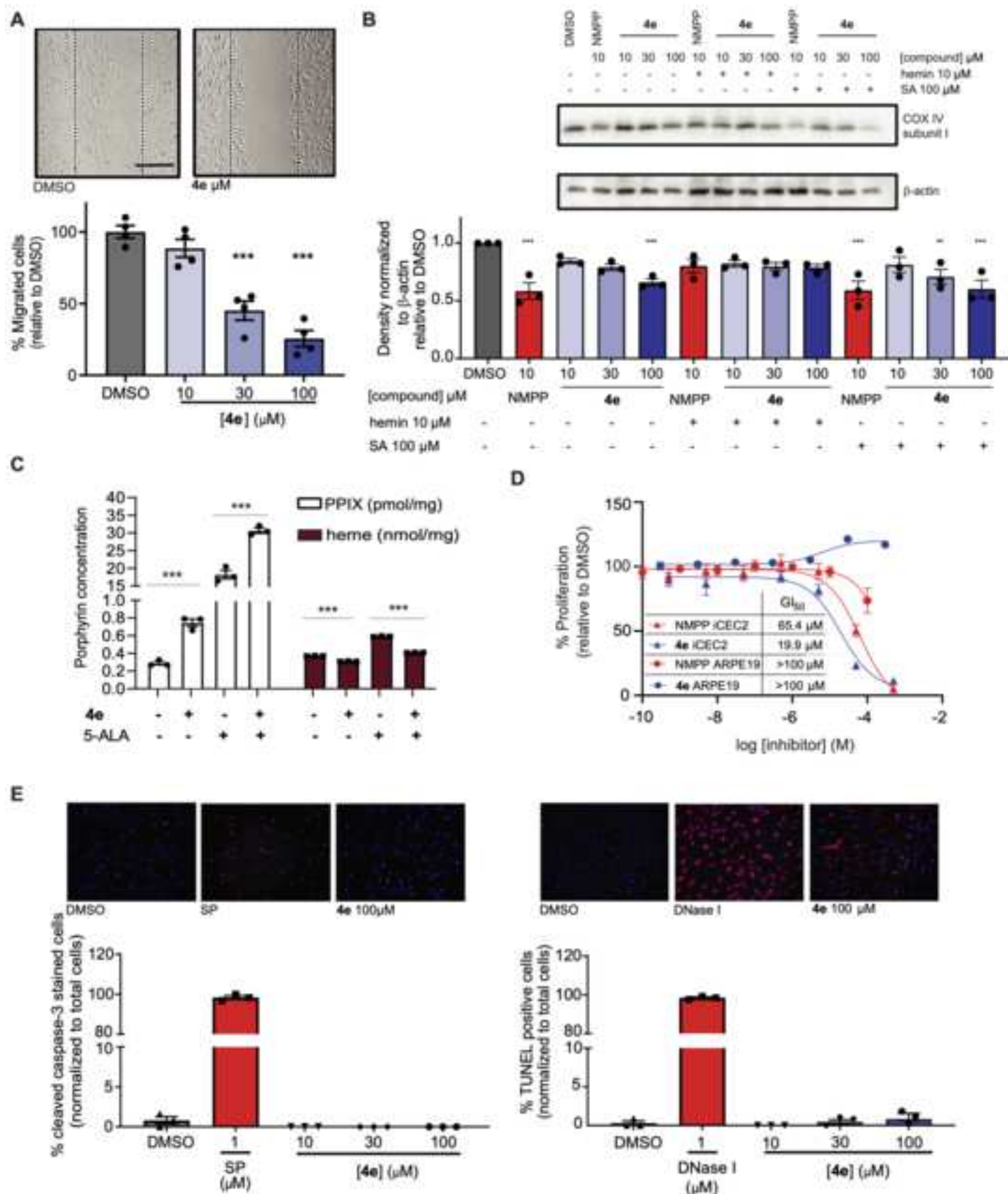


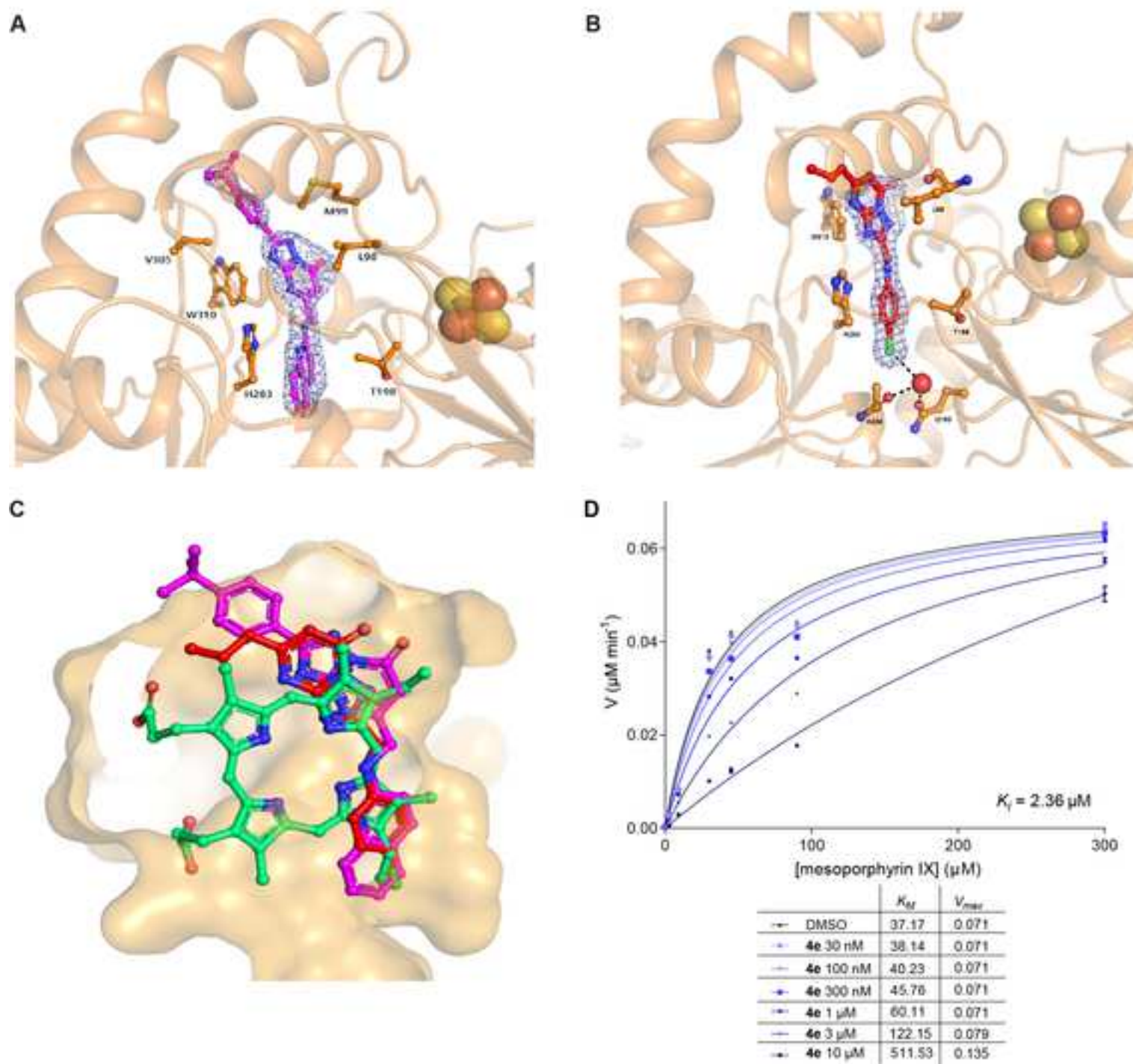
remaining hit compounds



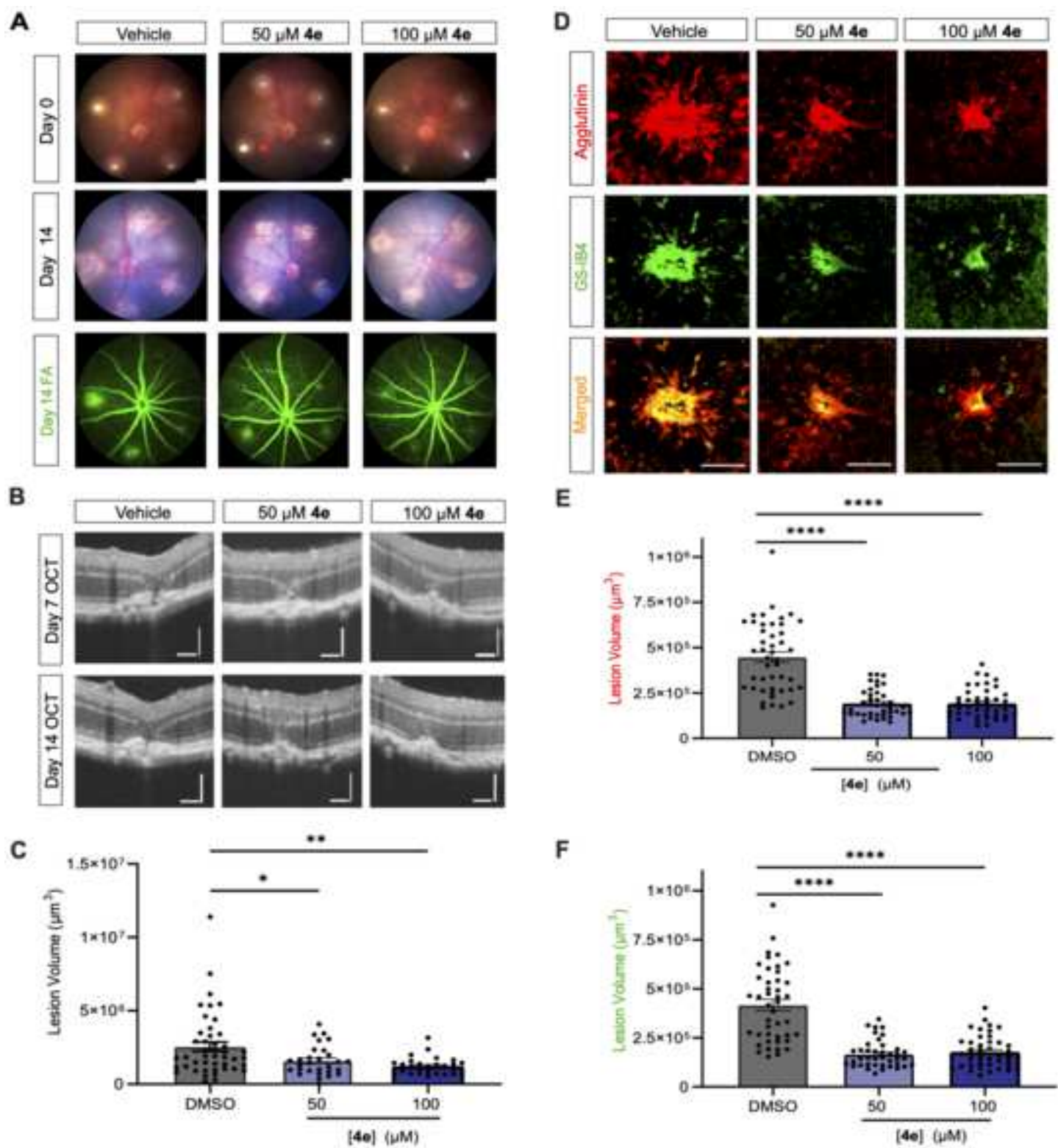


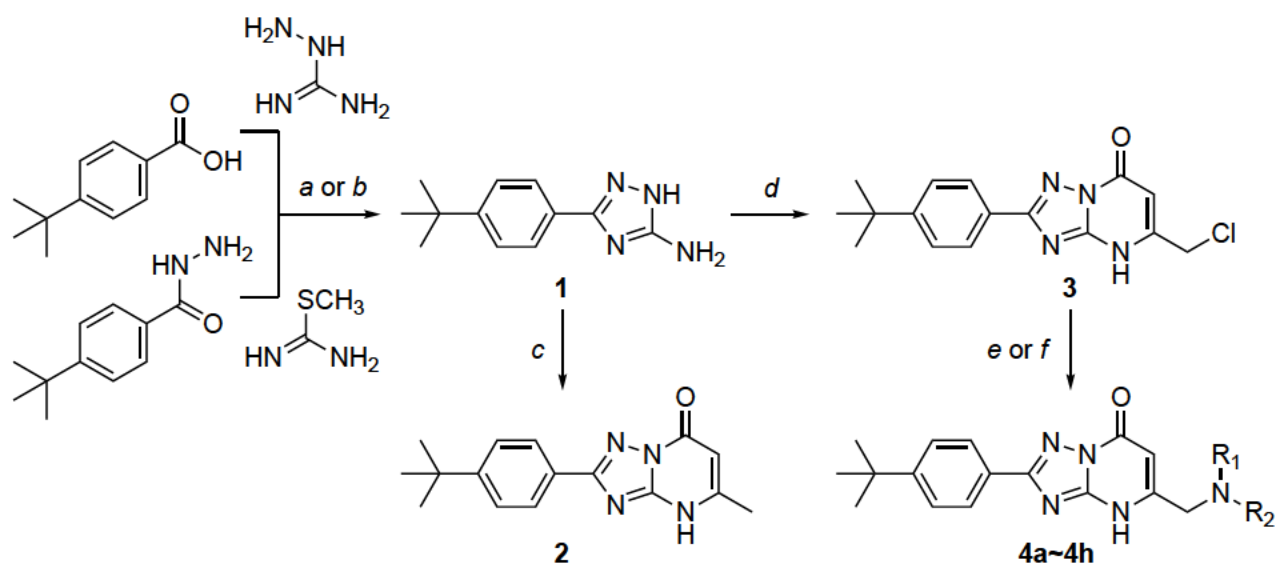


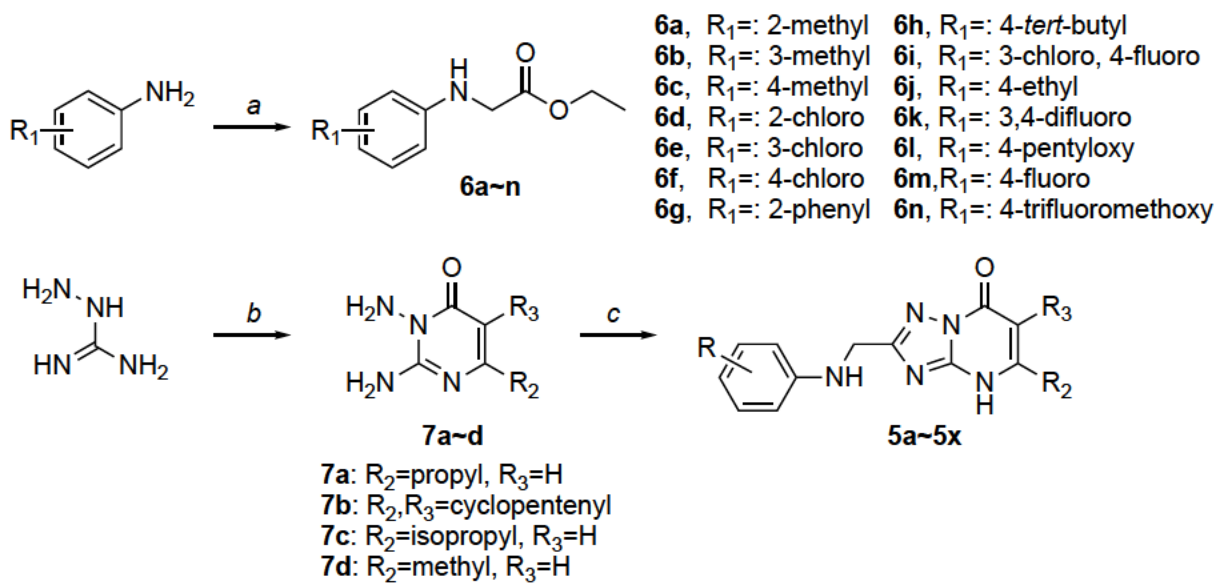












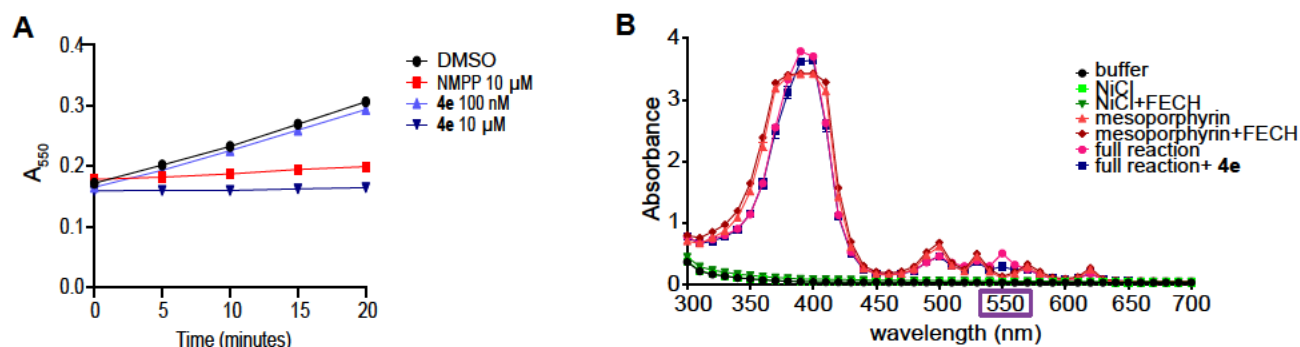


**Figure S1. FECH screening assay in detail**, Related to Figure 1

(A) Representative kinetic traces from screen showing inhibition of FECH activity over time with NMPP and 10  $\mu$ M **4e**. Absorbance at 550 nm measured over 20 minutes.

(B) Spectra traces of FECH assay with 10  $\mu$ M **4e** inhibition and all assay components. At 550 nm, components do not contribute to absorbance. A clean peak is observed with the full reaction mixture and that peak is diminished when **4e** is added. Data from individual wells shown.

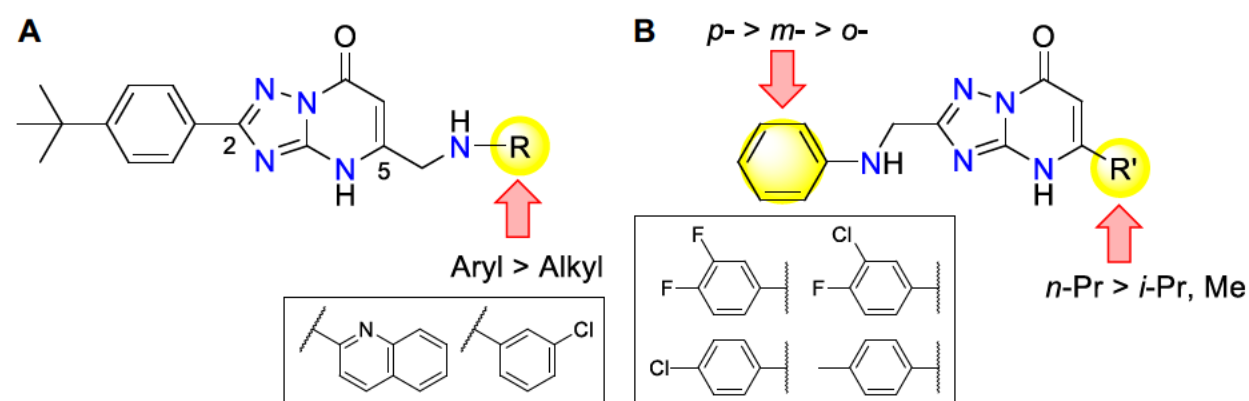


**Figure S2. Overview of SAR strategies and findings**, Related to Schemes 1 and 2

(A) 4-series triazolopyrimidinones modified on C5.

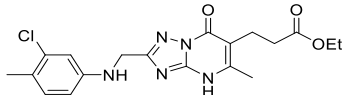
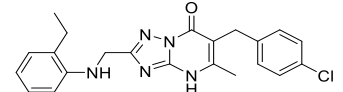
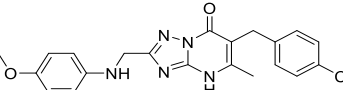
(B) 5-series triazolopyrimidinones modified on C2.

**Table S1.** Selected triazolopyrimidinone FECH inhibitor screening hits, with IC<sub>50</sub> against recombinant FECH and GI<sub>50</sub> against proliferation of HRECs. (ND = no data), Related to Figures 1 and 2

Library ID	Structure	FECH IC <sub>50</sub> (μM)	GI <sub>50</sub> on HRECs (μM)
D351-0414		0.346	>100
D351-0310		0.0981	42.3
D351-0312		1.39	>100
D351-0303		0.808	21.7
D351-0319		0.491	>100
D433-1741		2.86	1.61
D433-1725		4.39	1.17
D433-1750		2.15	>100
D433-1748		0.570	>100
D433-1800		0.751	ND
D433-1798		1.02	>100
D433-1831		1.57	>100
D433-1841		3.75	>100
D433-1839		1.05	81.5
D433-1848		0.227	>100



1  
2  
3  
4  
5  
6  
7  
8  
9  
10  
11  
12  
13  
14  
15  
16  
17  
18  
19  
20  
21  
22  
23  
24  
25  
26  
27  
28  
29  
30  
31  
32  
33  
34  
35  
36  
37  
38  
39  
40  
41  
42  
43  
44  
45  
46  
47  
48  
49  
50  
51  
52  
53  
54  
55  
56  
57  
58  
59  
60  
61  
62  
63  
64  
65

D433-1688		2.99	>100
D433-1585		1.25	74.6
D433-1582		0.0614	>100

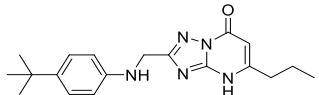
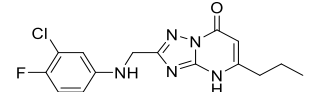
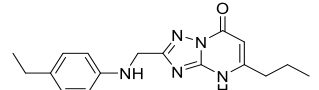
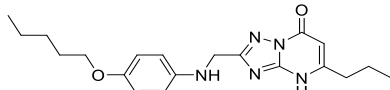
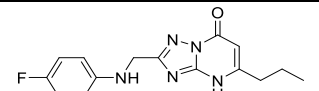
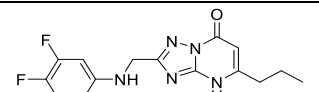
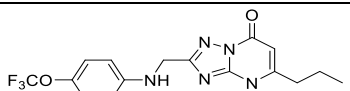
**Table S2.** Synthetic triazolopyrimidinones, with IC<sub>50</sub> against recombinant FECH and GI<sub>50</sub> against proliferation of HRECs, Related to Figure 2

Compound	Structure	FECH IC <sub>50</sub> (μM)	GI <sub>50</sub> on HRECs (μM)
<b>1</b>		>100	>100
<b>2</b>		>100	>100
<b>3</b>		>100	>100
<b>4a</b>		>100	>100
<b>4b</b>		>100	>100
<b>4c</b>		>100	>100
<b>4d</b>		>100	>100
<b>4e</b>		0.178	92.5
<b>4f</b>		>100	>100
<b>4g</b>		>100	>100
<b>4h</b>		0.511	>100

**Table S3.** Further synthetic triazolopyrimidinones, with IC<sub>50</sub> against recombinant FECH and GI<sub>50</sub> against proliferation of HRECs, Related to Figure 2

Compound	Structure	FECH IC <sub>50</sub> (μM)	GI <sub>50</sub> on HRECs (μM)
<b>5a</b>		92.0	75.5
<b>5b</b>		0.508	>100
<b>5c</b>		0.293	28.3
<b>5d</b>		>100	25.7
<b>5e</b>		0.346	>100
<b>5f</b>		0.0916	>100
<b>5o</b>		>100	>100
<b>5p</b>		9.34	>100
<b>5q</b>		3.62	>100
<b>5r</b>		17.9	>100
<b>5s</b>		28.1	>100
<b>5t</b>		16.8	>100
<b>5u</b>		77.2	>100
<b>5v</b>		18.7	>100
<b>5x</b>		22.5	>100
<b>5g</b>		27.3	>100

1  
2  
3  
4  
5  
6  
7  
8  
9  
10  
11  
12  
13  
14  
15  
16  
17  
18  
19  
20  
21  
22  
23  
24  
25  
26  
27  
28  
29  
30  
31  
32  
33  
34  
35  
36  
37  
38  
39  
40  
41  
42  
43  
44  
45  
46  
47  
48  
49  
50  
51  
52  
53  
54  
55  
56  
57  
58  
59  
60  
61  
62  
63  
64  
65

<b>5h</b>		>100	3.80
<b>5i</b>		0.0336	>100
<b>5j</b>		10.6	>100
<b>5l</b>		78.0	>100
<b>5m</b>		0.525	>100
<b>5k</b>		0.0429	>100
<b>5n</b>		34.1	>100

**Table S4.** Data collection and refinement statistics, Related to Figure 4

Data sets	FECH-5f complex	FECH-4e complex
Cell dimensions	$P2_12_12_1$	$P2_12_12_1$
$a, b, c$ (Å)	88.6, 93.8, 108.5	88.7, 93.7, 109.0
$\alpha, \beta, \gamma$ (°)	90.0, 90.0, 90.0	90.0, 90.0, 90.0
Wavelength (Å)	0.9790	0.9790
Resolution (Å)	2.0 (2.07-2.0)	2.0 (2.06-1.99)
No. reflections		
Observed	316,112 (31,477)	272,827 (27,152)
Unique	61,481 (6057)	61,965 (5753)
Redundancy*	5.1 (5.2)	4.4 (4.3)
Completeness (%)#	99.4 (99.4)	98.5 (92.4)
$I / \sigma(I)$	16.1 (2.4)	22.4 (2.1)
$R_{\text{merge}}^{\$}$	0.057 (0.772)	0.058 (0.660)
CC1/2	0.999 (0.919)	0.999 (0.911)
$R_{\text{p.m}}$	0.027 (0.364)	0.031 (0.350)
Refinement		
Resolution (Å)	2.0	2.0
$R / R_{\text{free}}^{**}$	0.191/0.222	0.207/0.221
rms deviation from ideal		
Bond lengths (Å)	0.007	0.009
Bond angles (°)	0.81	1.05
Ramachandran plot (%)		
Favored	96.9	97.2
Outliers	0.0	0.14
Rotamer outliers (%)	1.54	0.15
Clash score	4.21	5.58

Numbers in parentheses are given for the highest resolution shell. \*Redundancy is the number of observed reflections for each independent reflection. #Completeness in a percentage of independent reflections observed.  $R_{\text{merge}}^{\$}$  :  $\frac{\sum_{hi} \sum_i |I(h,i) - \langle I(h) \rangle|}{\sum_{hi} \sum_i I(h,i)}$ , where  $I(h,i)$  is the intensity value of the  $i$ th measurement of  $h$  and  $\langle I(h) \rangle$  is the corresponding mean value of  $I(h)$  for all  $i$  measurements; the summation is over the reflections with  $I/\sigma_I$  larger than -3.0.  $R_{\text{free}}^{**}$  is a free  $R$  factor of the refinement evaluated for the 10% of reflections that are excluded from the refinement.

**Table S5.** SafetyScan results for compound **4e**, Related to Figure 5

Target Class	Assay Name	Assay Target	Mode	Result Type	Value Prefix	RC <sub>50</sub> (μM)	Hill	Curve Bottom	Curve Top	Max Response
GPCR	Calcium Flux	ADORA2A	Agonist	EC <sub>50</sub>	>	100				4.72
GPCR	Calcium Flux	ADRA1A	Agonist	EC <sub>50</sub>	>	100				1.21
GPCR	Calcium Flux	AVPR1A	Agonist	EC <sub>50</sub>	>	100				7.18
GPCR	Calcium Flux	CCKAR	Agonist	EC <sub>50</sub>	>	100				0.21
GPCR	Calcium Flux	CHRM1	Agonist	EC <sub>50</sub>	>	100				0
GPCR	Calcium Flux	CHRM3	Agonist	EC <sub>50</sub>	>	100				0
GPCR	Calcium Flux	EDNRA	Agonist	EC <sub>50</sub>	>	100				0
GPCR	Calcium Flux	HRH1	Agonist	EC <sub>50</sub>	>	100				4.08
GPCR	Calcium Flux	HTR2A	Agonist	EC <sub>50</sub>	>	100				0
GPCR	Calcium Flux	HTR2B	Agonist	EC <sub>50</sub>	>	100				0
GPCR	Calcium Flux	ADORA2A	Antagonist	IC <sub>50</sub>	>	100				14.9
GPCR	Calcium Flux	ADRA1A	Antagonist	IC <sub>50</sub>	>	100				6.14
GPCR	Calcium Flux	AVPR1A	Antagonist	IC <sub>50</sub>	>	100				15.94
GPCR	Calcium Flux	CCKAR	Antagonist	IC <sub>50</sub>	>	100				1.88
GPCR	Calcium Flux	CHRM1	Antagonist	IC <sub>50</sub>	>	100				0
GPCR	Calcium Flux	CHRM3	Antagonist	IC <sub>50</sub>	>	100				0
GPCR	Calcium Flux	EDNRA	Antagonist	IC <sub>50</sub>	>	100				8.36
GPCR	Calcium Flux	HRH1	Antagonist	IC <sub>50</sub>	>	100				0
GPCR	Calcium Flux	HTR2A	Antagonist	IC <sub>50</sub>	>	100				0
GPCR	Calcium Flux	HTR2B	Antagonist	IC <sub>50</sub>	>	100				0
GPCR	cAMP	ADRA2A	Agonist	EC <sub>50</sub>	>	100				4.14
GPCR	cAMP	ADRB1	Agonist	EC <sub>50</sub>	>	100				0
GPCR	cAMP	ADRB2	Agonist	EC <sub>50</sub>	>	100				0
GPCR	cAMP	CHRM2	Agonist	EC <sub>50</sub>	>	100				34.46
GPCR	cAMP	CNR1	Agonist	EC <sub>50</sub>	>	100				37.9
GPCR	cAMP	CNR2	Agonist	EC <sub>50</sub>	>	100				40.8
GPCR	cAMP	DRD1	Agonist	EC <sub>50</sub>	>	100				0
GPCR	cAMP	DRD2S	Agonist	EC <sub>50</sub>	=	98.06407	0.57	0	100	53.12
GPCR	cAMP	HRH2	Agonist	EC <sub>50</sub>	>	100				0
GPCR	cAMP	HTR1A	Agonist	EC <sub>50</sub>	>	100				38.1
GPCR	cAMP	HTR1B	Agonist	EC <sub>50</sub>	>	100				27.67
GPCR	cAMP	OPRD1	Agonist	EC <sub>50</sub>	=	0.4734	2.28	-4.4	95.45	105.2
GPCR	cAMP	OPRK1	Agonist	EC <sub>50</sub>	>	100				30.81
GPCR	cAMP	OPRM1	Agonist	EC <sub>50</sub>	>	100				26.31

1	GPCR	cAMP	ADRA2A	Antagonist	IC <sub>50</sub>	>	100			0
2	GPCR	cAMP	ADRB1	Antagonist	IC <sub>50</sub>	>	100			41.8
3	GPCR	cAMP	ADRB2	Antagonist	IC <sub>50</sub>	>	100			42.53
4	GPCR	cAMP	CHRM2	Antagonist	IC <sub>50</sub>	>	100			0
5	GPCR	cAMP	CNR1	Antagonist	IC <sub>50</sub>	>	100			0
6	GPCR	cAMP	CNR2	Antagonist	IC <sub>50</sub>	>	100			0
7	GPCR	cAMP	DRD1	Antagonist	IC <sub>50</sub>	>	100			31.71
8	GPCR	cAMP	DRD2S	Antagonist	IC <sub>50</sub>	>	100			0
9	GPCR	cAMP	HRH2	Antagonist	IC <sub>50</sub>	>	100			39.06
10	GPCR	cAMP	HTR1A	Antagonist	IC <sub>50</sub>	>	100			0
11	GPCR	cAMP	HTR1B	Antagonist	IC <sub>50</sub>	>	100			0
12	GPCR	cAMP	OPRD1	Antagonist	IC <sub>50</sub>	>	100			0
13	GPCR	cAMP	OPRK1	Antagonist	IC <sub>50</sub>	>	100			0
14	GPCR	cAMP	OPRM1	Antagonist	IC <sub>50</sub>	>	100			0
15	Ion Channel	Ion Channel	CAV1.2	Blocker	IC <sub>50</sub>	>	100			3.68
16	Ion Channel	Ion Channel	GABAA	Blocker	IC <sub>50</sub>	>	100			12.03
17	Ion Channel	Ion Channel	hERG	Blocker	IC <sub>50</sub>	>	100			12.55
18	Ion Channel	Ion Channel	HTR3A	Blocker	IC <sub>50</sub>	>	100			0
19	Ion Channel	Ion Channel	KvLQT1/mi nK	Blocker	IC <sub>50</sub>	>	100			25.34
20	Ion Channel	Ion Channel	nAChR(a4/ b2)	Blocker	IC <sub>50</sub>	>	100			15.82
21	Ion Channel	Ion Channel	NAV1.5	Blocker	IC <sub>50</sub>	>	100			36.79
22	Ion Channel	Ion Channel	NMDAR (1A/2B)	Blocker	IC <sub>50</sub>	>	100			37.04
23	Ion Channel	Ion Channel	GABAA	Opener	EC <sub>50</sub>	>	100			0.51
24	Ion Channel	Ion Channel	HTR3A	Opener	EC <sub>50</sub>	>	100			0
25	Ion Channel	Ion Channel	KvLQT1/mi nK	Opener	EC <sub>50</sub>	>	100			9.85
26	Ion Channel	Ion Channel	nAChR(a4/ b2)	Opener	EC <sub>50</sub>	>	100			1.37
27	Ion Channel	Ion Channel	NMDAR (1A/2B)	Opener	EC <sub>50</sub>	>	100			5.64
28	Kinases	Binding	INSR	Inhibitor	IC <sub>50</sub>	>	100			0
29	Kinases	Binding	LCK	Inhibitor	IC <sub>50</sub>	>	100			12.26
30	Kinases	Binding	ROCK1	Inhibitor	IC <sub>50</sub>	>	100			39.22
31	Kinases	Binding	VEGFR2	Inhibitor	IC <sub>50</sub>	>	100			26.36
32	NHR	NHR Nuclear Translocati on	AR	Agonist	EC <sub>50</sub>	>	100			0
33	NHR	NHR Nuclear Translocati on	AR	Antagonist	IC <sub>50</sub>	>	100			17.15
34	NHR	NHR Protein Interaction	GR	Agonist	EC <sub>50</sub>	>	100			1.25
35	NHR	NHR Protein Interaction	GR	Antagonist	IC <sub>50</sub>	>	100			18.1

1  
2  
3  
4  
5  
6  
7  
8  
9  
10  
11  
12  
13  
14  
15  
16  
17  
18  
19  
20  
21  
22  
23  
24  
25  
26  
27  
28  
29  
30  
31  
32  
33  
34  
35  
36  
37  
38  
39  
40  
41  
42  
43  
44  
45  
46  
47  
48  
49  
50  
51  
52  
53  
54  
55  
56  
57  
58  
59  
60  
61  
62  
63  
64  
65

Non-Kinase Enzymes	Enzymatic	AChE	Inhibitor	IC <sub>50</sub>	>	100				0.26
Non-Kinase Enzymes	Enzymatic	COX1	Inhibitor	IC <sub>50</sub>	>	100				7.67
Non-Kinase Enzymes	Enzymatic	COX2	Inhibitor	IC <sub>50</sub>	>	100				3.31
Non-Kinase Enzymes	Enzymatic	MAOA	Inhibitor	IC <sub>50</sub>	>	100				0
Non-Kinase Enzymes	Enzymatic	PDE3A	Inhibitor	IC <sub>50</sub>	>	100				0.03
Non-Kinase Enzymes	Enzymatic	PDE4D2	Inhibitor	IC <sub>50</sub>	>	100				7.9
Transporter	Transporter	DAT	Blocker	IC <sub>50</sub>	>	100				22.27
Transporter	Transporter	NET	Blocker	IC <sub>50</sub>	>	100				28.22
Transporter	Transporter	SERT	Blocker	IC <sub>50</sub>	>	100				0